ANL/GTRI/TM-13/15

Argonne NATIONAL LABORATORY

Low Enriched Uranium Core Design for the Massachusetts Institute of Technology Reactor (MITR) with Un-finned 12 mil-thick Clad UMo Monolithic Fuel

Nuclear Engineering Division

About Argonne National Laboratory

Argonne is a U.S. Department of Energy laboratory managed by UChicago Argonne, LLC under contract DE-AC02-06CH11357. The Laboratory's main facility is outside Chicago, at 9700 South Cass Avenue, Argonne, Illinois 60439. For information about Argonne and its pioneering science and technology programs, see www.anl.gov.

Availability of This Report

This report is available, at no cost, at http://www.osti.gov/bridge. It is also available on paper to the U.S. Department of Energy and its contractors, for a processing fee, from:

U.S. Department of Energy
Office of Scientific and Technical Information
P.O. Box 62
Oak Ridge, TN 37831-0062
phone (865) 576-8401
fax (865) 576-5728
reports@adonis.osti.gov

ANL/GTRI/TM-13/15

Low Enriched Uranium Core Design for the Massachusetts Institute of Technology Reactor (MITR) with Un-finned 12 mil-thick Clad UMo Monolithic Fuel

prepared by

A. Bergeron, E.H. Wilson, G. Yesilyurt, F. E. Dunn, J.G. Stevens

GTRI Reactor Conversion Program, Nuclear Engineering Division
Argonne National Laboratory, 9700 S. Cass Avenue, Argonne, Illinois 60439

L. Hu and T.H. Newton Jr.

Massachusetts Institute of Technology Nuclear Reactor Laboratory
138 Albany Street, Massachusetts Institute of Technology, Cambridge, MA 02139

November 2013

This work is sponsored by the U.S. Department of Energy,
National Nuclear Security Administration Office of Global Threat Reduction (NA-21)

(This page intentionally left blank)

EXECUTIVE SUMMARY

This report contains the results of reactor fuel element design for conversion of the Massachusetts Institute of Technology Reactor (MITR) from the use of highly enriched uranium (HEU) fuel to the use of low enriched uranium (LEU) fuel. The analyses were performed by staff members of the Global Threat Reduction Initiative (GTRI) Reactor Conversion Program at the Argonne National Laboratory (ANL) and the Massachusetts Institute of Technology Nuclear Reactor Laboratory. The core conversion to LEU is being performed with financial support of the U. S. government.

The goal of this work was to design an MITR LEU fuel element that could safely replace the current MITR HEU fuel element and maintain mission performance while requiring minimal, if any, changes to the reactor system. As a means to accomplish this, neutronic and steady-state thermal hydraulic performance of the MITR was analyzed with various LEU fuel element designs. The evaluation included the impact of assumed manufacturing tolerances and other uncertainties in reactor parameters.

Documents that were reviewed as bases for the design and safety evaluations were the MITR design drawings and historic analyses of the facility. All of the information and data needed to construct the reactor models and perform the analyses were provided by MITR. The current HEU fuel element has 15 plates that are 0.080 inch thick with 0.010 inch deep grooves along the length of the plate. These grooves serve as fins to increase heat transfer area to the coolant. The HEU aluminide fuel contains uranium with a ^{235}U enrichment of 93 wt%, and is 0.030 inch thick in each plate. The Al-6061 aluminum cladding at the base of the grooves on the HEU plates is 0.015 inch thick.

Prior LEU element design analyses with high-density monolithic alloy fuel have obtained equivalent performance and fuel cycle with an 18-plate element with 0.020 inch thick fuel and 0.010 inch cladding thickness (at the base of the fins). Whereas this prior MITR LEU design was based upon cladding thickness of 0.010 inch, recent manufacturing development experience has led to a re-evaluation of the minimum cladding thickness for reliable fabrication. These core and element design activities were undertaken to determine if additional cladding thickness could be incorporated into an MITR LEU element design. Since increased cladding thickness would displace water and degrade core reactivity, removal of the fins was also explored as a goal of the work. Removal of the fins would not only increase water to metal ratio in the core, but would also improve the economics of an MITR LEU element by eliminating this fabrication step, which is unique to MITR fuel design among U.S. high performance research reactors which refuel with HEU. In order to compensate for the loss of heat transfer area, an increased core coolant flow rate has been considered, and distinct fuel thicknesses were introduced in the outer plates of each element to limit heat flux peaking.

The proposed LEU fuel element designs have the same overall design and exterior dimensions as the current HEU fuel elements, except for altering the number of fuel plates from 15 to either 18 or 19 plates; incorporating distinct thinner fuel plates in the outer plates of each element; altering the interior and end channel dimensions; and removing the surface grooves. Furthermore, whereas the HEU aluminide dispersion fuel is 0.030 inch thick, the proposed LEU fuel element designs have fuel meat thicknesses of 0.020, 0.025, or 0.030 inch for interior plates, and thinner fuel zones in the outer plates. Each proposed LEU design incorporates three distinct thicknesses of fuel so that the fuel in the outer plates is progressively thinner with an outermost fuel thickness of 0.011-0.016 inch, depending on the design. For all designs the fuel consists of U-10Mo monolithic foils containing uranium with a ^{235}U enrichment of 19.75%. The cladding consists of Al-6061 aluminum and a thin layer of zirconium

between the fuel foil and aluminum. The thinnest nominal combined zirconium and aluminum thickness on the fuel plates is 0.012 inch of cladding.

For stability, all plates of an element have the same exterior thickness (for a given element design), and so cladding is thicker in the outer plates of the element where the fuel is thinner. Plate thicknesses among the various designs ranged from 0.044 to 0.059 inch thick, which is thicker than the prior LEU design due to either thicker cladding, or thicker cladding and fuel. The cladding thickness is based on feedback from the Fuel Development (FD) and Fuel Fabrication Capability (FFC) pillars to the Reactor Conversion (RC) pillar of the GTRI U.S. High Performance Research Reactor Conversion program to reliably manufacture the fuel plates. The LEU U-10Mo monolithic alloy fuel is not yet qualified as driver fuel in research reactors, but is under intense development under the auspices of the GTRI FD and FFC programs.

To design the proposed MITR LEU element, optimization analyses were performed to limit power peaking factors so that acceptable shutdown and safety margins will still exist with the LEU fuel. The designs were also required to maintain experimental performance comparable to the current HEU core and, at a minimum, fuel cycle performance equivalent to the prior LEU design which was analyzed assuming a 47 day typical LEU cycle; and refueling on a quarterly, or less frequent, basis each year. Experimental performance evaluations demonstrated that a power up-rate to 7 MW is needed to maintain neutron fluxes at key irradiation locations. Consequently, all future study of safety margins should be evaluated relative to the uprated power of 7 MW. The HEU core has as a criterion for the Limiting Safety System Settings (LSSS) avoidance of the onset of nucleate boiling (ONB). For the LEU cores all designs were required to have sufficient margin to ONB (> 20% margin) so that the reactor may operate at 7 MW with a margin at least equivalent to the current HEU core.

Given the constraints described above, element design parameters investigated include the number of plates, fuel thickness(es), cladding thickness, removal of fins, lower fuel loading in the outer plates, end channel size, and increased core coolant flow rate. Margin to ONB was calculated for each element design by statistically sampling the effect of tolerances and uncertainties for both all-fresh and depleted cores representative of MITR fuel management. In order to perform a whole core analysis, the limiting location for each design was determined by finding the element, channel, stripe, and axial with the minimum margin to ONB. Both fresh and depleted cores were analyzed in this manner. For many designs considered, the depleted cores representative of current MITR fuel management were more limiting than fresh cores; however each core loading requires individual analysis.

A systematic variation of parameters was carried out that allowed down selection of designs. These calculations determined a range of LEU element designs with an adequate fuel cycle at the 7 MW LEU power required to maintain performance equivalent to 6 MW HEU operation. Six candidate LEU element designs with 0.012 inch cladding and no fins also demonstrated sufficient margin to ONB, provided that core coolant flow rates can be increased, by approximately 10-20%. While the increased core coolant flow rate has been demonstrated during pre-operational tests with the current pumps, further evaluation is required. Complete safety analysis after selection of the most promising element design is also required to determine steady state core flow rates and temperatures, and to finalize related uncertainty assumptions presented is this report. The performance of the LEU element design under accidents and transient scenarios also requires evaluation. The design selection will follow this report with any input available regarding fabrication from the FFC pillar, and fuel performance constraints from the FD pillar.

TABLE OF CONTENTS

TABLE OF FIGURES

LIST OF TABLES

LIST OF TABLES (Cont'd)

1 INTRODUCTION

The Massachusetts Institute of Technology Reactor (MITR-II) is a research reactor designed primarily for experiments using neutron beam and in-core irradiation facilities. It delivers a neutron flux comparable to current light water power reactors in a compact 6 MW core using Highly-Enriched Uranium (HEU) fuel.

In order to reduce the threat related to the dissemination of weapons-grade uranium materials, the international community presently aims to minimize and if possible eliminate the use of HEU fuel from civilian activities. As a part of this global effort, most HEU-fueled research and test reactors worldwide have started a program of conversion to the use of Low-Enriched Uranium (LEU) fuel.

Previous work has analyzed an MITR-II LEU fuel element for both performance and safety margins [1-11]. The reference LEU fuel considered for the conversion of MITR-II is a new type of high density Uranium-Molybdenum (UMo) alloy. This fuel is currently under development [12].

The goal of this work was to design an MITR LEU fuel element that could safely replace the current MITR HEU fuel element and maintain performance while requiring minimal, if any, changes to the reactor system. As a means to accomplish this, neutronic and steady-state thermal hydraulic performance of the MITR was analyzed with various LEU fuel element designs. The evaluation included the impact of uncertainties due to tolerances assumed in manufacturing.

Prior LEU element design analyses with high-density monolithic alloy fuel have obtained equivalent performance and fuel cycle with an 18-plate element with 0.020 inch thick fuel and 0.010 inch cladding thickness (at the base of the fins). Whereas this prior MITR LEU design was based upon cladding thickness of 0.010 inch [13], recent manufacturing experience has led to a re-evaluation of the minimum cladding thickness for reliable fabrication. These core and element design activities were undertaken to determine if additional cladding thickness could be incorporated into an MITR LEU element design.

2 MITR REACTOR AND REFERENCE LEU DESIGN

This section provides basic information on the MITR-II HEU and reference LEU element designs as previously described in detail [3, 6].

2.1 General Description of the Core

The MITR-II facility is currently licensed to operate at 6 MW thermal power. It is a hexagonal core containing 27 rhomboidal-shaped fuel locations in three radial layers (later referred to as rings A, B and C) as shown in Figure 1. The 27 elements may be referred to with either the ring designation, or sequentially counting from element 1 (A-1) to 27 (C-15). Typically three of these positions (two in the A-ring and one in the B-ring) are filled with either an in-core experimental facility or a solid aluminum dummy (to reduce power peaking and increase shutdown margin).

The core is cooled by light water circulated upward through the core from bottom to top and is surrounded by a D_2O reflector. Boron impregnated stainless steel control blades are present at the periphery of the core at each side of the hexagon. The control blades have sufficient reactivity worth to shut down the reactor at any time. Each blade can be controlled independently but the 6 blades are typically banked for normal operation.

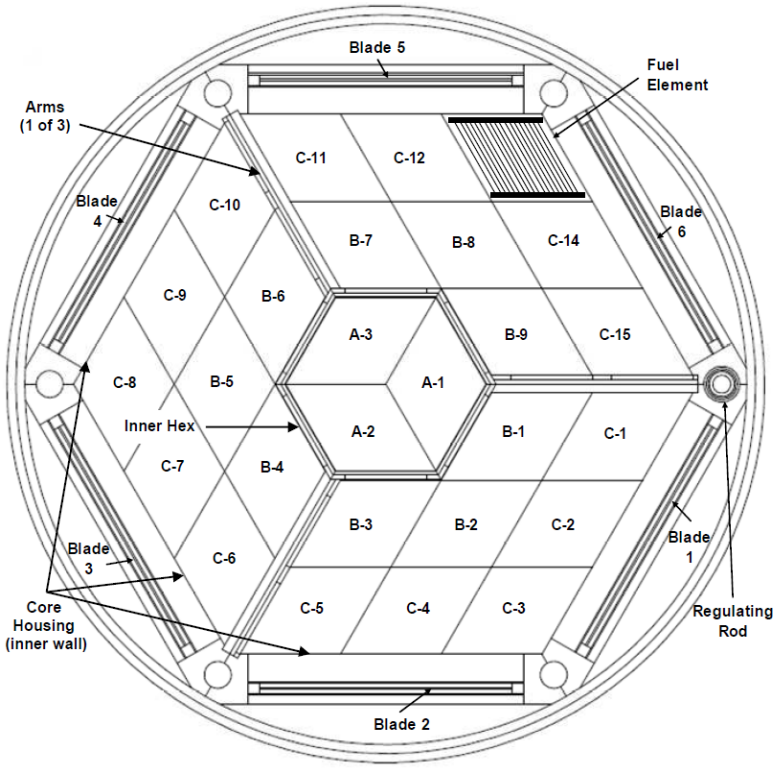

Figure 1. Layout of the MITR-II Reactor Core.

Several reentrant thimbles are installed inside the D_2O reflector, delivering greater thermal neutron flux to the beam ports outside the core region. Beyond the D_2O reflector, a secondary reflector of graphite exists in which several horizontal and vertical thermal neutron irradiation facilities are present. In

addition, a fission converter facility is installed in the graphite reflector. This facility contains eleven partially spent MITR fuel elements for delivery of a beam of primarily epithermal neutrons to the medical facility for use in Boron Neutron Capture Therapy (BNCT).

2.2 LEU Reference Element Design

The reference LEU element has been extensively discussed in [3, 5, 6]. The reference LEU element contains 18 fuel plates made of aluminum clad and UMo monolithic fuel. The UMo fuel is enriched up to 19.75wt% of ^{235}U and contains 10wt% of Mo for an overall fuel density of 17.02g/cc. The fuel composition modeled is given in Table 1. As illustrated in Figure 2 and Figure 3, the reference LEU element design contains 18 plates with fins. The cladding is made of 6061 aluminum which has a thin layer (nominally 1 mil or 25µm) of zirconium at the fuel/cladding interface. The zirconium layer is used as a diffusion barrier to avoid the undesirable chemical reaction between the fuel foil and the aluminum of the cladding. The fuel thickness is 0.508mm (20 mil), its width is 5.288cm (2.082inch) and its length is 56.833cm (22.375inch). Note that 1 mil corresponds to 0.001 inch. The cladding thickness is 0.254mm (10 mil). In order to increase the heat transfer to the coolant there are 110 0.254mm (10 mil) longitudinal fins in addition to the 0.254mm cladding. The thickness of the plate is 1.524mm (60 mil) from fin-tip to fin-tip. The gaps between fuel plates form the interior channels. Their thickness is 1.8288mm (72 mil) from fin-tip to fin-tip. The end channel thickness is 50.5 mil from fin-tip to nozzle. Important dimensions of the reference LEU element design are given in Table 2 which also gives the equivalent dimensions of the HEU element. The data regarding the HEU and prior reference LEU element design are being presented since the purpose of the analyses is to re-design the LEU element so that it performs adequately while incorporating cladding thicker than 0.010 inch.

Table 1. LEU U-10Mo Monolithic Fuel Composition Modeled.

Isotope	Atomic Density (atom/barn-cm)	Density (g/cc)
^{92}Mo	1.578E-03	2.408E-01
^{94}Mo	9.857E-04	1.537E-01
^{95}Mo	1.699E-03	2.677E-01
^{96}Mo	1.781E-03	2.837E-01
^{97}Mo	1.021E-03	1.644E-01
^{98}Mo	2.584E-03	4.202E-01
^{100}Mo	1.033E-03	1.713E-01
^{234}U	1.025E-04	3.983E-02
^{235}U	7.751E-03	3.025E+00
^{236}U	1.798E-04	7.046E-02
^{238}U	3.082E-02	1.218E+01
total	**4.953E-02**	**1.702E+01**

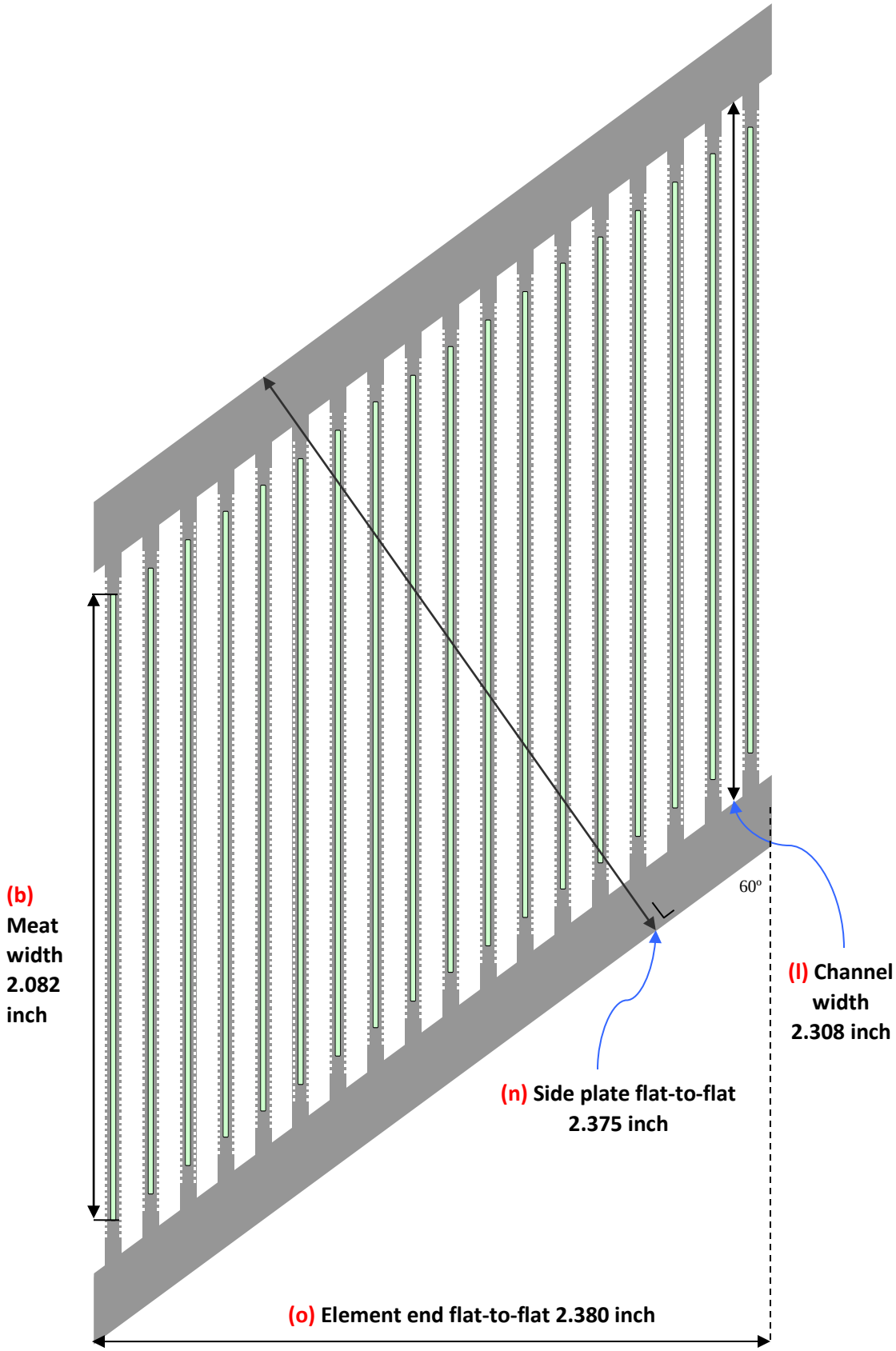

Figure 2. Reference LEU Fuel Element with Fins.

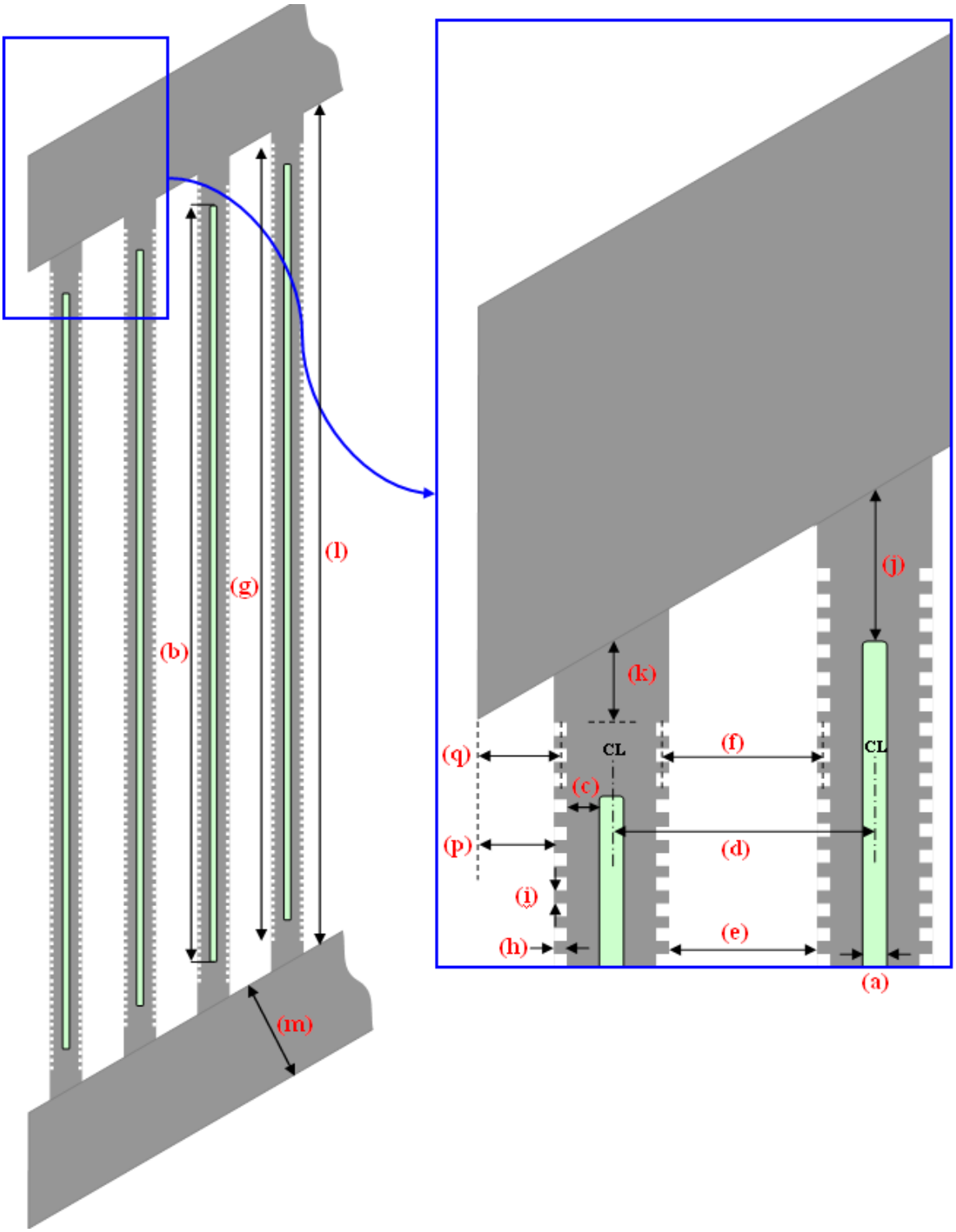

Figure 3. Schematic of Prior MITR LEU Reference Element Outer 4 Plates (letters indicate dimensions listed in Table 2).

Table 2. HEU and Prior Reference LEU Element Dimensions.

Plate and Channel Dimensions (Schematic Labels Figs. 2-3)	HEU	LEU
Fuel plate length (inch)	23	23
Fuel meat length (inch)	22.375	22.375
Fuel plates per assembly	15	18
Interior (full) channels per assembly	14	17
End (partial) channels per assembly	2	2
(a) Fuel meat thickness (mil)	30	20
(b) Fuel meat width (inch)[a]	2.082	2.082
(c) Clad thickness, base of fin to fuel surface (mil)	15 (6061 Al)	10 (6061Al + Zr)
(d) Plate to plate pitch, CL to CL (mil)	158	132
(e) Interior channel water gap, fin tip-to-tip (mil)	78	72
(f) Effective interior channel thickness (mil)	88	82
(g) Finned width (inch) [a]	2.2	2.2
Number of fins per plate	110 per side	110 per side
(h) Fin depth (mil)	10	10
(i) Fin width (mil)	10	10
(j) Width between fuel meat and side plate (mil)	113	113
(k) Width between fins and side plate (mil)	54	54
(l) Channel width (inch) [a]	2.308	2.308
(m) Side plate thickness (mil)	188	188
(n) Side plate flat-to-flat, outer edge of one side plate to outer edge of second side plate on element (inch)	2.375	2.375
(o) Element end flat-to-flat (inch)	2.380	2.380
(p) Outer plate fin-tip to side plate end plane (mil)	44	38
(q) Effective outer plate gap to side plate end plane (mil)	49	43
Outer plate fin-tip to nozzle at full width (mil)	56.5	50.5
Effective outer plate gap to nozzle at full width (mil)	61.5	55.5

[a] For thermal hydraulic analysis, channel width is the fuel meat width of 2.082 inch (0.052883 m)

3 TOOLS, METHODS AND SCOPE OF THE ANALYSIS

An acceptable LEU design must demonstrate acceptable performance and acceptable safety margins. Acceptable performance means that the magnitude of the neutron flux in the experimental facilities matches the current level that is obtained with a 6 MW HEU core. Also, fuel lifetime should at least match that of the HEU core, and preferably exceed that of the reference LEU design. Safety margins include reactivity shutdown margins and the margin to Onset of Nucleate Boiling (ONB) [14]. Simulation of a complete fuel management scheme is complicated and computationally expensive. This is why the element design process has followed a two-step process.

At first, as discussed in Section 4, modifications to the design have been made considering a fresh core since calculations are based on a single core configuration. Impacts on performance and safety margins have been analyzed. A down-selection of the most promising combinations of design modifications has been carried out based upon these results. In the second step, as discussed in Section 5, these most promising candidates have been analyzed in a representative MITR fuel management scheme where performance and safety margins have been re-evaluated at each relevant time step. Section 3.1 describes explicitly the different neutronic parameters taken into consideration in this analysis and what tools and methods have been used to evaluate them. Section 3.2 describes the implementation of fuel management and Section 3.3 the thermal hydraulic methods used for both fresh and depleted core analysis.

3.1 Neutronic Parameters and Tools in the Scope of the Fresh Core Design Selection Analysis

All steady-state neutronic parameters have been evaluated using the Monte-Carlo code MCNP. The MCNP model of the MITR reactor has been validated through benchmarking [3]. Depletion calculations have been carried out with the MIT depletion code MCODE which is described in more details in Section 3.2.2.

3.1.1 Neutron Flux in Experimental Facilities

The neutron flux is evaluated, for the critical state, at five distinct locations which are considered representative of the overall performance of both the in-core and ex-core experimental facilities.

In-core:

- In-Core Experimental Facilities
  - Utilized for fast flux irradiation of samples
  - Three experiments can be loaded simultaneously with two in the A-ring (currently A1 A3 B3)
  - An in-core sample assembly (ICSA) loaded into the A-ring, position A3, has been modeled as a reference location for comparison of performance
  - The A ring ICSA modeled is a helium-filled (two inch) diameter titanium tube surrounded by solid aluminum within the A-3 core position. The central sample 7.6-inch tall region of the tube was tallied empty for comparative purposes to be independent of particular sample loadings.

A unique feature of MITR's in-core experiment capabilities is high temperature irradiation. The high temperature ICSA capsule has been demonstrated for up to 850°C, and a High Temperature Irradiation Facility (HTIF) was demonstrated up to 1400°C using gamma heating. Additional evaluation of the

performance of high temperature experiments is being conducted separately; however, thermal assessments and associated re-design of the experimental devices is beyond the scope of the present element design analyses.

Four ex-core facilities that follow are, similar to the ICSA, modeled for comparative purposes empty and without sample-related materials.

Ex-core:

- Twelve-inch Beam Port 12SH1
  - Facility is representative of beam port facilities located just below the core, used in neutron scattering and other applications

- Two-inch Pneumatic Facility
  - High flux pneumatic facility located in the six-inch radial port 2PH1 is tallied
  - Neutron activation analysis and isotope production
  - Positioned closer to core centerline than the horizontal ports such as 12SH1

- Fission Converter Window
  - Fourteen-inch square window in the graphite reflector directly adjacent to the fission converter facility is tallied. This area is representative of the thermal flux impingent upon the fission converter fuel tank and is directly proportional to the epithermal flux available to the medical facility for BNCT clinical trials

- Below-core Thermal Beam Facility
  - Water shutter below D2O reflector directly under core is tallied
  - Facility now in use as a thermal beam
  - Modeled with “open” water shutter (helium filled)

While many other in-core and ex-core facilities are utilized at MITR, these five metrics are considered representative of performance since they cover the diverse regions and functions of the majority of experiments and facilities. The variety of locations covered by these ex-core facilities is illustrated in Figure 4.

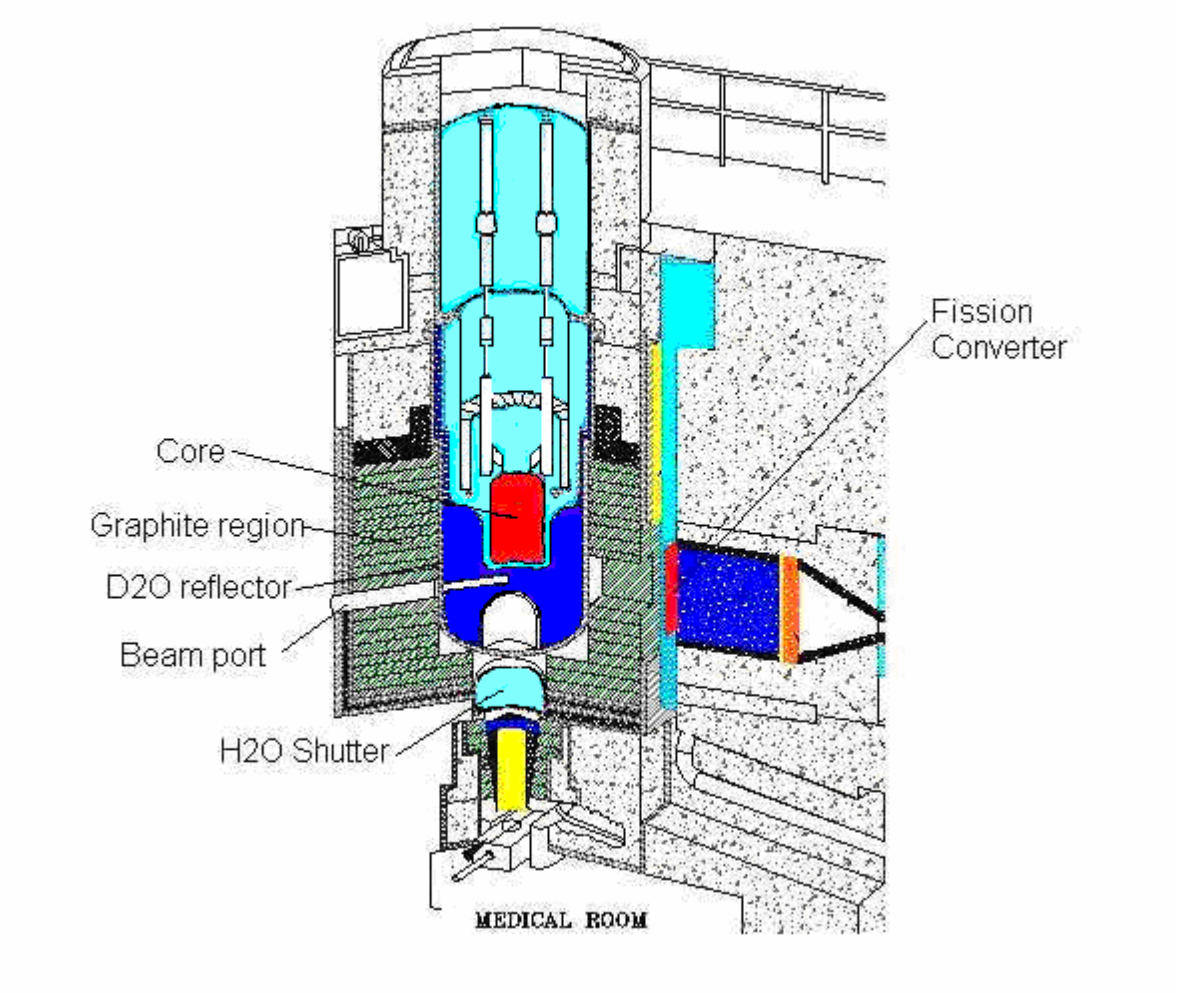

Figure 4. Schematic of the MITR Reactor Facility.

3.1.2 Shutdown Margin

Shutdown margins are evaluated at BOC with the reactor in a cold state (entire reactor at 10°C) as described in Reference [3]. Shutdown margin requirements are met if there is at least 1% Δk/k negative reactivity margin, for a xenon-free condition, with both the most reactive shim blade and the regulating rod fully withdrawn and all experimental samples in their most reactive state.

3.1.3 Rundown Core Lifetime

Rundown depletion core lifetime calculations have been performed at the reference LEU power with all shim blades and regulating rods withdrawn and starting with 24 fresh elements. As a figure of merit of the designs, the core cycle rundown lifetime is reported as the time necessary for the excess reactivity to be reduced to zero. This depletion calculation is not used to evaluate the fuel element consumption but to provide an important insight into how the core will perform during more realistic fuel management operations.

3.2 Neutronic Fuel Management Methods and Tools

3.2.1 MITR Fuel Management

MITR has flexible fuel management incorporating 24 elements in three radial rings where elements can be rotated and/or flipped. Elements can be used in-core over the course of several years, or held in storage for future reloading. Fuel management representative of 12 cores, and approximately two years, of historical operation was modeled. The results of these analyses were used to identify the best candidate LEU element designs under conditions representing anticipated operations.

The computational complexity is increased for depleted cores since these cores reproduced over 80 fuel shuffling operations required for MITR fuel management on 57 elements over this two year historical period, including fuel movements, flips and rotations. These depleted cores may contain several fresh elements loaded in order to increase reactivity, or may be loaded entirely of elements which have been irradiated previously.

Nuclear fuel management entails making core loading decisions that influence how a reactor core's spatial distribution of flux, power and burnup vary. The power density spatial distribution drives the thermal-hydraulic performance of the core, which is constrained by various safety performance limits such as heat flux, margin to ONB, and limiting materials temperatures. The objective of nuclear fuel management for conversion to LEU is to maintain reactor capabilities for experimental applications as closely as possible to that for HEU fuel, while satisfying all constraints imposed.

Core fuel management modeling was utilized to meet the following objectives:

- to model a series of depleted cores that can generate a representative LEU fuel history;
- to shuffle the fuel effectively throughout the reactor operation over many cycles in order to ensure that core parameters remain within the approved operating limits across a range of cores and time-points in the cycle;
- to validate core operating strategies in order to obtain maximum operating flexibility and optimum fuel utilization while at the same time remaining within the established safety limits;
- to ensure that the cycle length of the new core is consistent with expectations.

Fuel management calculations were performed for the MIT Reactor (MITR) to ensure that the reactor is operating at full power within the safety limits at the critical state. Both the MCODE-2 [15] and MCODE-FM [16] codes were utilized to perform the fuel management analysis.

3.2.2 Neutronic Fuel Management Tools

The code package MCODE (MCNP - ORIGEN coupled Depletion) [15, 17] links the continuous-energy Monte Carlo code MCNP5 [18] with the point-depletion code ORIGEN2.2 [19] as detailed in other works [5], and reiterated here. It uses the predictor-corrector method to calculate nuclide concentrations for each time-step, which has been shown to be more accurate than the methods used in other similar codes that use only the beginning-of-step or middle-of-step reaction rates for the depletion matrix in the Bateman equations. Also, MCODE provides a more user-friendly interface for depleting a significantly larger number of regions than was previously feasible. This is of particular interest for full-core modeling of MITR-II.

MCODE-FM [16], written in Python, was developed to replace the previous generation of MITR-II fuel management utilities produced in the 1970s which were centered around the finite-difference diffusion theory. It uses MCODE to deplete the fuel regions of a series of core configurations, optionally utilizing a criticality search algorithm to track critical blade movement. The logic of MCODE-FM is rather straightforward. It takes as input the material definitions for any number of fuel assemblies as well as series of core loading configurations using those elements. Next it creates an MCODE input file for the first core configuration by writing the MCNP cells, surfaces, and materials cards into the specified location of a template MCNP skeleton file of the MITR-II core.

This core configuration is depleted with MCODE, and then the subsequent core configurations are constructed with the appropriate material concentrations for each fuel assembly. This facilitates the automation of long fuel shuffling simulations without the need to manually move materials around to create MCNP/MCODE input files for each new core configuration. The user can specify how the depletion materials are treated to balance accuracy and speed. Axially, a number of surfaces are written to divide the fuel plates into any number of axial regions. Likewise, fuel plates can be grouped together radially into any number of regions less than the number of fuel plates. For instance, if one radial region is used for an assembly each plate will be depleted in MCODE using the same MCNP material. Unlike prior works, in this design study each plate was depleted separately, not grouped with any other plates other than for the reference LEU design which follows Reference [6]. Although the complexity of the generated MCNP inputs is higher, and the number of reaction rate tallies needed for MCODE depletion larger, the computational expense was reasonable. This versatile functionality facilitates whole core neutronic analysis by allowing the user to control the tradeoff between accuracy and computational expense.

3.2.3 Burnup and Fuel Behavior

Due to the effect of fission, fuel swelling occurs and can be calculated as per Kim and Hofman [20]:

$$(\Delta V/V_o)_f = 5.0 f_d, \quad \text{for} \quad f_d \leq 3$$

$$(\Delta V/V_o)_f = 15 + 6.3(f_d - 3) + 0.33(f_d - 3)^2, \text{ for } f_d > 3$$

where $(\Delta V/V_o)_f$ is the fuel swelling due to both fission product solids and gas in percent and f_d is fission density in units of 10^{-21} cm^{-3}. Note $(\Delta V/V_o)_f$ is not fractional but is given in units of percent. This uses the original volume, V_o , and the change in volume ΔV. The ^{235}U burnup is estimated to represent the fission density for the purposes of this study. This neglects the swelling arising from fissions due to other actinides; however, on the whole, somewhat overestimates the swelling due to the non-fission reactions, e.g. (n,γ), consuming ^{235}U.

Local swelling of the fuel meat was estimated using a combined local fission density and lateral power peaking factor as described in [22]. This was done since the fuel was not subdivided in the lateral direction for depletion. The lateral power peaking factor from the MCNP power distribution analysis has been applied to obtain an estimate of peak local burnup values.

Using the above method including lateral peaking, the axially averaged swelling for each stripe in the channel may be computed. As discussed in Section 5, an evaluation of the thermal hydraulic reduction in channel (stripe) flow area has been performed in this manner.

3.3 Thermal Hydraulic Methods and Tools

This section discusses the method implemented in a computer program to perform analysis of the steady state thermal hydraulic safety basis for MITR. Since the conversion from HEU to LEU will involve a number of significant changes to the core, a new steady-state and transient thermal hydraulic safety analyses is required. The number of required new safety analysis cases may be quite large. Optimization of the new fuel element design as detailed in this report requires analysis of a large number of design options. Also, since there is great flexibility in MITR reactor fuel shuffling and reloading, it may be necessary to repeat at least part of the safety analysis in the future for every fuel reloading. The main goal is to provide a standardized and automated procedure and tool for the safety analysis. The work described in this section only addresses steady-state analysis as codified in the Stat7 program. Transient analysis of accidents is also required, but the transient analysis is not within the scope of this report [20].

For steady-state operation, safety limit analysis is performed in order to protect against critical heat flux (CHF) or departure from nucleate boiling (DNB). Since onset of flow instability (OFI) can lead to DNB, OFI is also to be avoided. In order to provide additional margin, the limiting safety system settings are based on avoiding onset of nucleate boiling (ONB) [14]. ONB will occur before either OFI or DNB.

The original thermal hydraulics approach was to calculate the margin to ONB at each axial node of the limiting fuel plate stripe in the core. The stripes run the length of the fuel, from axial node 1 at the bottom of the fuel to axial node 18 at the top of the fuel. For nominal dimensions before accounting for uncertainties, the stripe with the maximum stripe power will be the most limiting; but it may also be necessary to analyze the stripe containing the peak spot power to determine which stripe is limiting. Since then, the steady-state thermal hydraulics calculations have been automated to the point that the current practice is to calculate the margin to ONB for each axial node of each stripe of each plate of each element in the core.

3.3.1 Channel Treatment

Figure 5 illustrates a cross section of the channel geometry used for thermal hydraulics calculations where a number of axial nodes are modeled in this manner in the vertical direction.

Both interior channels and end channels must be considered. A simple interior ‘half-channel’ models the middle of the fuel to the middle of the adjacent interior coolant channel. There are a number of possible end channel geometries. An end channel models the region from the middle of the fuel of an end plate, including the whole end coolant channel, to the surface of the side plate of an adjacent assembly. This effectively models a coolant channel heated on one side but with wall friction on both sides. Variations on this type of end channel include end coolant channels that face the core housing, the inner hex or an arm (see Fig. 1). Qualitatively these situations are similar, but the end coolant gap size depends on what the end channel is facing. Another possibility is that the end coolant channel of one element could face the end coolant channel of another element, creating one larger coolant channel heated on both sides.

Originally the calculations done for this work included only half of one fuel plate and half of an adjacent coolant channel for an interior channel or an end channel heated on both sides. The entire adjacent coolant channel was used for an end channel facing an unheated surface. Only a minor modification to

the computational procedure was required to add the option to treat a coolant channel heated on both sides. With this option an interior channel was modeled from the middle of plate 1 to the middle of plate 2, as shown in Fig. 3.3-1. Also, an end channel heated on both sides can be treated more accurately. The treatment has been extended to simultaneously treat every plate and every coolant channel in an element.

In this channel treatment, the width of a sub-channel is equal to the width of a single stripe in the fuel. The non-fueled sides of the plate and the coolant in contact with the non-fueled sides are ignored. Lateral coolant mixing between stripes is ignored. Also lateral conduction between stripes in the fuel and clad is ignored.

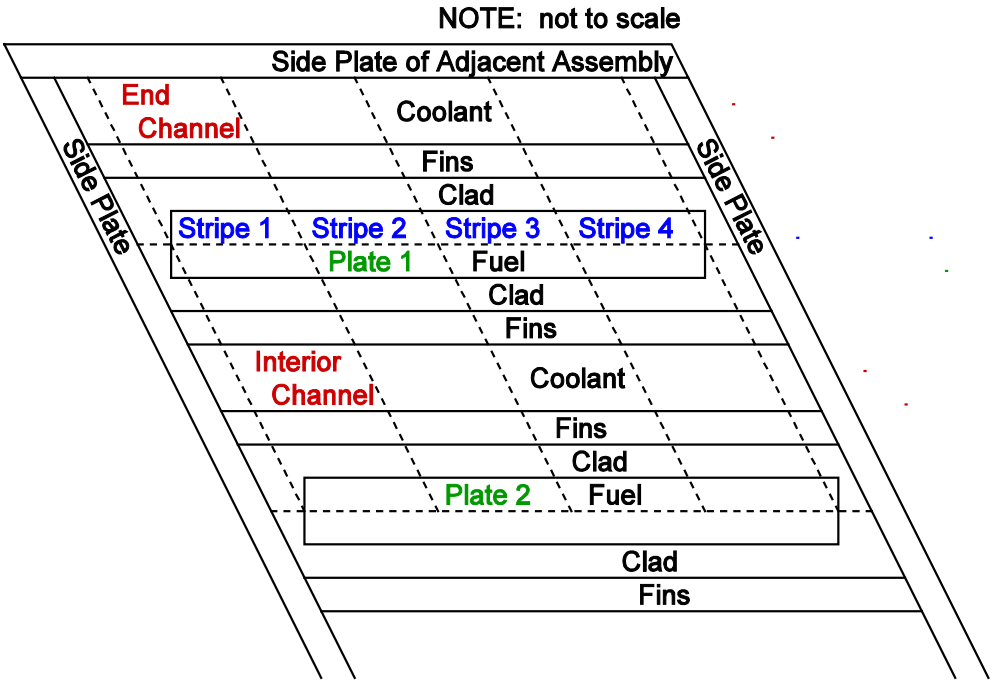

Figure 5. Channel Geometry for 4 Stripes.

3.3.2 How Many Stripes Are Necessary?

One of the issues addressed by this work is the question of how many lateral stripes are necessary to obtain an accurate or conservative evaluation of peak clad temperatures. The plate power profiles are peaked fairly sharply at the sides of the fuel near the side plate since beyond the edges of the fuel there is less fuel self-shielding of the thermal neutron flux, which causes most of the fissions. Absorption and fission in the fuel reduces the thermal neutron flux in the fuel. The fuel is a source for high energy fission neutrons but a sink for thermal neutrons.

Lateral thermal conduction in the fuel and the clad can reduce the peaking in lateral temperature profiles. To investigate this situation a multi-stripe model, as shown in Fig. 3.3-2, was set up for the RELAP5-3D code [22]. Eighteen channels were used to model the region from the middle of the end plate fuel to the surface of the side plate of the adjacent assembly. Channels 1 to 16 model 16 stripes in

the fueled part of the plate. Channels 0 and 17 model the plate and coolant between the sides of the fuel foil and the side plates. Axial power profiles for a peak power LEU case were obtained with the MCNP code for each of the 16 fueled stripes [24]. A number of variations on this model were run, with and without lateral conduction between adjacent channels or axial conduction in the plate. Also, adjacent fueled channels were combined to make 4 channels or 8 channels in the fuel for additional cases. In all cases coolant mixing or direct lateral heat transfer between coolant channels was ignored.

RELAP5-3D is mainly a transient code. It does not provide a direct steady-state solution for this type of case. Therefore, a null transient, starting from uniform temperatures everywhere, was run. For the null transient the power levels, coolant inlet temperature, and total coolant flow rate were held constant; and the transient was run until the temperatures reached steady-state.

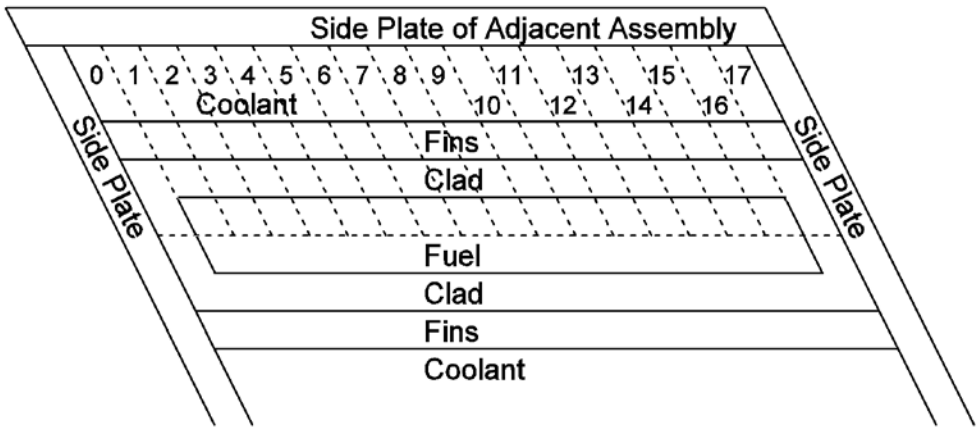

Figure 6. Multi-stripe RELAP5-3D Model.

Results from these RELAP5-3D multi-stripe runs are shown in Fig. 3.3-3. Axial conduction makes no significant change in the peak clad temperatures, so no axial conduction cases are shown in this figure. With no lateral conduction the peak clad temperature rise from the inlet temperature is proportional to the stripe power, so the no lateral conduction results indicate the lateral power peaking. Lateral conduction significantly reduces the peak clad temperature. The peak clad temperature for 4 stripes and no lateral conduction is higher than that for 8 or 16 stripes and with lateral conduction. Therefore, 4 stripes are conservative for a multi-stripe steady-state calculation with no lateral conduction.

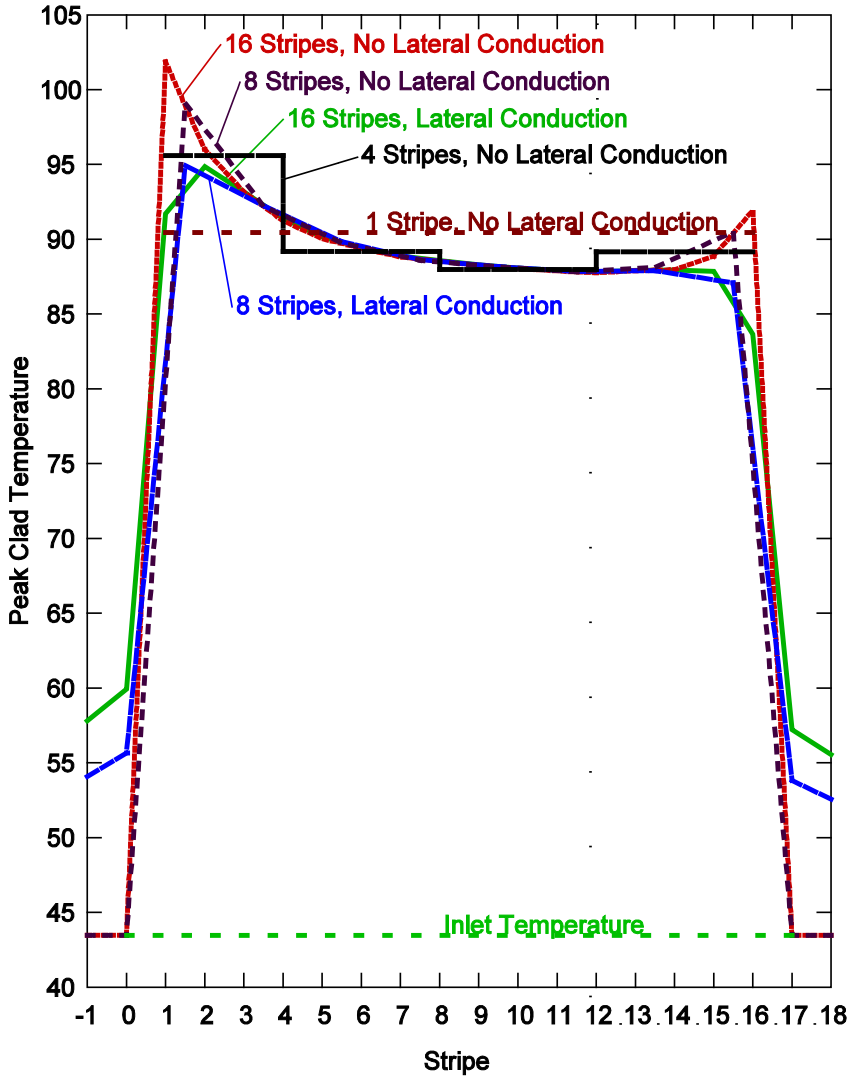

Figure 7. Peak Clad Temperature Results from RELAP5-3D for Various Stripe Discretization of the Fuel Plate and the Coolant Channel, both with and without Lateral Heat Conduction in the plate.

3.3.3 Treatment of Uncertainties using Statistical Approach

For the thermal hydraulics calculations to support the LSSS settings, uncertainties in important parameters are treated with a Monte-Carlo statistical propagation approach. For a given nominal (measured) value of the total reactor power, a large number of histories are run. For each history the values of important parameters are set based on random sampling from the uncertainty distributions for respective parameters. Then a steady-state thermal hydraulics calculation is done for the channel. If the clad surface temperature exceeds the ONB limit at any axial node, then the ONB count is increased by one. Note that for a given history the result used in the statistical analysis is either a 0 (no ONB anywhere) or a 1 (ONB at one or more axial nodes of one or more plates). The amount by which ONB is exceeded in a history is not used. The ONB probability for the specified nominal operating parameters is then given by the ratio of the number of ONB histories to the total number of histories. An iteration process is used to repeat the calculations for additional nominal reactor powers until the power at

which a specific probability of ONB occurring is predicted. During the reactor power iteration the nominal values of all other parameters are held constant. Currently the specified probability of ONB occurring is 0.00135, which corresponds to a 3-sigma confidence level of 99.865%.

The parameters whose uncertainties are treated with the statistical propagation approach are listed in Table 3. The uncertainties listed in this table are treated as 3-sigma values, and normal distributions are assumed for the uncertainties. For LEU designs the coolant gap size uncertainty may have to be reevaluated.

Table 3. Parameters and Uncertainties.

Parameter	3-sigma Uncertainty (%)
Reactor power	5
Local power	14.1 [a]
Pump flow	5
Fin-to-fin interior channel coolant gap size	6.9 [b]
Film heat transfer coefficient	20

a) The uncertainty considered in this work is 14.1% based upon the RMS combination of an assumed 10% uncertainty in the calculated power distribution, and a 10% uncertainty on power due to local fuel homogeneity [4]. This manufacturing assumption is among those requiring confirmation using fabrication data, and depends in part on the fuel foil thicknesses considered in the alternate element designs.
b) Value presented in this section for comparison to previous work [7]. See Appendix A for assumed LEU interior channel tolerances, based upon the same fractional variation of 5.7% at 3-sigma (1.9% at 1-sigma) for all alternate element designs considered. Note that the coolant gap size uncertainty for an end channel must be evaluated separately from the interior channel values in this table.

3.3.4 Code Implementation, the Stat6 Code

A small FORTRAN program, the Stat code, was written to implement and automate the thermal hydraulics calculations for the statistical propagation method for MITR-II. The Stat code is not integrated with neutronics. One neutronic calculation for each core configuration of interest must be made to generate for the whole core stripe powers and axial power shapes used in the Stat thermal hydraulic analysis.

A Stat6 case calculates the nominal reactor power level at which a specified ONB probability occurs for one channel representing a stripe in one element. The input for a Stat6 case includes design information such as that in Table 2, plus axial fuel plate power shapes for a stripe in one or two plates and the fraction of the total reactor power in the stripe for the plate or plates, plus the standard deviations in the probability distributions for the parameters listed in Table 3. Other inputs include the ONB probability level, the number of Monte-Carlo histories for each reactor power iteration, and the first value of the nominal power for the power iteration.

The output from a Stat6 case is mainly the nominal reactor power level at which the specified ONB probability occurs. Also output is some statistical information on the standard deviation of the ONB probability for the final power iteration.

3.3.4.1 Thermal Hydraulics Calculations for a History

At the start of the thermal hydraulics calculations for a history, the nominal reactor power, P_r, is known from the power iteration. The coolant outlet temperature, T_x, and the nominal pump flow are set by the input. After some initialization, the calculations for a history go through the following steps in order. Note that there is no over-all iteration in the thermal hydraulics calculations for a history, although there are two-step iterations within some individual steps to make temperature-dependent coolant properties consistent with the coolant temperatures.

Nominal Stripe Power and Flow

The nominal hot stripe power, P_s, is calculated as:

$$P_s = P_r f_c f_s/(N_e N_p N_s) \quad (1)$$

Where

P_r = nominal core power
f_c = the fraction of the fission power deposited in the core region (calculated value = 0.965)
f_s = hot stripe power/core average stripe power
N_e = number of elements
N_p = number of plates per element
N_s = number of stripes/plate

If the 2-plate option is used, then the nominal stripe 2 power, P_{s2}, is calculated the same way using f_{s2}, the stripe 2 power/core average power, instead of f_s.

The nominal interior channel stripe coolant flow, W_i, is calculated as

$$W_i = W_p f_f d_f f_{in} f_{sf}/(N_e N_p N_s) \quad (2)$$

Where

W_p = Nominal pump flow
f_f = Coolant core flow fraction. This accounts for bypass flow.
d_f = Plenum flow disparity factor; accounts for element to element flow variation
f_{in} = Ratio of the average interior channel flow to the average channel flow. This accounts for the average end channel flow being different from the average interior channel flow.
f_{sf} = Fraction of the coolant channel flow in the stripe region. This accounts for neglecting the flow between the side plate and the edge of the fuel foil.

This section is skipped except for the first history of each reactor power iteration, since the results are the same for later histories.

Reactor Power and Pump Flow

The statistical sampling value, $[P_r]$, for the reactor power is randomly sampled from the probability distribution function about the nominal value, P_r.. Also, the sample value, W_p, for the pump flow is randomly sampled from the probability distribution function for the nominal value, W_p, which uses its standard deviation.

Coolant Inlet Temperature

The coolant inlet temperature, T_{in}, is obtained from

$$T_{in} = T_x - [P_r] f_c/([W_p] C_p) \quad (3)$$

where f_c is the fraction of the power deposited in the core region (value assumed conservatively to be 0.965 and is to be reevaluated for final design). C_p is the heat capacity of the water. T_x is the outlet temperature, at the outlet of each axial node. A two-step iteration is used to obtain some consistency between the temperature-dependent value of C_p and the average core coolant temperature. In the first step, C_p is calculated using Tx as the coolant temperature. In the second step Eq. 3 is repeated with the temperature used for C_p based on the average of T_x and the first step value for $T_{in.}$

Hot Stripe Gap Size, Coolant Flow Area and Hydraulic Diameter

The statistical sampling value, $[G]$, for the hot stripe gap size is obtained from the nominal value, G, and the standard deviation. The coolant flow area, A_G, and hydraulic diameter, D_{hG}, for this gap size are then calculated.

Hot Stripe Coolant Flow Rate

If the core channel pressure drop is mainly due to friction with a turbulent friction factor proportional to the Reynolds number raised to the -0.25 power, then a channel flow rate will be proportional to the flow area times the hydraulic diameter to the 0.714 power. Thus, the hot stripe coolant flow rate, W_s, is obtained from

$$W_s = W_i ([W_p]/W_p)(A_G/A_0)(D_{hG}/D_{h0})^{0.714} \quad (4)$$

Where

A_0 = nominal interior channel stripe flow area

D_{h0} = nominal interior channel stripe hydraulic diameter

Note that although Eq. (2) applies to the nominal interior channel, Eq. (4) can be used for either an interior channel or an end channel if the appropriate values are used for A_G and D_{hG}.

Hot Stripe Axial Node Power Uncertainties

The axial node plate power in the stripe, $[p_j]_j$, for axial node j is obtained from

$$[p_j] = \theta_j [u_j] P_s \quad (5)$$

where

θ_j = input axial power shape, normalized to sum to 1.0

$[u_j]$ = local power uncertainty factor, obtained by statistical sampling from the local power distribution.

The code has options to obtain a separate value for u_j for each axial node or to use the same value for all nodes in a plate.

Axial Node Coolant Temperatures

The axial node coolant temperature, T_{wj}, at the bottom of node j is obtained by starting with the inlet temperature for node 1 and then using

$$T_{wj+1} = T_{wj} + p_{wj} / (W_s C_p) \quad (6)$$

where the value of p_{wj}, the power in the coolant, depends on the options being used. For an interior channel for the single plate option and a full coolant channel, p_{wj} is equal to $[p_j]$. For an interior channel with the two plate option, p_{wj} is the average of the $[p_j]$ for the two plates. For an end channel facing an unheated surface, p_{wj} is half of $[p_j]$.

A two-step iteration is used for each axial node to make the temperature-dependent value of C_p consistent with the calculated coolant temperatures.

Axial Node Coolant Pressures and Saturation Temperatures

The coolant pressure at the top of the core is calculated, based on the height of the water above the core and the coolant outlet temperature. Then the pressure drop in each axial node is calculated, based on friction and gravity head. The saturation temperature at each node is obtained after the pressures are calculated.

Axial Node ONB Temperatures

The Bergles-Rohsenow correlation predicts the fuel clad temperature at which ONB occurs [25].

$$T_{clad,ONB} = T_{sat} + 0.556\left[\frac{q''}{1082 \cdot p^{1.156}}\right]^{0.463 \cdot p^{0.0234}} \quad (7)$$

Where

$T_{clad,ONB}$ is the fuel clad temperature (°C) at which ONB occurs,

T_{sat} is the saturation temperature (°C),

q" is the local heat flux (W/m^2), and

p is the pressure (bar).

Carnavos Fin Heat Transfer Coefficients and Clad Surface Temperatures

The fin heat transfer coefficients are calculated using the Carnavos correlation [26]. The Carnavos correlation is an empirical correlation based on 11 finned tubes of different number of fins, fin height,

fin helix angles and tube diameters. Carnavos fitted experimental data from these tests to obtain this correlation within 10% error. The correlation is given as:

$$Nu = 0.023 \cdot \mathrm{Re}_a^{0.8} \cdot \mathrm{Pr}^{0.4} \cdot \left(\frac{A_{fa}}{A_{fc}}\right)^{0.1} \cdot \left(\frac{A_n}{A_a}\right)^{0.5} \cdot \sec^3 \alpha \qquad (8)$$

where $\mathrm{Nu} = \mathrm{h}\, D_{ha} / \mathrm{k}$

Nu, Re and Pr are Nusselt, Reynolds and Prandtl Number, respectively. Other terms in the Carnavos correlation and their counterparts in MITR are summarized in Table 4.

The clad surface temperatures are calculated from the coolant temperatures, the heat transfer coefficients and the clad heat fluxes.

Table 4. Geometry Parameters in the Carnavos Correlation and Derived Values for LEU Fuel Element.

Symbol	Meaning	Counterpart in MITR element
A_{fa}	Actual free flow area	Stripe Width × (water gap* + 2×fin height) – number of fins per stripe × single fin area
A_{fc}	Open core free flow area at fin inner diameter	Stripe width × water gap*
A_n	Nominal heat transfer area based on tube inner diameter as if fins were not present	Nominal heated perimeter × fuel length
A_a	Actual heat transfer area	Actual heated perimeter × fuel length
α	Helic angle in finned tube	0
D_{ha}	Actual hydraulic diameters	(4×actual flow area)/(actual wetted perimeter)

* water gap refers to the fin-tip to fin-tip distance

3.3.5 Statistical Sampling

The statistical sampling method is taken from a mathematical handbook [27]. A random variable Y is said to be normally distributed with mean m and standard deviation σ if the probability, I_p, that Y is less than or equal to y is given by

$$I_p(Y \le y) = \frac{1}{\sigma\sqrt{2\pi}} \int_{-\infty}^{y} e^{\frac{-(t-m)^2}{2\sigma^2}} dt \qquad (9)$$

or if $x = (y - m)/\sigma$, then

$$I_p(x) = \frac{1}{\sqrt{2\pi}} \int_{-\infty}^{x} e^{-\frac{t^2}{2}} dt \quad (10)$$

Define $I_q(x) = 1 - I_p(x)$

Then if a random number, r, evenly distributed from 0 to 1 is obtained from a random number generator, then sampling from a normal distribution is obtained by obtaining the value of x for which

$$r = I_p(x) \quad (11)$$

Alternatively, one can obtain random sampling from a normal distribution by using

$$r = I_q(x) \quad (12)$$

Reference 27 gives a rational approximation for $x(r)$ where $r = I_q(x)$

for $r \leq 0.5$

$$x(r) = v - (c_0 + c_1 v + c_2 v^2)/(1 + d_1 v + d_2 v^2) + \varepsilon(r) \quad (13)$$

$$v = \sqrt{\ln \frac{1}{r^2}}$$

$c_0 = 2.515517$ $d_1 = 1.432788$
$c_1 = 0.802853$ $d_2 = 0.189269$
$c_2 = 0.010328$ $d_3 = 0.001308$

$|\varepsilon(r)| < 4.5 \times 10^{-4}$

for $r > 0.5$

$$x(r) = -x(1 - r) \quad (14).$$

3.3.6 Comparison with Oracle-Crystal Ball Results

A consistent series of cases for various coolant outlet temperatures was run with the Oracle Crystal Ball approach [28] and with the Stat code. Fig. 3.3-4 shows the results. For an outlet temperature of 60°C, the results are almost identical, indicating that both approaches are equivalent.

Note that, for this comparison only, the uncertainty on local power was 10% (3-sigma). The slight difference in slopes in Fig. 3.3-4 is probably due to differences in the treatment of the temperature dependence of water properties where Stat calculates temperature-dependent water properties using the axial node temperatures for each history.

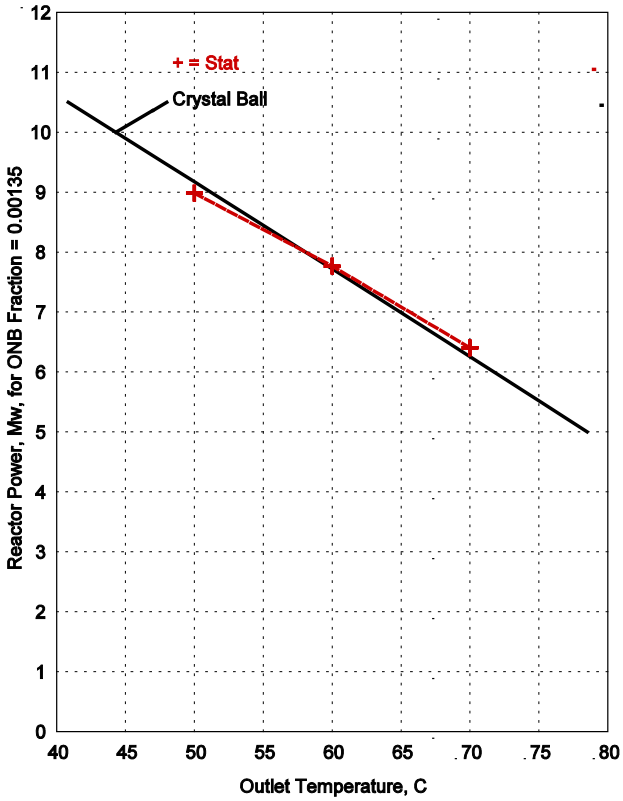

Figure 8. Comparison of Stat and Oracle-Crystal Ball Results.

There are three advantages to the Stat code over the Oracle-Crystal Ball approach. The first advantage is that setting up the Stat input and running the code is much simpler and less time consuming. Oracle-Crystal Ball requires hand iteration to obtain a consistent solution. All iteration in Stat is done internally by the code. Another advantage is that the Stat code can be easily expanded and integrated into a 3-D fuel management program. The third advantage is computing speed. The Stat calculations for one outlet temperature for 250,000 histories and ONB tests at all 18 axial nodes run in seconds. The Oracle-Crystal Ball computer time is substantially longer because it is a general purpose software with a spreadsheet interface.

3.3.7 The Stat7 Code

The Stat7 code is an expansion of the Stat6 code to treat N_{ch} coolant channels and $N_{pl} = N_{ch} + 1$ plates. This code can model one stripe of all of the plates and coolant channels in an element, from end channel through the internal channels to the other end channel. When modeling an element containing N_{fp} fuel plates there are $N_{fp} - 1$ internal channels and 2 end channels. Also, an extra plate is added before the first end channel and another after the last end channel to account for whatever is beyond the end channels. If the end channel butts up against the end channel of an adjacent element, then the extra plate can model half of the end fuel plate of the adjacent element, with a zero heat flux boundary condition at the middle of the plate. If the end channel butts up against an unheated side plate of an adjacent element or against an unheated structural wall, then the only impact of the extra

plate is to contribute to the wetted perimeter used in computing the hydraulic diameter of the end channel.

3.3.7.1 Power Splits

When calculating steady-state temperatures for a series of plates separated by coolant channels, zero heat flux boundary conditions at the centers of the plates cannot be assumed. Instead, a power split, f_{ps}, must be calculated for each axial node of each plate. The power split for a plate surface is defined as the ratio of the heat flux from the surface to the sum of the heat fluxes from both surfaces. The approach taken in Stat7 for calculating power splits involves assuming that the plate power density is uniform across the thickness of the fuel. Then a zero heat flux boundary condition occurs a fraction f_{ps} of the way across the thickness of the fuel. The value of the flow split is set so that the peak fuel temperature calculated starting from the bulk coolant temperature on one side of the plate equals the peak fuel temperature calculated starting from the other side. For the extra plates at the ends, the power split is assumed to be 0.5 at all axial nodes.

3.3.7.2 Comparison of Stat7 Results with RELAP5 Results

For verification of the Stat7 thermal hydraulic calculations, a comparison was made of the results from a Stat7 case and from a RELAP5 case that was set up to be equivalent to the Stat7 case. One stripe of an 18 fuel plate element with fins was modeled in both codes. The fins are 8 mils high, 10 mils wide and 10 mils apart, giving a surface area of 1.8 times as high as a no-fins case. Stat7 uses a Carnavos film heat transfer fin factor of 0.75 for this case. RELAP5 does not have a fin treatment, but fin heat transfer effects were accounted for by multiplying the plate surface area by 1.8 x 0.75 = 1.35. In order to obtain the correct temperatures in the plates, the clad and fuel thermal conductivities used in RELAP5 were divided by 1.35.

Stat7 calculates steady-state coolant flow rates and temperatures. RELAP5 does not have a steady-state solver, so the RELAP5 case was run as a null transient with powers, total element flow, and the coolant inlet temperature held constant at the Stat7 values for 300 seconds. The RELAP5 transient results settled down to steady-state values well before 300 seconds.

Figure 9 shows the coolant mass flow rates by channel. For this case the end channels both had the same gap size, and all interior channels had a second same gap size. The small differences between the Stat7 results and the RELAP5 results are probably mainly due to the change in water viscosity with temperature: an effect that is not included in the Stat7 calculation.

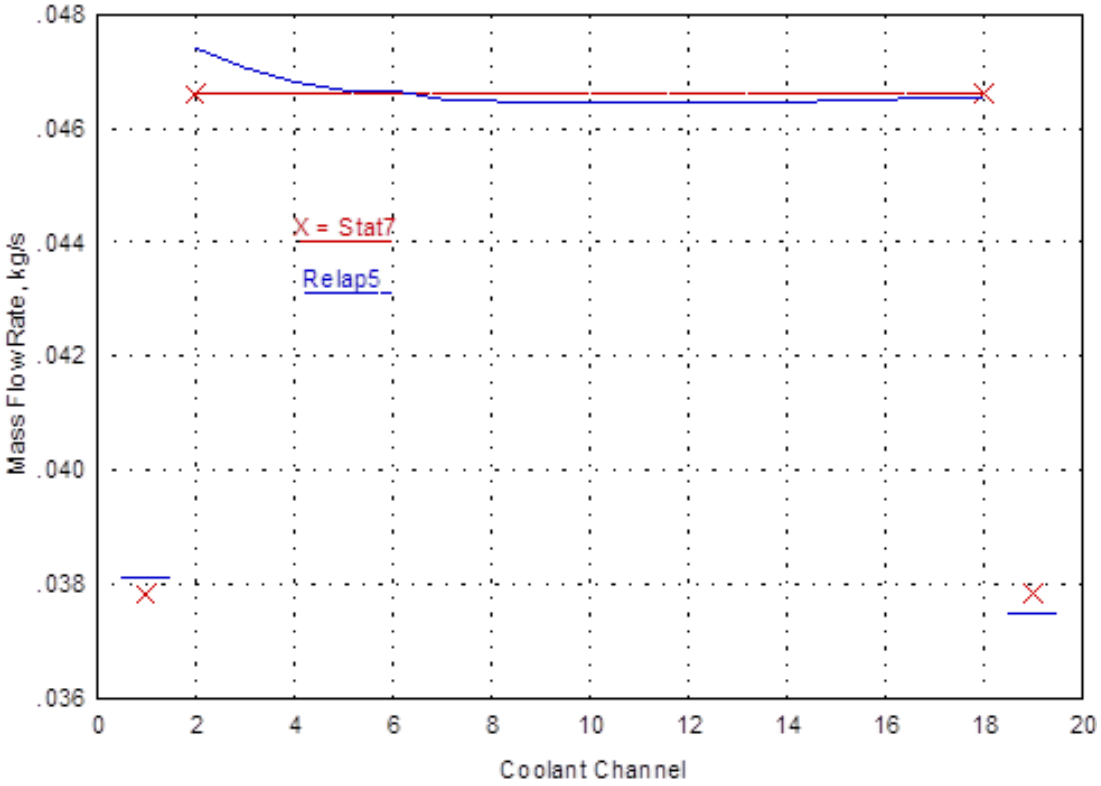

Figure 9. Comparison of Stat7 and RELAP5 End Channel and Interior Channel Flow Rates.

Figure 10 shows the coolant temperatures for the end channel and for the first two interior channels. One slight complication is that RELAP5 prints axial node coolant temperatures at the outlet (upper boundary) of the node and uses these node boundary coolant temperatures in the calculations for the axial node plate temperatures. Stat7 uses coolant temperatures at the middle of the axial node in the calculations for the axial node plate temperatures. The Stat7 temperatures in Figure 10 are mid-node temperatures and are plotted at the middles of the nodes. The RELAP5 temperatures in this figure are node boundary values plotted at the node boundaries. Thus the coolant temperatures in Figure 10 are plotted consistently. On the other hand, the axial node plate temperatures calculated by RELAP5 are based on node boundary coolant temperatures but node average heat fluxes. In the following figures for plate temperatures, the axial node plate temperatures for both Stat7 and RELAP5 are plotted at the middle of the node. For RELAP5, the film temperature rise, based on the node-average heat flux, is larger than the bulk coolant temperature rise in half of an axial node.

Figure 11 and Figure 12 show the comparisons for the clad surface temperatures and the peak fuel temperatures. Figure 13 shows the comparisons for the plate power splits at each axial node.

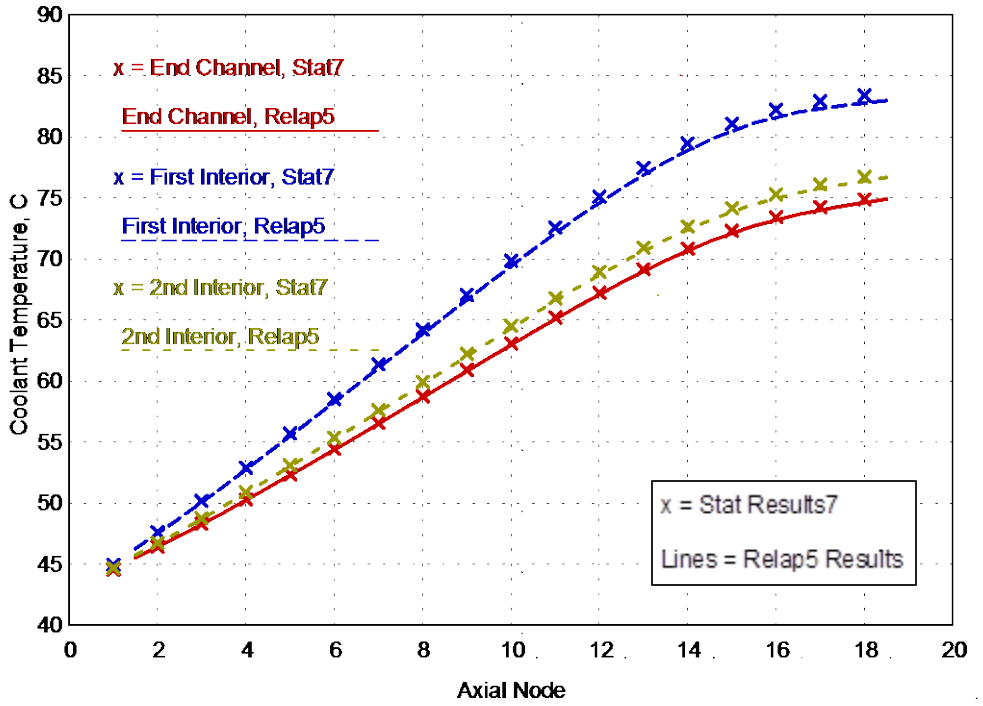

Figure 10. Comparison Between Stat7 and RELAP5 Coolant Temperatures for an End Channel and the First Two Interior Channel.

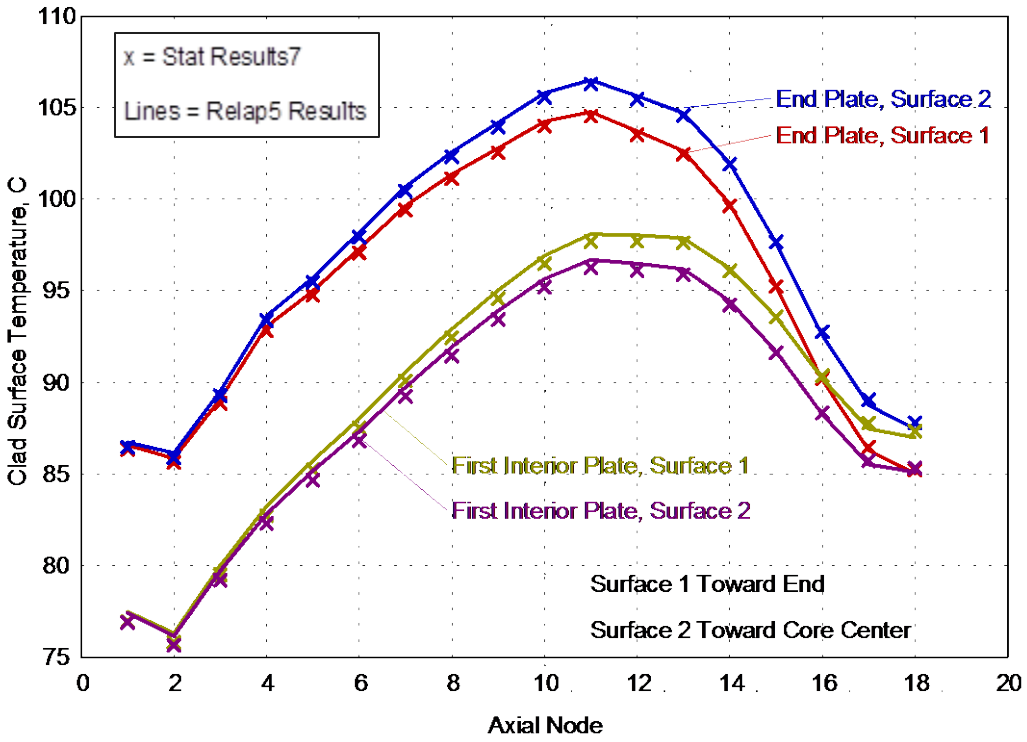

Figure 11. Comparison Between Stat7 and RELAP5 Clad Surface Temperatures for an End Plate and the First Interior Plate.

The comparisons between Stat7 results and RELAP5 results show, for this family of channels verified, that the thermal hydraulic calculations in Stat7 have been implemented correctly. Also, the method used to account for fins in RELAP5 is consistent with the Carnavos treatment in Stat7. Also, the comparisons in Section 3.3.5 between Stat6 and Oracle-Crystal Ball results show that the statistical methods are equivalent. Stat7 is a key tool that in this work has been used for optimization of the new fuel element design.

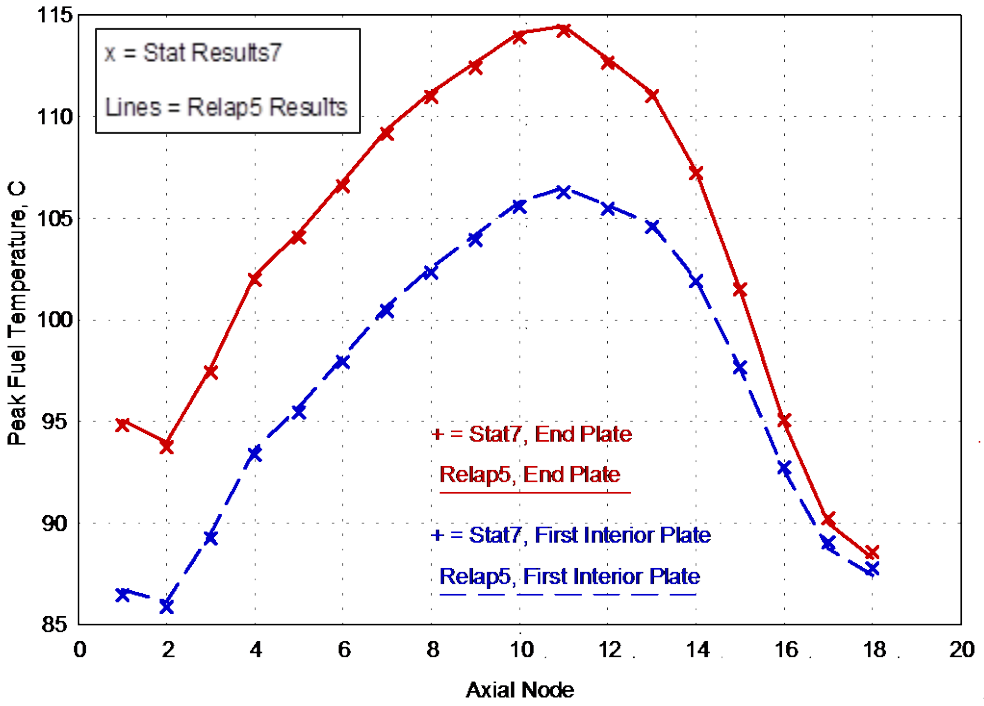

Figure 12. Comparison Between Stat7 and RELAP5 Peak Fuel Temperatures for an End Plate and the first Interior Plate.

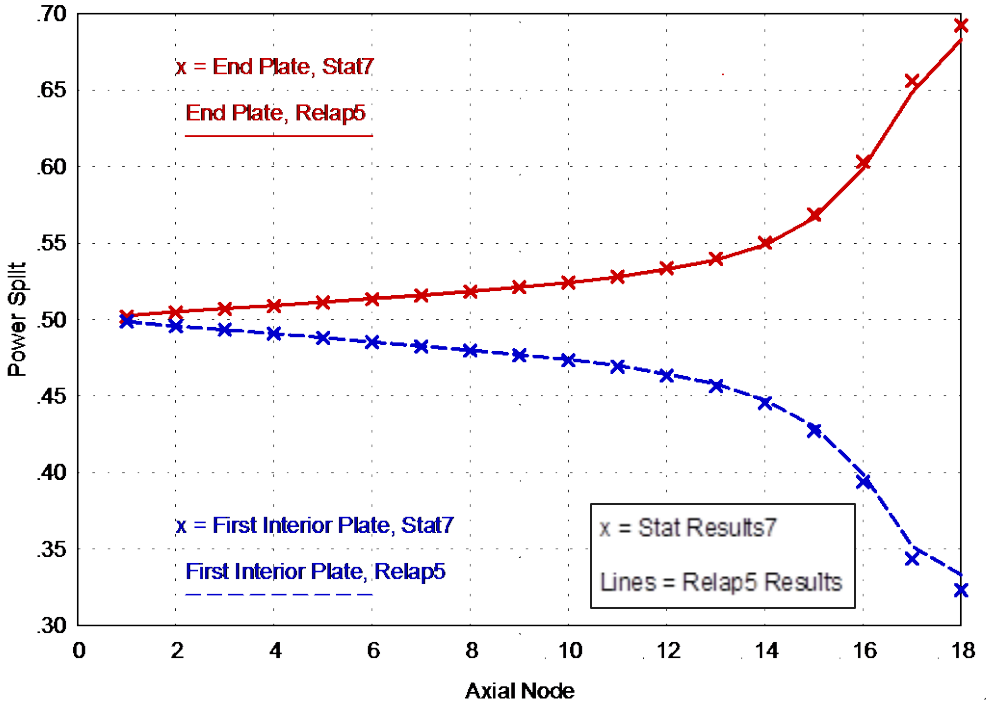

Figure 13. Comparison Between Stat7 and RELAP5 for Power Splits in an End Plate and the First Interior Plate.

3.3.8 Determination of LSSS

In summary, the Limiting Safety System Settings (LSSS) are based on Onset of Nucleate Boiling (ONB) in the core. Uncertainties are accounted for in the analysis by using Monte Carlo uncertainty propagation of the parameters influencing ONB, as discussed above. The requirement is that the measured total reactor power should have at least 20% margin to the power at which the ONB (P_{ONB}) is found to occur with a 3-sigma confidence level of 99.865%. The margin between HEU licensed power and LSSS power is 20%, and so this should be maintained in the LEU case in order to provide an equivalent margin [14,29].

Using a 3-sigma confidence level of 99.865%, the probability of ONB occurring in the most limiting element is 0.135% at P_{ONB}. As is the case in the HEU core, it is proposed that the total core reactor power, P_r, should have an additional 20% margin to the ONB power, P_{ONB}, such that $P_r = P_{ONB} / 1.2$. All channels of an element are analyzed, including end channels. Each element is analyzed in this manner so that a whole core analysis may identify the most limiting locations for each core configuration considered. It should be noted that margin to Critical Heat Flux (CHF) or Onset of Flow Instability (OFI) are not treated in these analyses. A large margin to CHF has been previously demonstrated for MITR and is not anticipated to be limiting; however, both CHF and OFI will be analyzed in detail in subsequent safety analysis [14].

4 LEU ELEMENT DESIGN WITH FRESH CORES

This section describes the different design modifications that have been considered to develop an acceptable alternative LEU design without fins on the cladding. The section starts by presenting the characteristics of the reference LEU design (with fins) and then re-evaluates these parameters using the same fuel element configuration without the fins. In this portion of the LEU element design, modifications to the design have been made considering a fresh core since calculations are based on a single core configuration before proceeding to calculations which include fuel management as found in Section 5.

4.1 Evaluation of the Reference LEU Design

The reference LEU design, and all other fresh core design candidates, considered in this section contains 22 fresh LEU UMo monolithic elements, four dummy elements (positions A-2, B-3, B-6 and B-9) and one experimental non-fueled element (position A-3) as shown in Figure 1. The light water circulating through the core is set at 46^{o}C. The heavy water reflector is modeled at a temperature of 54^{o}C. While the heavy water temperature modeled matches normal operation of the HEU core, the light water temperature of the LEU core may slightly differ due to several parameters. The mixed mean core coolant temperature has been previously used to represent the reactor [3]. This mean temperature depends on the reactor power, inlet temperature, and coolant flow rate. Since reactor power and core coolant flow rate are design variables in this study, and the inlet temperature may be varied in later design analysis, the fixed temperature of 46^{o}C is considered representative and will require final determination during future plant and safety analysis which will include the core coolant flow rate. However, given the expected 7 MW operating power, flow rates assumed in this study up to 2200 gpm, and inlet temperatures anticipated to be at, or lower than, the current 44^{o}C inlet temperature, the light water temperatures modeled should compare reasonably within a few degrees Celsius. These assumptions provide the required level of accuracy in order to make determinations regarding element design selections. In these assumed conditions, the reference LEU design critical blade position is 22.78cm (8.97inch) withdrawn.

4.1.1 Performance

The neutron flux was evaluated in the five reference locations described in Section 3.1.1. At 6 MW, the neutron flux drops by 8% to almost 13%, depending upon the location, compared to the HEU core operating in the same conditions (fuel location, temperature and power). The detailed results are presented in Table 5, with statistical uncertainty at 1-σ <2%. The LEU power (this applies only to the fresh core of this design) needs to be increased to 6.9 MW to match the HEU 6 MW core neutron flux performance everywhere. The reference power for the LEU core is therefore chosen to be 7 MW, which is the same value used in previous analyses.

Table 5. Neutron Flux Performance of the Reference LEU Core.

	Experimental facility				
	In-Core Irradiation (A2)	**Twelve-inch Beam Port**	**Two-inch Pneumatic Facility**	**Fission Converter Window**	**Below-core Thermal Beam Facility**
Energy	>0.1 MeV	<0.4 eV	<0.4 eV	<0.4 eV	<0.4 eV
LEU 6 MW flux / HEU 6 MW flux (%)	92%	89%	87%	89%	89%
LEU power equivalent to HEU 6 MW performance (MW)	6.5	6.8	6.9	6.8	6.7

4.1.2 Shutdown Margins

The shutdown margins obtained with this reference configuration are given in Table 6. The maximum uncertainty associated does not exceed 0.05% Δk/k within one standard deviation. These margins are evaluated with the reactor in a cold state (10^{o}C) with 5 blades fully inserted and one of the 6 blades and the regulating rod fully withdrawn. The margins remain relatively close in the six cases considered (3.05 to 3.20%). The limiting blade is the one that yields the smallest shutdown margin. It is seen from Table 6 that blade 2 is the limiting blade. For every case, the margins are well above the 1% Δk/k requirement.

Table 6. Shutdown Margins for Reference LEU Configuration.

	Blade fully withdrawn (with regulating rod fully withdrawn)					
	#1	#2	#3	#4	#5	#6
Δk/k (%)	3.15	3.05	3.20	3.15	3.20	3.10

4.1.3 Power Distribution and ONB Margins

Local power distributions were calculated using MCNP tallies. The power distributions calculated with 3D detail, resolved to each axial segment of each stripe, of each fuel plate loaded in the core. Minimum ONB Margin of each core configuration was then calculated by the Stat7 code, statistically sampling the effects of uncertainties and tolerances in addition to the local power detail.

Peak spot and peak stripe heat flux values are reported in Table 7. The maximum tally uncertainty associated with local power tallies is below 1% within one standard deviation. The location is designated as EvPwSxAxySUz (with v the element number; w the plate number; x the stripe number; y the axial node number; z the plate surface, if it applies). In this report, the fuel has been divided in 18 axial nodes. Axial node 1 represents the bottom of the fuel, and axial node 18 the top of the fuel. The axial sequence used in this report is consistent with the sequential direction of flow in the channel. The surface number indicates in which channel P_{ONB} occurs. Surface number is 1 if it refers to the channel before the plate and 2 if it refers to the channel after the plate. For instance, surface 1 of plate 1 refers to the end channel and surface 2 refers to the channel located between plate 1 and 2. The location presented in Table 4 matches that given previously except for the axial location [6]. The slight variation is expected due to control blade position change. In this report the fresh core differed from the prior reference

element analysis only in the presence of an ICSA, and the coolant temperature assumed as discussed earlier in Section 4.1. These peak locations are, in general, a good indication of where the limiting ONB spot will occur. For nominal dimensions (before accounting for uncertainties) the stripe with the maximum stripe power will be the most limiting. However, once the hot channel factors are included the most limiting spot may shift to another location. It has been observed that the most limiting location with respect to ONB is ordinarily just above (i.e., down-stream from) the location of peak power in the stripe.

The Limiting Safety System Settings (LSSS) are based on Onset of Nucleate Boiling (ONB) in the core as discussed in Section 3. The evaluation of the margin to ONB has been carried out for all nodes in the core as described in Section 3. For the reference LEU configuration, the minimum ONB power is found to be 9.71 MW with a 3-sigma confidence level of 99.865% at 1800 gallons per minute (gpm) core flow rate and otherwise using uncertainties detailed in Appendix A. It occurs in location E27P1S1Ax8SU1 which is in the end channel of element C15 (element 27), in the stripe and plate where the peak heat flux spot occurs. The ONB Margin for the all-fresh core of reference LEU elements is 39% (i.e., 9.71 MW / 7.0 MW).

Table 7. Peak Heat Flux Values for Reference LEU Configuration.

CORE PEAKS	Peak spot	Peak stripe
Heat flux (W/cm^2)	87.6	55.5
Peak/Core average	2.98	1.89
Location	E27P1S1Ax5	E27P1S1

4.1.4 Rundown Core Lifetime

A depletion calculation has been carried out with the reference LEU configuration but with 24 fresh LEU elements instead of 22 as used previously. The 2 dummy elements are located in positions A-1 and B-3, and one experimental non-fueled element (ICSA) is located in A-3. For depletions, 24 elements are more representative of typical loading of the MITR variable core configuration. These calculations are referred to as 'rundown' calculations since there are no fuel management operations to re-position fuel or load fresh fuel. The control blades are withdrawn, and the reactor is depleted until subcritical. These depletion calculations have been carried out at a constant power of 7 MW. Figure 14 shows k-effective as a function of time. As can be seen in Figure 14, the rundown core lifetime for this configuration is about 320 days (the time for the excess reactivity to be zero).

This core lifetime is not believed to be representative of the real fuel consumption during a fuel management irradiation for a core containing fuel at a variety of burnups. Nonetheless, it provides a good indication of how well the core will perform. It has previously been shown that the reference LEU design provides sufficient core lifetime in a given reference fuel management scheme [6]. In the remainder of Section 4 discussion of design modifications, the rundown core lifetime will be used as an indicator of how well the reactor could perform. Representative performance will be evaluated in cores operated under a selected fuel management scheme in Section 5. Core lifetime of design candidates is gauged, prior to fuel management calculations, against the reference LEU design which was calculated with a 1-σ uncertainty estimated at ± 5 days.

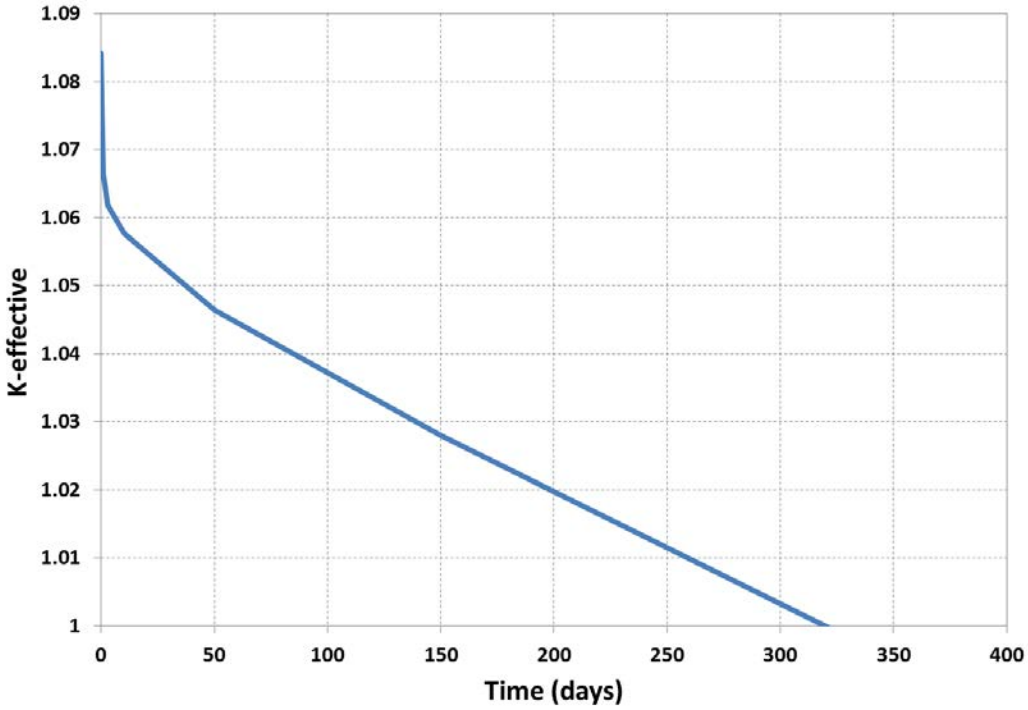

Figure 14. K-effective During Irradiation at 7 MW of 24 Fresh LEU Elements Using the Reference LEU Configuration.

4.2 Removing the Fins of the Reference Design

The relevant parameters of the reference LEU design have been established in the previous section. In this section, the configuration used is the same as the reference one but the cladding has no fins. The neutronic model is identical since the fins were not explicitly modeled but homogenized (cladding thickness of 15 mil) and the cladding thickness of the model without fins is also 15 mil.

Since in this case the neutronic models are identical, all neutronic related parameters such as performance (neutron flux and core lifetime) shutdown margins and power distribution are unchanged. However, margin to ONB (and other thermal-hydraulic margins) will be impacted by the change since the cooling surface area is reduced by removal of the fins.

4.2.1 Power Distribution and Margin to ONB

Removing the fins decreases the heat transfer surface area, which in return increases the fuel and clad temperatures. To illustrate this point, the axial cladding temperature profile of element C-15, plate 1, stripe 1 obtained at 8 MW with the configuration with and without fins is presented in Figure 15 for an example case with otherwise identical but randomly sampled uncertainties. Recall that the power distribution used to calculate the temperature is identical. As one can see the temperature increase due to removal of the fins is significant since it leads, at this power, to an increase of about 30^{o}C in the hottest region. Consequently the limiting ONB power decreases substantially as shown in Table 8. The new limiting power of 5.01 MW is well below the LSSS requirement of 8.4MW. The location is on the same stripe of the same plate, but it is shifted by one axial node.

Table 8. Limiting ONB power and Corresponding Location for Reference Configuration with and without Fins.

	Limiting ONB power	Location
Reference LEU with fins (MW)	9.71	E27P1S1Ax8SU1
Reference LEU no-fins (15 mil clad) (MW)	5.01	E27P1S1Ax7SU1
Variation no-fins / fins (%)	-48.4%	

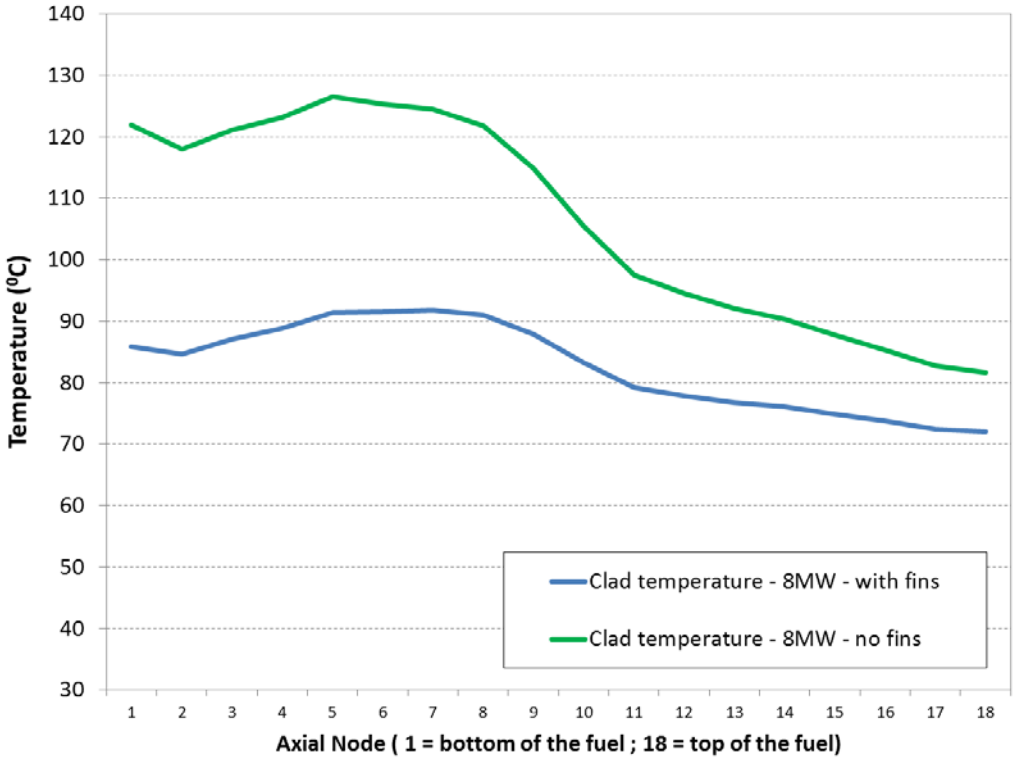

Figure 15. Axial Cladding Temperature Profile in Element C15, Plate 1, Stripe 1 for Reference LEU Configuration With and Without Fins at 8MW.

4.3 Design Parameters Used to Increase ONB Margin

From the previous analyses, as expected, removing the fins from the reference LEU design leads to a significant reduction of the ONB margin. The following section presents the different solutions that have been considered to increase the ONB margin to an acceptable level.

4.3.1 Increased End Channel Dimension

The minimum margin to ONB occurs in the reference design in the end channel adjacent to the first plate. Accordingly the influence on the ONB margin of the end channel size relative to the others has been investigated. The ratio of the end channel gap thickness dimension to the interior channel dimension has been explored, and is hereafter referred to as the end channel ratio (ECR). By increasing the ECR, the interior channel gap thickness decreases. This leads to a redistribution of the flow and an increase in the coolant velocity in the end channels. By having more coolant circulating through the end channels and at higher speed, the end plates are expected to be cooled more efficiently, increasing the margin to ONB by making that location less limiting.

In the reference LEU configuration the ECR is 67.7%. In this work, the ECR has been varied over a substantial range. The limiting ONB power versus the ECR for the reference LEU design is presented in Figure 16. As expected, the ONB limiting power increases with the increase of ECR. As can be seen however, the improvement is relatively limited: about 10% with an ECR of 90%. Consequently, modifying the ECR cannot be the only design modification considered. In the following sections, the ECR has been set at 88% which leads to an increase of 10% in the limiting ONB power. No significant impact on the other parameters (neutron flux, core lifetime, shutdown margins) has been observed by changing the ECR to 88%.

Due to the uncertainties in the fabrication of the end channels, tolerances may be substantial as discussed in Section 2.2 of Reference [6]. It is advantageous for fabrication, as well as for safety margin, to have an element which is not limited by the end channel. This ECR value is considered reasonable pending results presented in Section 5 for cores incorporating fuel management of depleted fuel. This and other changes analyzed in Sections 4.3 and 4.4 are made so that each design feature is added cumulatively as changes to the reference LEU design in order to determine the incremental benefit to the element performance.

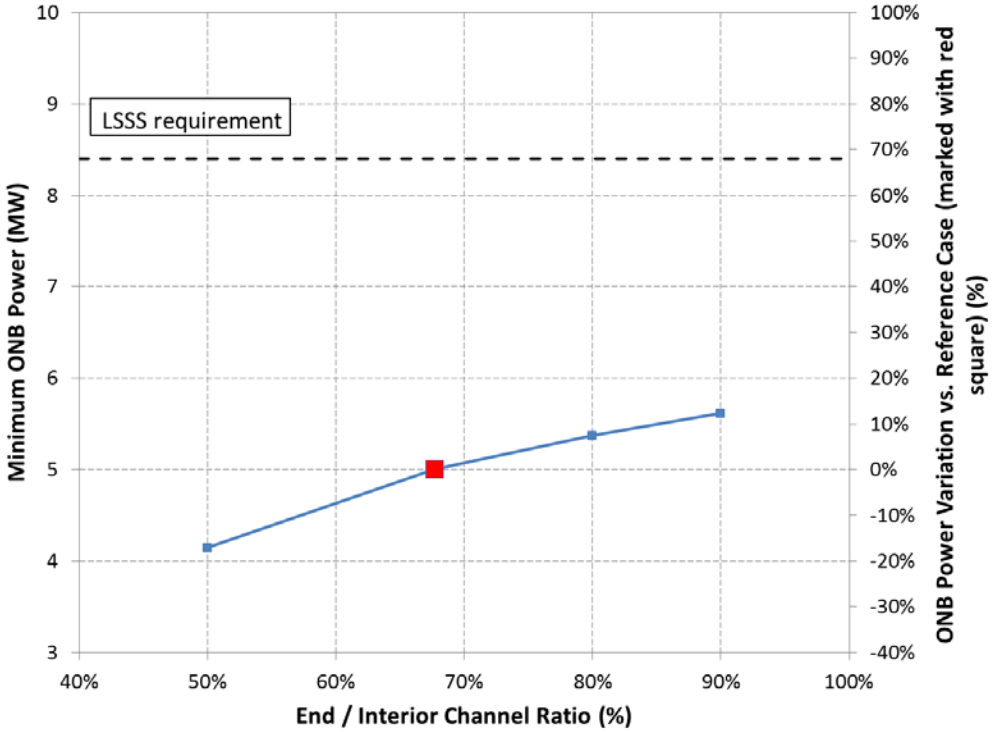

Figure 16. Limiting ONB Power vs. End Channel Ratio.

4.3.2 Increased Core Coolant Flow Rate

The HEU core currently has an LSSS primary coolant flow rate of 1800 gallons per minute (gpm) circulating through the core [14]. The nominal flow rate through the HEU core is 2000 gpm which corresponds to roughly a 2 m/s average channel velocity. If the flow rate could be increased substantially, consideration to designs with significant economic advantages could be pursued (e.g. elements with significantly fewer plates). The reactor facility has had limited experience with higher flow rates through the core during zero power testing with a fueled core. In 2010, many of the secondary cooling components and pipes were upgraded or replaced. Hence, pre-operational tests were conducted at flow rates up to 2400 gpm for short durations without observing any unusual effects, and the current pumps installed are rated up to a combined 2400 gpm.

Significantly higher flow rates than this, however may be unattainable, because some sections of primary piping have an inner diameter as small as 7.25 inch in locations that would present significant difficulty to retrofit. The performance of piping of this diameter would further require evaluation if significantly higher flows than 2400-2600 gpm were utilized. For this reason, and since the secondary system is designed to reject heat with a similar temperature rise across the core, flow rates higher than the capacity of the current pumps have not been considered in this report.

The minimum ONB power, P_{ONB}, for the core versus the flow rate has been calculated using an ECR of 88%. Results are shown in Figure 17. The limiting ONB power increases nearly linearly with the flow as expected. A flow rate increase of 25% (from 1800 to 2250 gpm) leads to an increase of almost 25% (from 5.5MW to 6.8MW) in the limiting power. Though this increase in margin is significant, it is still insufficient to satisfy the LSSS requirement (8.4MW for an operating power of 7 MW). An assumption that the core can maintain LSSS core flow rates of 2200 gpm is made through the remainder of this report. Evaluation of the required and feasible flow should continue in future conversion activities.

As noted in Section 4.1, flow rate impacts the coolant temperature rise across the core. Since the core average coolant temperature varies only slightly across the range of designs, no changes in the neutronic model regarding temperature have been made in this or later cases examined. As an example, in the cases shown in Figure 7, the impact of the core flow rate change on reactivity is expected to be at most a modest 0.06% Δk/k.

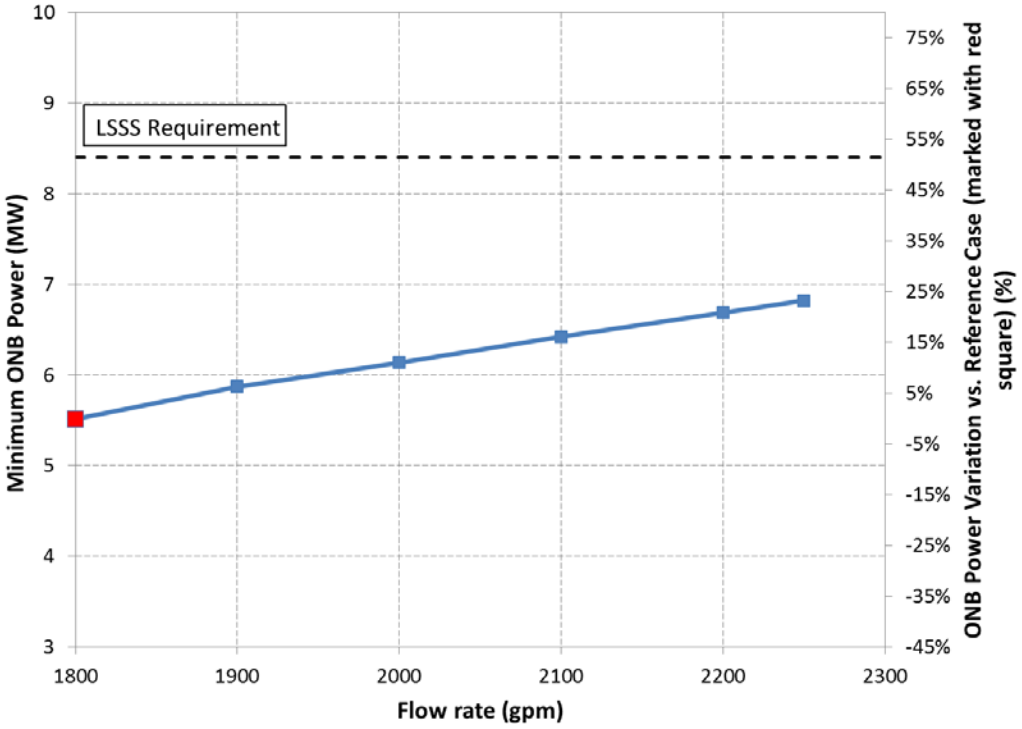

Figure 17. Limiting ONB Power Versus Flow Rate through the Core (reference LEU configuration without fins and ECR of 88%).

4.3.3 Increasing the Number of Plates

The impact of a change in the number of fuel plates has been explored. At a given power and flow rate, the increase in plate number would reduce the amount of heat per unit surface and also increase the coolant velocity through the core leading to better heat removal and increased margin to ONB. Figure 8 presents the minimum ONB power, P_{ONB}, vs. the number of plates for a 2200 gpm flow rate and elements with 88% ECR, 15 mil cladding, no fins, and matching the reference LEU design in other respects. The number of plates has been varied from 17 to 20 due to expected limitations in hydraulic margin for cases with fewer plates, and due to low fuel lifetime with additional plates displacing moderator. The evolution of the limiting ONB power with the number of plates has been analyzed using a volumetric flow rate of 2200gpm and ECR of 88%. Results are presented in Figure 18. As one can see, increasing the number of plates has a limited impact on the ONB margin not exceeding 5% for a 20-plate configuration.

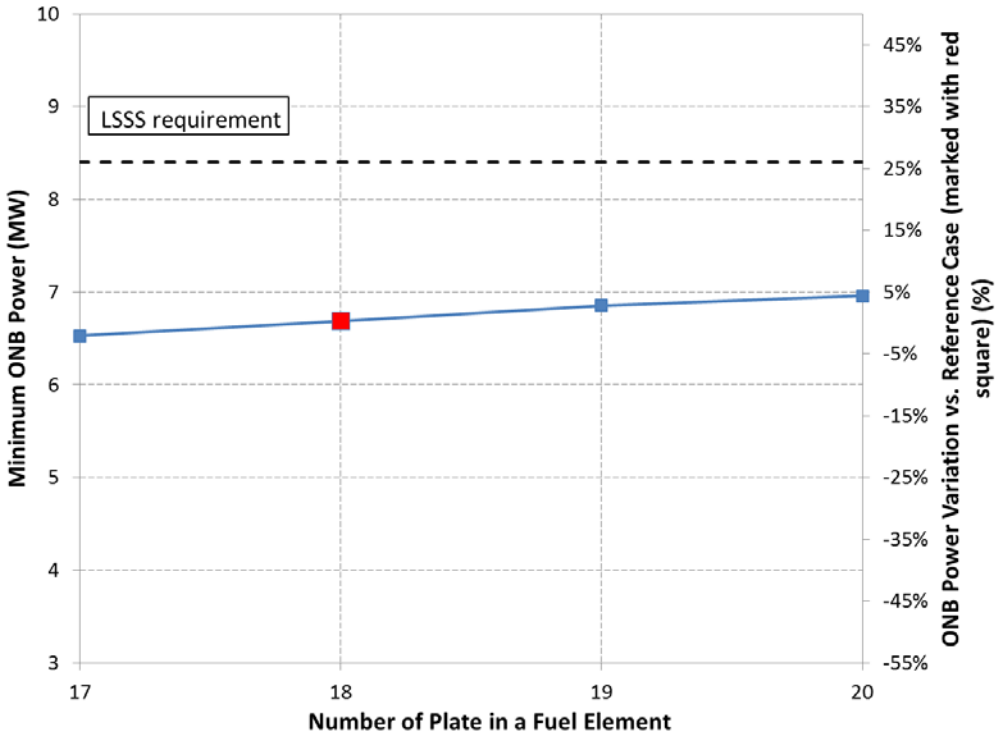

Figure 18. Limiting ONB Power vs. the Number of Plates (The scale on the right axis indicates the change in percent compared to the initial value marked in red on the graph).

4.3.4 Reducing the Meat Thickness of the Outer Plates

Since the limiting ONB power occurs on the edges of the element, the impact of a meat thickness reduction in the outer plates, on both sides, of the element has been considered. The ONB power can be increased by reducing power of the outer plates of the element which have been limiting in both fresh and depleted core designs analyzed previously [6, 8]. Although the concept of flattening power profiles has been used throughout reactor design, implementing this into a core conversion is challenging due to the combination of competing effects. Although thinner plates aid in reducing power peaking, they also degrade fuel lifetime. Since MITR loads into 3 radial rings and can rotate elements, plates on both sides of the element must be thinned, which lowers fuel loading throughout the reactor in addition to the plates immediately adjacent to the reflector. Additionally, the degree to which plates should be thinned cannot be predicted a priori without implementing representative fuel management capable of analyzing the power distributions found in depleted cores.

Since this is a problem requiring optimization with multiple constraints, and results require complex fuel management calculations, four combinations of meat reduction have been tested. In each case, the fuel thickness of 3 or 4 plates on each side of the element is reduced. For reasons of economy of fabrication it has been assumed as a constraint that there would be three distinct fuel foil thicknesses, and no more, in each element design. The thickness of all the plates is however kept constant. In other words, if a plate has a reduced meat thickness, the cladding thickness increases accordingly in order to end up with the same plate thickness as the others. The selected combinations are presented in Table 9.

Table 9. Selected Combination of Meat Thickness Reduction.

Combination	Fraction of nominal meat thickness (%)			
	1st plates	2nd plates	3rd plates	4th plates
A	45	60	60	100
B	55	70	70	100
C	50	50	70	70
D	60	60	80	80

In this section, the selected meat reduction combinations have been tested with an element containing 18 plates, 15 mil cladding, no fins, ECR of 88%, matching the reference LEU design in other respects, and for a core flow of 2200 gpm.

The selected combinations decrease the edge power significantly as illustrated in Figure 19 to Figure 23. Figure 19 shows the axial heat flux profile obtained in element C-15, plate 1, stripe 1 for the reference configuration as well as for the four combinations tested. Maximum heat flux uncertainty is below 1% within one standard deviation. It is clear that the magnitude of the maximum heat flux decreases significantly with the meat thickness reduction (from 25 to 35%, depending on the combination considered).

Figure 20 through Figure 23 show the heat flux profile by plate in element C-15, stripe 1, at the axial node 12 for the reference configuration as well as for combinations A, B, C and D. This location has been selected because it has been found to be limiting in previous analyses. The plots also show the corresponding fuel thickness which is read on the right axis. These plots show clearly the power decrease on the edges and the power migration to the interior plates. Combination A has reduced the outer plate fuel thickness sufficiently to have the maximum power peak in the interior, full thickness, plates. However, the limiting plates are still observed to be in the thinned outer plates for combinations B, C, and D. The most appropriate level of thinning will need to be determined in concert with other factors such as core lifetime and ONB power for depleted cores operated over many cycles with representative fuel management.

The corresponding limiting ONB power obtained considering a flow rate of 2200 gpm and ECR of 88% are given in Table 10, where uncertainty on cycle length is estimated at ± 5 days. The four meat thickness reduction combinations give margin to ONB higher than the required 20% which show the effectiveness of the edge meat reduction on improving core safety margins.

The core lifetime is however expected to decrease due to the significant decrease in uranium mass with the outer meat reduction. Core lifetime calculations for the 4 meat reduction combinations have been carried out at 7 MW with 24 elements (same fuel location as described in section 4.2). Results are presented in Figure 24. As expected the core lifetime drops substantially (from 25% to 40% depending on the combination considered). The core lifetimes of these designs are considered too short to be acceptable.

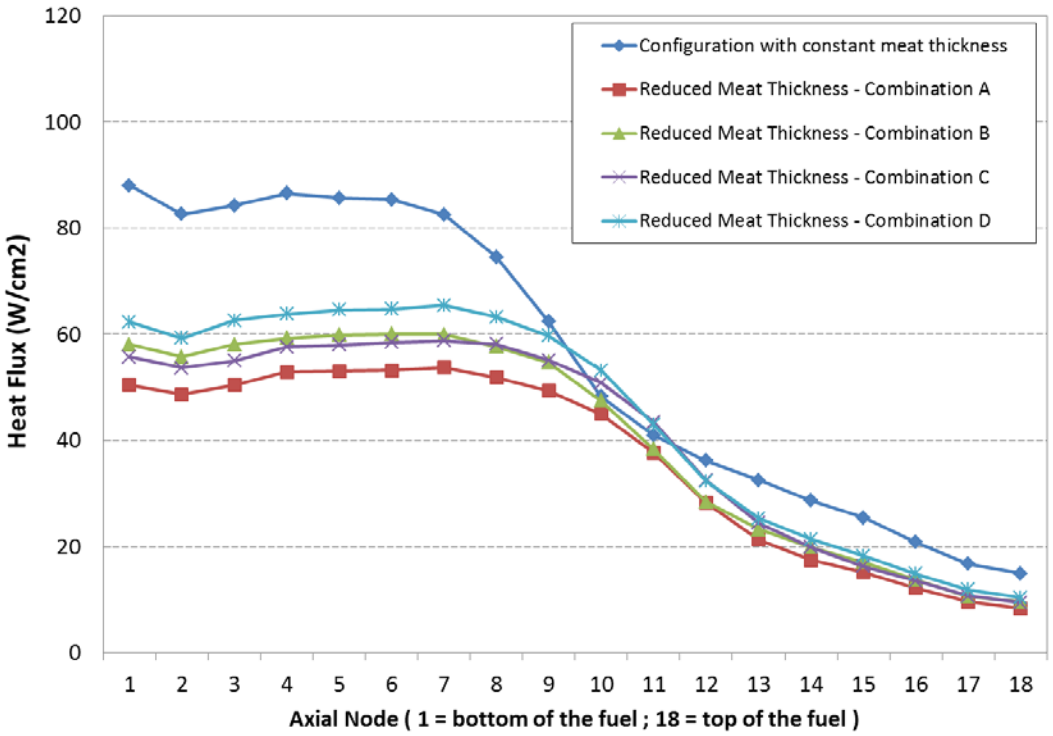

Figure 19. Axial Heat Flux Profile in Element C15, Plate 1, Stripe 1 for 7 MW 18-plates LEU Configuration with Nominal Meat Thickness as well as for the Different Combinations of Meat Reduction.

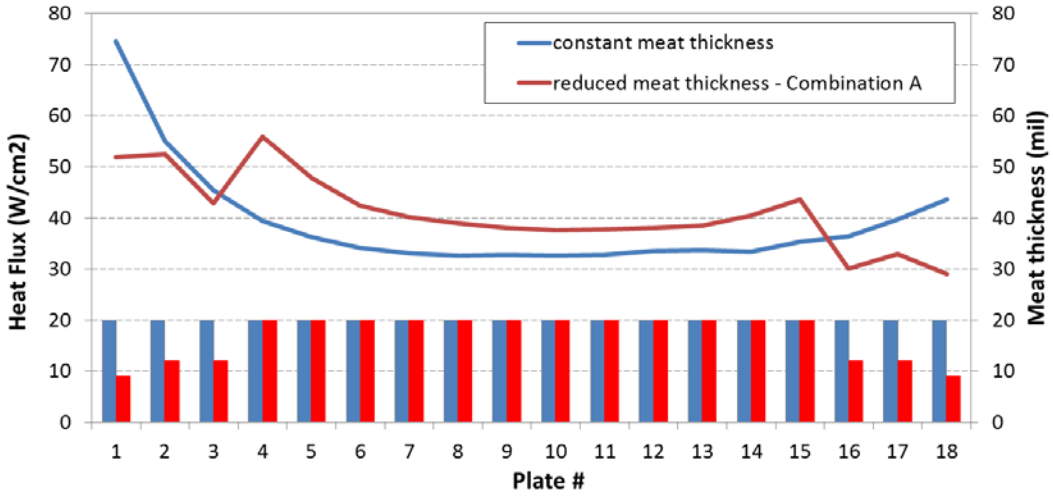

Figure 20. Heat Flux Profile through the Plate in Element 27, Stripe 1, Axial Node 12 for Configuration with Constant Meat Thickness and Reduced Meat Thickness as in Combination A.

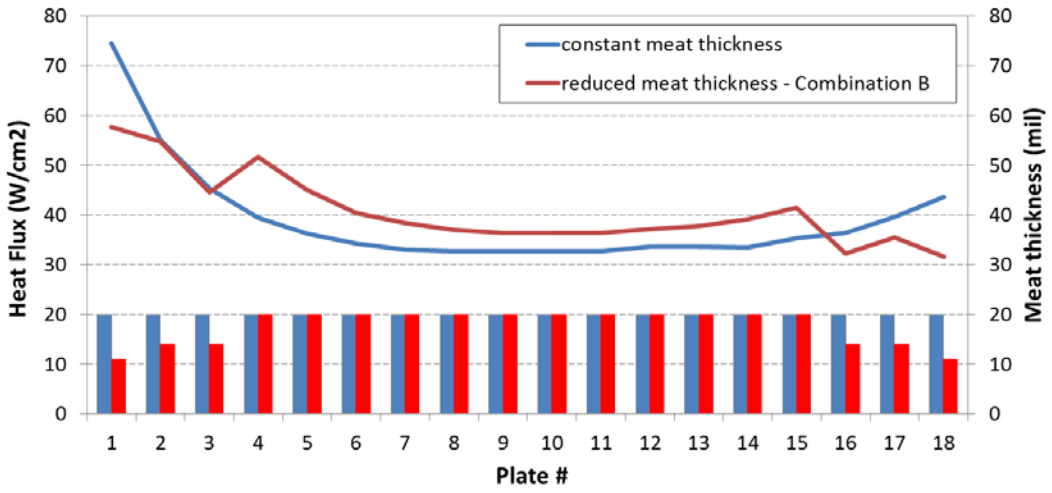

Figure 21. Heat Flux Profile through the Plate in Element 27, Stripe 1, Axial Node 12 for Configuration with Constant Meat Thickness and Reduced Meat Thickness as in Combination B.

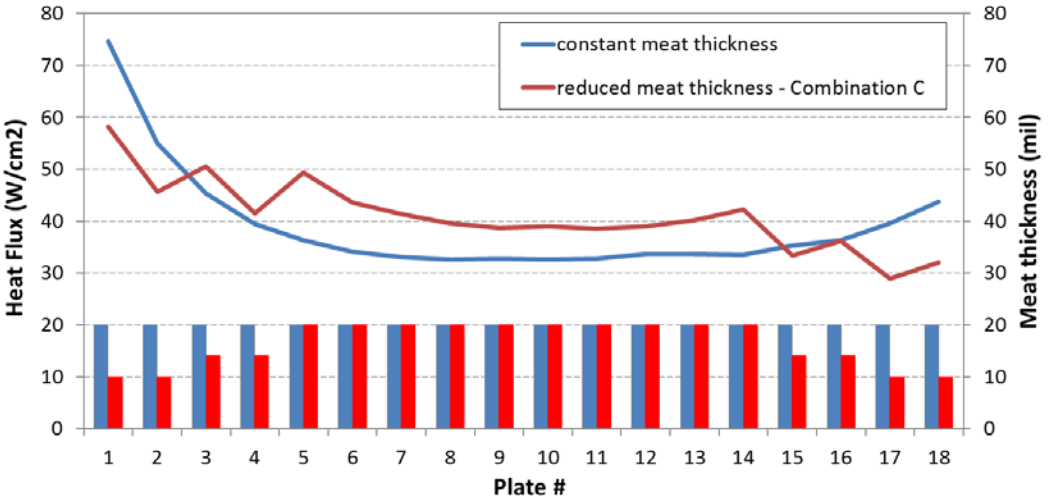

Figure 22. Heat Flux Profile through the Plate in Element 27, Stripe 1, Axial Node 12 for Configuration with Constant Meat Thickness and Reduced Meat Thickness as in Combination C.

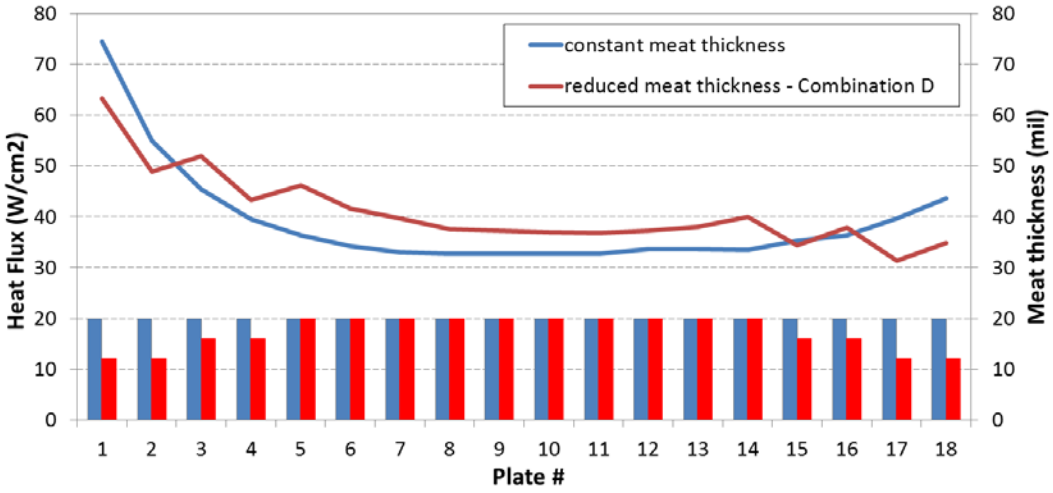

Figure 23. Heat Flux Profile through the Plate in Element 27, Stripe 1, Axial Node 12 for Configuration with Constant Meat Thickness and Reduced Meat Thickness as in Combination D.

Table 10. Limiting ONB Power for the Four Reduced Meat Combinations with a Flow Rate of 2200 gpm.

Configuration	Limiting ONB power (MW)	Location
LEU reference design except no fins, and ECR 88%	6.8	E27S1P1Ax8SU1
A	9.6	E13S4P15Ax9SU1
B	9.7	E27S1P1Ax8SU1
C	9.8	E14S4P14Ax9SU1
D	8.9	E27S1P1Ax8SU1

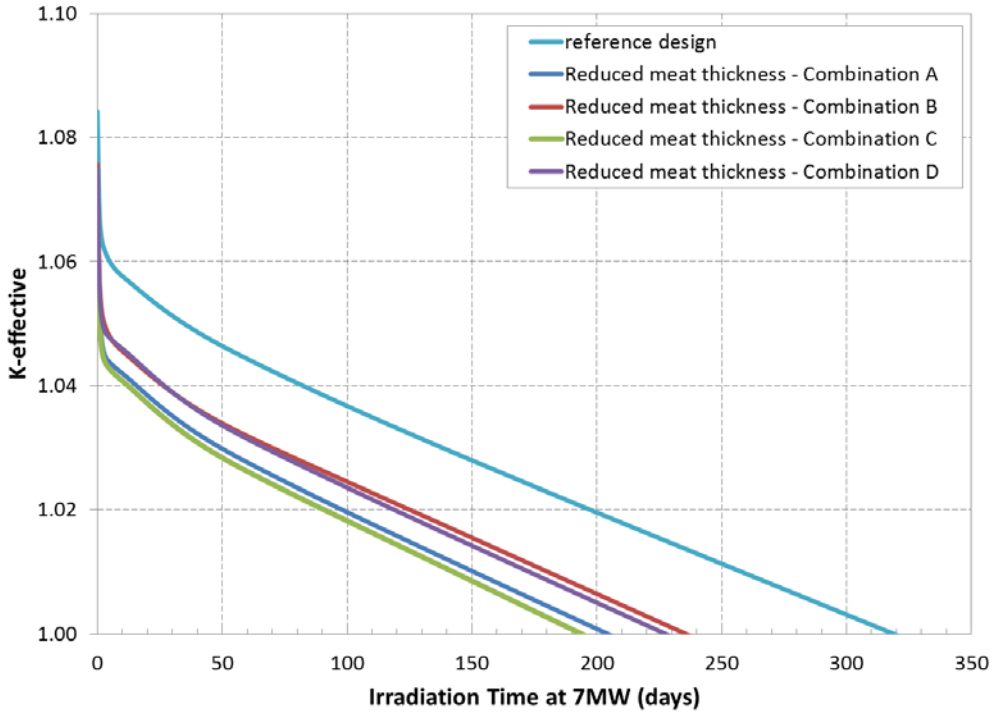

Figure 24. K-effective vs. Irradiation Time through Depletion at 7 MW.

4.4 Increase in Cycle Length

In the previous section, different solutions have been explored to increase the margin to ONB of the LEU design without fins. The most efficient solution consists in a reduction of the meat thickness in the outer fuel plates of the element. While the distinct meat thicknesses provide acceptable margin to ONB, the approach significantly penalizes the core lifetime. The following section describes the solutions that have been considered to increase the core lifetime of the reduced thickness fuel meat designs.

4.4.1 Decrease in Cladding Thickness

Decreasing the cladding thickness will have the effect to increase the volume of water in the core which may increase the reactivity, if the coolant to heavy metal ratio becomes more favorable, and increase the cycle length. However there is a trade-off since, at a given flow rate, the coolant velocity would decrease, leading to a decrease of ONB margin.

Four reduced meat thickness configurations have been tested with a nominal clad thickness reduced from 15 mil to 12 mil. Core lifetime and limiting ONB power are compared to the 15 mil clad configurations in Table 11, where acceptable configurations in terms of core lifetime and limiting ONB power at 2200 gpm are highlighted in green. The favorable impact of the clad reduction on the core lifetime is significant since it leads to a lifetime increase of 30% to more than 60%, depending on the configuration considered. Two of the four configurations tested have core lifetime slightly exceeding that of the reference configuration. The impact on the ONB margin is a decrease of 0.6% - 14 % depending on the configuration. As a result the 18 plate LEU configurations without fins, an ECR of 88%, a flow of 2200 gpm and a meat thickness reduction as described with combination B or D (the two combinations with lower thinning fraction) gives acceptable performance and acceptable margin to

ONB. Although the 15 mil cladding was shown to have unacceptably poor lifetime, the designs with 12 mil cladding can be further considered.

Table 11. Core lifetime and limiting ONB Power obtained with the four reduced meat configurations considering a nominal clad thickness of 12 mil and a flow rate of 2200 gpm.

Combination	15 mil cladding		12 mil cladding		Variation 12/15 mil cladding	
	Core lifetime (days)	Limiting ONB power (MW)	Core lifetime (days)	Limiting ONB power (MW)	Core lifetime (%)	Limiting ONB power (%)
A	230	9.6	300	8.29	+30.4%	-13.6%
B	235	9.7	330	8.77	+40.4%	-9.6%
C	195	9.8	285	8.77	+46.2%	-10.5%
D	205	8.9	330	8.95	+61.0%	+0.6%

4.4.2 Increase the Meat Thickness

The effect of a meat thickness increase has also been explored. Additional uranium mass could increase the core lifetime but at the same time reduce the core coolant/meat ratio. Consequently the reactivity of the core would decrease, which would reduce the core lifetime. But at a given coolant mass flow rate, that would also increase the coolant velocity and increase the ONB margin.

In order to find an optimal solution design options are considered here with nominal meat thickness increased from 20 to 30 mil in increments of 5 mil. The nominal cladding thickness is 12 mil. The results are given in

Table 12 where acceptable configurations in terms of core lifetime and limiting ONB power at 2200 gpm are highlighted in green. The meat thickness increase tends to increase the core lifetime by about 6% to 12% depending on the configuration considered. There is also no clear advantage to increase the fuel thickness from 25 to 30 mil. However, the limiting ONB powers do not present a single pattern for all combinations. Using the reduced meat combination A, the margin to ONB increases as meat thickness is increased. For combination B and C, the margin to ONB increases slightly using a 25 mil thickness, and decreases at 30 mil. Combination D shows that an increase in meat thickness would lead to a drop in ONB margin. It is concluded that 8 of the 12 configurations have acceptable core lifetimes and margins to ONB, before consideration of the effects of fuel management as described in Section 5.

Table 12. Impact of the Meat Thickness Increase on the Core Lifetime and Limiting ONB power for the four 18 Plates Meat Reduced Configuration Using a Nominal Clad Thickness of 12 mil and a Flow Rate of 2200 gpm.

Combination	Nominal meat thickness (mil)	Core lifetime (days)	Limiting ONB power (MW)	Variation from 20mil configuration	
				core lifetime (%)	limiting ONB power (%)
A	20	300	8.29	-	-
	25	330	8.92	+10.0%	+7.6%
	30	330	9.54	+10.0%	+15.1%
B	20	330	8.77	-	-
	25	360	9.12	+9.1%	+4.0%
	30	360	8.45	+9.1%	-3.6%
C	20	285	8.77	-	-
	25	320	9.18	+12.3%	+4.7%
	30	315	8.64	+10.5%	-1.5%
D	20	330	8.95	-	-
	25	350	8.33	+6.1%	-6.9%
	30	355	7.95	+7.6%	-11.2%

4.5 Seeking the Best Combinations of Design Modifications

Whereas only fresh cores without fuel management have been analyzed for performance (or rundown lifetime), the performance of the selected designs under representative depleted cores must also be considered. Fresh cores have been used to select more promising core design options in the analyses presented to this point. However, a final range of all-fresh core designs are presented in order to allow a down-selection of designs which will undergo representative fuel management and performance analysis. The intent is to show that at every relevant cycle, the core lifetime, neutron flux performance and margin to ONB requirements are met. The evolution of these parameters during a shuffling scheme is difficult to predict since the core loading will vary at each cycle, mixing elements with various depletions with a few fresh elements. This is why an appropriate down-selection to the most promising design requires fuel management analyses. In order to increase the likelihood of finding the best combination of performance and design, the previous analyses regarding the calculation of core lifetime and limiting ONB power have been expanded to configurations with 17 to 19 fuel plates and flow rates in the range of 1800 gpm to 2200 gpm, by increments of 100 gpm.

Table 13 through Table 17 present the results obtained with flow rates of 2200, 2100, 2000, 1900 and 1800 gpm, respectively. Acceptable configurations (having adequate core lifetimes and adequate margins to ONB) are highlighted in green on these tables. At 2200 gpm, acceptable configurations are obtained with 17, 18 and 19 plates. The fewer the number of plates, the higher is the core lifetime but the lower is the margin to ONB. Element designs with 18 plates have the highest number of acceptable configurations. They are the best compromise for core lifetime and ONB margin. However by decreasing the mass flow rate, the margin to ONB drops substantially while, of course, the lifetime remains unchanged. Thus at flow rates between 1900 and 2100 gpm, the best designs are seen to be elements with 19 plates. At 1800 gpm (existing nominal mass flow rate used in the reactor), only one configuration has both an acceptable core lifetime and acceptable ONB margin (prior to evaluation under representative fuel management).

For the fuel shuffling and burnup calculations, eleven configurations were selected for performance and safety, while also retaining a variety of number of plates and fuel thicknesses. For the selection, two tiers have been defined. The first tier takes configurations that have at least 30% margin to ONB as well as a rundown core lifetime of at least 310 days. The second tier takes from the remaining configurations the ones that have at least 25% margin to ONB and rundown core lifetime of at least 330 days. A summary of the characteristics of the selected design are given in Table 18. These configurations have been analyzed under representative fuel management as described in Section 5 where fuel meat thicknesses have modeled as an integer (in mils), and configuration specific uncertainties used in the Stat7 analyses are described in Appendix A.

Table 13. Core Lifetime and Limiting ONB Power for Reduced Meat Configurations at a Flow Rate of 2200 gpm.

Plate	Meat reduction Combination	Nominal meat thickness (mil)	Power to match HEU 6 MW performance (MW)	Required LSSS limiting power (MW)	Core lifetime (days)	Limiting ONB power (MW)
17	A	20	7.2	8.6	310	7.59
		25	7.0	8.4	355	7.98
		30	6.9	8.3	360	8.78
	B	20	7.3	8.7	335	8.00
		25	7.1	8.5	380	8.56
		30	6.9	8.3	395	8.23
	C	20	7.1	8.5	290	7.76
		25	7.0	8.4	330	8.35
		30	6.9	8.2	340	8.26
	D	20	7.2	8.7	320	8.16
		25	7.1	8.5	360	8.07
		30	6.9	8.3	380	7.60
18	A	20	7.0	8.4	300	8.29
		25	6.9	8.3	330	8.92
		30	6.8	8.2	330	9.54
	B	20	7.1	8.5	330	8.77
		25	6.9	8.3	360	9.12
		30	6.8	8.2	360	8.45
	C	20	7.0	8.4	285	8.77
		25	6.9	8.3	320	9.18
		30	6.8	8.2	315	8.64
	D	20	7.1	8.5	330	8.95
		25	6.9	8.3	350	8.33
		30	6.8	8.2	355	7.95
19	A	20	6.9	8.3	290	9.31
		25	6.8	8.2	310	9.98
		30	6.8	8.1	300	10.05
	B	20	6.9	8.3	325	9.76
		25	6.8	8.2	345	9.28
		30	6.8	8.1	325	8.84
	C	20	6.9	8.3	280	9.48
		25	6.8	8.2	305	9.62
		30	6.8	8.1	285	9.12
	D	20	6.9	8.3	315	9.32
		25	6.8	8.2	330	8.63
		30	6.8	8.1	320	8.20

Table 14. Core Lifetime and Limiting ONB Power for Reduced Meat Configurations at a Flow Rate of 2100 gpm.

Plate	Meat reduction Combination	Nominal meat thickness (mil)	Power to match HEU 6 MW performance (MW)	Required LSSS limiting power (MW)	Core lifetime (days)	Limiting ONB power (MW)
17	A	20	7.2	8.6	310	7.29
		25	7.0	8.4	355	7.67
		30	6.9	8.3	360	8.42
	B	20	7.3	8.7	335	7.68
		25	7.1	8.5	380	8.22
		30	6.9	8.3	395	7.92
	C	20	7.1	8.5	290	7.48
		25	7.0	8.4	330	8.02
		30	6.9	8.2	340	7.95
	D	20	7.2	8.7	320	7.87
		25	7.1	8.5	360	7.76
		30	6.9	8.3	380	7.31
18	A	20	7.0	8.4	300	7.97
		25	6.9	8.3	330	8.56
		30	6.8	8.2	330	9.17
	B	20	7.1	8.5	330	8.43
		25	6.9	8.3	360	8.76
		30	6.8	8.2	360	8.12
	C	20	7.0	8.4	285	8.42
		25	6.9	8.3	320	8.82
		30	6.8	8.2	315	8.29
	D	20	7.1	8.5	330	8.59
		25	6.9	8.3	350	8.00
		30	6.8	8.2	355	7.64
19	A	20	6.9	8.3	290	8.94
		25	6.8	8.2	310	9.57
		30	6.8	8.1	300	9.66
	B	20	6.9	8.3	325	9.35
		25	6.8	8.2	345	8.92
		30	6.8	8.1	325	8.49
	C	20	6.9	8.3	280	9.09
		25	6.8	8.2	305	9.24
		30	6.8	8.1	285	8.75
	D	20	6.9	8.3	315	8.95
		25	6.8	8.2	330	8.30
		30	6.8	8.1	320	7.87

Table 15. Core Lifetime and Limiting ONB Power for Reduced Meat Configurations at a Flow Rate of 2000 gpm.

Plate	Meat reduction Combination	Nominal meat thickness (mil)	Power to match HEU 6 MW performance (MW)	Required LSSS limiting power (MW)	Core lifetime (days)	Limiting ONB power (MW)
17	A	20	7.2	8.6	310	7.00
		25	7.0	8.4	355	7.35
		30	6.9	8.3	360	8.07
	B	20	7.3	8.7	335	7.36
		25	7.1	8.5	380	7.88
		30	6.9	8.3	395	7.60
	C	20	7.1	8.5	290	7.15
		25	7.0	8.4	330	7.69
		30	6.9	8.2	340	7.62
	D	20	7.2	8.7	320	7.54
		25	7.1	8.5	360	7.44
		30	6.9	8.3	380	7.00
18	A	20	7.0	8.4	300	7.63
		25	6.9	8.3	330	8.20
		30	6.8	8.2	330	8.79
	B	20	7.1	8.5	330	8.08
		25	6.9	8.3	360	8.39
		30	6.8	8.2	360	7.78
	C	20	7.0	8.4	285	8.07
		25	6.9	8.3	320	8.45
		30	6.8	8.2	315	7.96
	D	20	7.1	8.5	330	8.25
		25	6.9	8.3	350	7.68
		30	6.8	8.2	355	7.31
19	A	20	6.9	8.3	290	8.57
		25	6.8	8.2	310	9.17
		30	6.8	8.1	300	9.25
	B	20	6.9	8.3	325	8.96
		25	6.8	8.2	345	8.55
		30	6.8	8.1	325	8.14
	C	20	6.9	8.3	280	8.73
		25	6.8	8.2	305	8.85
		30	6.8	8.1	285	8.38
	D	20	6.9	8.3	315	8.58
		25	6.8	8.2	330	7.95
		30	6.8	8.1	320	7.54

Table 16. Core Lifetime and Limiting ONB Power for Reduced Meat Configurations at a Flow Rate of 1900 gpm.

Plate	Meat reduction Combination	Nominal meat thickness (mil)	Power to match HEU 6 MW performance (MW)	Required LSSS limiting power (MW)	Core lifetime (days)	Limiting ONB power (MW)
17	A	20	7.2	8.6	310	6.70
		25	7.0	8.4	355	7.03
		30	6.9	8.3	360	7.72
	B	20	7.3	8.7	335	7.05
		25	7.1	8.5	380	7.53
		30	6.9	8.3	395	7.27
	C	20	7.1	8.5	290	6.84
		25	7.0	8.4	330	7.35
		30	6.9	8.2	340	7.29
	D	20	7.2	8.7	320	7.20
		25	7.1	8.5	360	7.13
		30	6.9	8.3	380	6.71
18	A	20	7.0	8.4	300	7.30
		25	6.9	8.3	330	7.85
		30	6.8	8.2	330	8.40
	B	20	7.1	8.5	330	7.73
		25	6.9	8.3	360	8.03
		30	6.8	8.2	360	7.44
	C	20	7.0	8.4	285	7.72
		25	6.9	8.3	320	8.10
		30	6.8	8.2	315	7.61
	D	20	7.1	8.5	330	7.91
		25	6.9	8.3	350	7.35
		30	6.8	8.2	355	7.00
19	A	20	6.9	8.3	290	8.19
		25	6.8	8.2	310	8.78
		30	6.8	8.1	300	8.83
	B	20	6.9	8.3	325	8.58
		25	6.8	8.2	345	8.18
		30	6.8	8.1	325	7.77
	C	20	6.9	8.3	280	8.33
		25	6.8	8.2	305	8.48
		30	6.8	8.1	285	8.02
	D	20	6.9	8.3	315	8.22
		25	6.8	8.2	330	7.60
		30	6.8	8.1	320	7.22

Table 17. Core Lifetime and Limiting ONB Power for Reduced Meat Configurations at a Flow Rate of 1800 gpm.

Plate	Meat reduction Combination	Nominal meat thickness (mil)	Power to match HEU 6 MW performance (MW)	Required LSSS limiting power (MW)	Core lifetime (days)	Limiting ONB power (MW)
17	A	20	7.2	8.6	310	6.35
		25	7.0	8.4	355	6.66
		30	6.9	8.3	360	7.31
	B	20	7.3	8.7	335	6.68
		25	7.1	8.5	380	7.13
		30	6.9	8.3	395	6.90
	C	20	7.1	8.5	290	6.48
		25	7.0	8.4	330	6.96
		30	6.9	8.2	340	6.91
	D	20	7.2	8.7	320	6.82
		25	7.1	8.5	360	6.77
		30	6.9	8.3	380	6.36
18	A	20	7.0	8.4	300	6.92
		25	6.9	8.3	330	7.43
		30	6.8	8.2	330	7.96
	B	20	7.1	8.5	330	7.32
		25	6.9	8.3	360	7.62
		30	6.8	8.2	360	7.04
	C	20	7.0	8.4	285	7.31
		25	6.9	8.3	320	7.67
		30	6.8	8.2	315	7.21
	D	20	7.1	8.5	330	7.49
		25	6.9	8.3	350	6.96
		30	6.8	8.2	355	6.63
19	A	20	6.9	8.3	290	7.75
		25	6.8	8.2	310	8.30
		30	6.8	8.1	300	8.36
	B	20	6.9	8.3	325	8.11
		25	6.8	8.2	345	7.73
		30	6.8	8.1	325	7.35
	C	20	6.9	8.3	280	7.89
		25	6.8	8.2	305	8.04
		30	6.8	8.1	285	7.59
	D	20	6.9	8.3	315	7.78
		25	6.8	8.2	330	7.20
		30	6.8	8.1	320	6.83

Table 18. Characteristics of the Eleven LEU Element Design Configurations Selected for Fuel Management Calculations.

Element Design	# of plates	Nominal fuel meat thickness (mil)	Plate thickness (mil)	1st plate on both ends	2nd plate on both ends	3rd plate on both ends	4th plate on both ends	^{235}U mass per element (g)	Power to match HEU BOC 6 MW performance (MW)	Required LSSS limiting power (MW)	Limiting ONB power at 2200 gpm (MW)	Margin to ONB at 2200 gpm (%)	Core lifetime 24 fresh elements (days)	Minimum shutdown margins (%)
19A25	19	25	49	11	15	15	25	940	6.8	8.2	9.98	46%	330	3.7
19B20	19	20	44	11	14	14	20	781	6.9	8.3	9.76	41%	325	2.5
18A30	18	30	54	13	18	18	30	1,058	6.8	8.2	9.54	40%	330	4.0
19B25	19	25	49	13	17	17	25	968	6.8	8.2	9.28	36%	345	3.4
19D20	19	20	44	12	12	16	16	767	6.9	8.3	9.32	34%	315	2.4
18C25	18	25	49	12	12	17	17	845	6.9	8.3	9.18	33%	320	3.0
18B25	18	25	49	13	17	17	25	910	6.9	8.3	9.12	32%	360	2.4
19B30	19	30	54	16	21	21	30	1,169	6.8	8.2	8.84	31%	325	4.6
18A25	18	25	49	11	15	15	25	882	6.9	8.3	8.92	29%	330	2.7
18D20	18	20	44	12	12	16	16	721	7.1	8.5	8.95	27%	330	1.7
17A30	17	30	54	13	18	18	30	988	6.9	8.3	8.78	27%	360	3.0

5 ELEMENT DESIGN RESULTS WITH FUEL MANAGEMENT

For the eleven configurations selected in the previous section, LEU depleted cores were generated using fuel management representative of MITR. As discussed in Section 3.2, burnup modeling using the ORIGEN2-MCNP coupling code MCODE has been used to compare parameters of recent core configurations using the actual operating history and refueling movements of twelve HEU MITR core configurations in the period 2007-2009 in order to benchmark and validate the model [3,6].

Due to the number of cores between 1976 and the present, elements entering the fuel cycle were generated by depleting a fresh core to 3 effective full power years, and inserting elements with matching element average burnup into the historical twelve core sequence. MITR HEU cores on average operated with control blades considerably (70%) withdrawn. For this reason, and since elements may be flipped, the initialization depletion, without fuel movements, was modeled without control blades inserted. This however only approximates the element burnup shape entering the twelve core loadings modeled until the elements are depleted in the specific locations used during fuel management.

For depletion, each fuel element was discretized into independent depleting regions as listed in Table 19, where power distribution regions were further subdivided into locations as small as 4 cm2, as shown in an example with 18 plates. Regions were equally distributed (such as the plate division into 4 lateral stripes, each 56.8 cm axially and 1.3 cm laterally). Each of the 24 elements in the depleted cores modeled individual plates discretely in the geometry without homogenization.

Table 19. Discretization of the LEU depletion zones and power regions to used generate representative depleted cores.

Regions	Geometry	Depletion	Power Shape
Plate Division	Each plate discrete	Each plate individual	Each plate individual
Fuel Axial Division	Continuous	6	18
Fuel Lateral Division	Continuous	1	4
Per LEU Core	-	864	31104

LEU depleted cores analogous to HEU historical cores 179-190 were generated in this same manner for each of the 11 designs considered with fuel management. Also generated were depleted cores with the reference LEU design for comparison, and as a verification of consistency with prior calculations. Depleted elements for the 11 designs were generated so that the ^{235}U mass burnup matched the reference LEU design element burnup at the introduction into the fuel management cycle. Determination of the exact fuel cycle utilization is beyond the scope of this work; however, so long as the control blades are stable the fuel cycle should perform at least as well as the reference LEU design. Fuel management was performed according to the records presented in Table 20 consistent with the work performed previously [6]. The operational history was modeled from the 179 BOC, and all fuel operations were enabled including flipping of fuel (rotating end-to-end in place) and rotating in place by 180°. There are a total of 57 fuel elements. Some of them are fresh and the others are partially depleted, coming from storage.

Table 20. Fuel Management of New and Depleted Elements.

Core	178	179	180	181	182	183	184	185	186	187	188	189	190
Location	5/4/07	7/17/07	10/13/07	1/5/08	3/8/08	5/23/08	6/4/08	7/25/08	9/23/08	12/17/08	2/7/09	3/13/09	5/28/09
A1	Non-fuel solid dummy element with cooling hole												
A2	MIT-323					MIT-339f						MIT-345	
A3	Non-fuel solid dummy element with cooling hole												
B1	MIT-335				MIT-344 new							MIT-354 new	
B2	MIT-338					MIT-331				MIT-351 new			
B3	Non-fuel solid dummy element with cooling hole												
B4	MIT-336	MIT-341 new						MIT-347 new				MIT-355 new	
B5	MIT-339				MIT-345 new					MIT-352 new			
B6	MIT-331	MIT-342 new						MIT-348 new					
B7	MIT-337				MIT-346 new							MIT-356 new	
B8	MIT-340					MIT-336f				MIT-353 new			
B9	MIT-334	MIT-343 new						MIT-349 new					
C1	MIT-302			MIT-325(C14)f						MIT-325r	MIT-299(C15)		MIT-299r
C2	MIT-303	MIT-303r	MIT-288(C2)		MIT-282fr	MIT-282r			MIT-326f				
C3	MIT-300	MIT-300r	MIT-319(A2)					MIT-301f			MIT-290(C8)		
C4	MIT-305			MIT-332(B2)	MIT-303fr			MIT-303r	MIT-340f				
C5	MIT-282	MIT-281(C2)			MIT-304(C6)f	MIT-304r			MIT-307(C14)				MIT-341f
C6	MIT-279			MIT-330(B4)	MIT-295(C11)			MIT-306f			MIT-306r	MIT-297(C7)	MIT-342f
C7	MIT-324			MIT-305		MIT-305r	MIT-334f						
C8	MIT-306				MIT-306r			MIT-295f			MIT-323		
C9	MIT-318		MIT-326(B5)		MIT-288fr	MIT-288r	MIT-324f			MIT-324r			
C10	MIT-322		MIT-292(C1)f			MIT-292r			MIT-294(C10)			MIT-330fr	
C11	MIT-301					MIT-333(B6)f							MIT-333r
C12	MIT-285			MIT-300			MIT-293(C9)f			MIT-332f	MIT-332r		
C13	MIT-327									MIT-317(A2)	MIT-317f		
C14	MIT-328				MIT-328r			MIT-328r		MIT-338f			
C15	MIT-329					MIT-337						MIT-335	
# of fuel moves	22 to begin model	4	4	5	8	5	3	6	4	6	4	7	2

Notes: "f " indicated element is flipped before insertion
"r" indicated element is rotated before insertion
"( )" indicates core location element occupied prior to storage

5.1 Critical Control Blade Position of Depleted Cores

Among the 36 designs presented in Section 4.5, a 0.5 MW range of power for performance equivalent to HEU was predicted based upon all-fresh core neutron flux levels. However, for the 11 design configurations selected as most promising for fuel management, the power for performance equivalent to HEU was 6.8-7.1 MW, depending on the design. Results presented later in Section 5.4 discuss performance with fuel management and confirm that the selected 7 MW depletion power level is adequate. Note that for fresh cores without fuel management, depletion calculations were performed at the specific power required to achieve beginning of life equivalent neutron flux performance, as described in Section 4.5.

Currently MITR operates with quarterly refueling each year and so the goal was to maintain that capability. The MCODE depletion was performed with MCNP5 generated flux and reaction rates at BOC, 1, 3, 10, 40, and 47 days during each cycle. An exception was LEU core 182 which was ended at 35 days. As discussed in Reference [6], this is consistent with HEU core 182, which had limited excess reactivity, and preceded core 183 which had a significantly shorter operating time than the other HEU cores. So long as cores maintain sufficient reactivity with this fuel cycle, quarterly refueling will remain achievable with the new element designs.

For the reference LEU design, and 9 of the 11 element designs, the reactivity of the cores throughout the cycle was sufficient so that the control blades remained lower than the fully withdrawn position of 21 inch (53.34 cm). Designs 18C25 and 19B20 however were significantly less than critical during the course of the depletion even with a fully withdrawn control blade position and so failed to complete the fuel management sequence. These two configurations had insufficient reactivity to maintain a fuel cycle equivalent or better than the reference LEU design, and so are not considered in the remainder of this report. The critical blade height during the progression of fuel management in cores 179-190 is depicted in Figure 25 for the reference LEU design and the nine remaining element designs with 12 mil cladding. Effective Full Power Days (EFPD) is based on a 7 MW operating power.

Design 19D20 was also slightly less than critical during the course of the depletion cycle 188. Since a reduction of only 4 days of its cycle length was enough to allow this configuration to complete the sequence, this design has not been discarded. Control blade heights can also be compared with the reference LEU design results in Appendix C. Most of the configurations generated comparable results with the reference LEU design.

In Figure 25 LEU blade heights are seen to transition during the first cores as both burnup shape and reactivity impacts of the 47 day LEU cycle are established in the modeling. As a consequence, power distributions and neutron flux from the second half of the LEU cores series (core 185-190) are used as representative of LEU fuel management. Since MIT analyzes the adequacy of thermal hydraulic margins prior to each core loading, the loading and analysis of each core remains flexible to meet MITR experimental missions.

Since optimizing the cycle length by design was not performed, Table 21 instead lists the average change in blade height from the prior core at both BOC and EOC for cores 185-190. Each design, other than 18C25 and 19B20, remained negative as was the reference LEU data [6]. The negative values indicate

additional reactivity available. Thus from the 11 configurations, only nine will continue to be considered to provide sufficient fuel cycle performance.

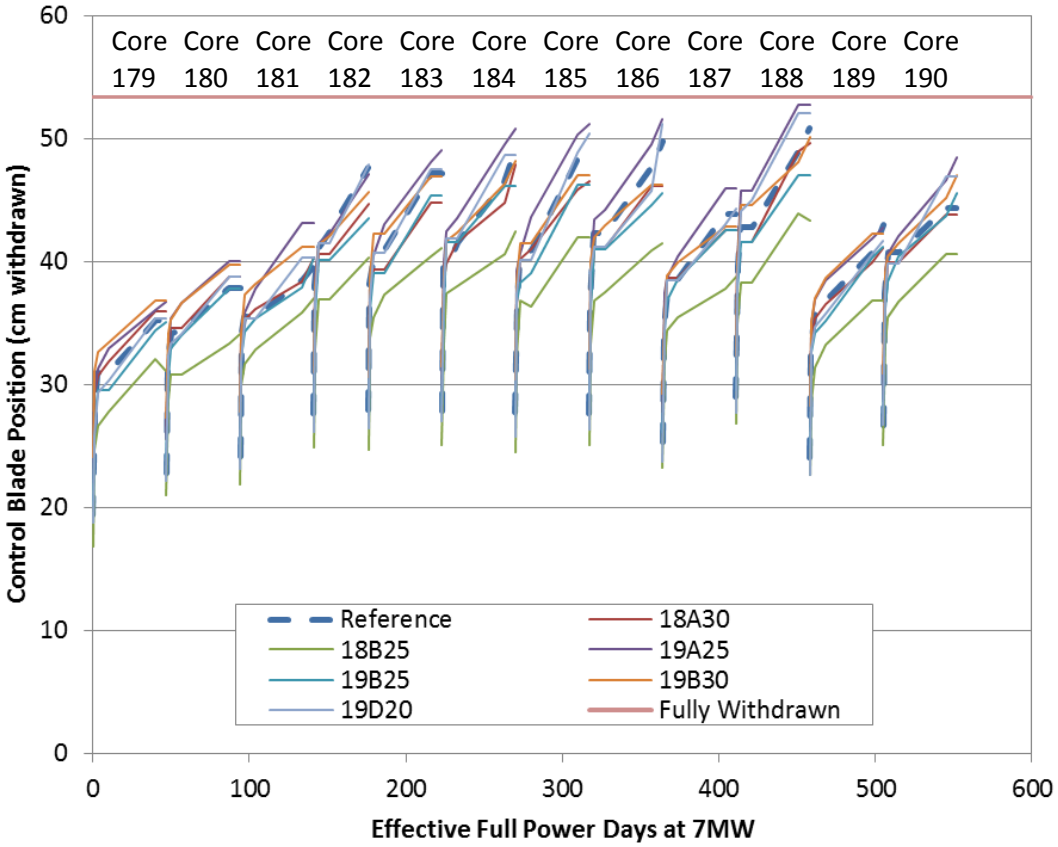

Figure 25. Critical Control Blade Position Throughout LEU Cores 179-190 for Alternate Element Designs.

5.2 ONB Margin Evaluation of Depleted Cores

The ONB margins of the nine remaining configurations and the reference design with and without fins have been calculated by Stat7. ONB power has been calculated in each channel of each element for each configuration from cycle 185 to 190 considering 3 core states per cycle: beginning of cycle (BOC), day 3 xenon equilibrium (Xenon eq.), and end of cycle (EOC). The volumetric flow rate was fixed at 2200 gpm. The purpose of these analyses is to discard the configurations that do not provide sufficient ONB margins through the fuel management sequence. Among the six cycles considered, the minimum ONB power is always found to occur in core 189 which is the freshest core.

From these calculations, 3 configurations were found inadequate: 17A30, 18A25 and 18D20 did not present sufficient margin to ONB for some of the time steps analyzed (limiting ONB power > 8.4MW). Limiting ONB powers for each core state and corresponding location obtained for these 3 configurations are presented in Table 21. The minimum ONB power occurs at cycle 189 BOC in element 10 which is a fresh element in the first channel adjacent to plates with full-thickness fuel.

Table 21. Alternate Element Designs without Adequate Margin to ONB.

		17A30		18A25		18D20	
Cycle	**Core state**	**ONB power (MW) & location**		**ONB power (MW) & location**		**ONB power (MW) & location**	
185	BOC	8.35	E10-S1-P4-Ax11-Surf2	8.71	E10-S1-P4-Ax11-Surf2	8.59	E10-S1-P5-Ax11-Surf2
	Xenon Eq.	8.60	E10-S1-P4-Ax11-Surf2	9.03	E7-S1-P4-Ax11-Surf2	8.80	E10-S1-P5-Ax11-Surf2
	EOC	8.76	E10-S1-P4-Ax12-Surf2	9.14	E10-S1-P4-Ax12-Surf2	9.04	E10-S1-P5-Ax13-Surf2
186	BOC	8.74	E10-S1-P4-Ax11-Surf2	9.00	E10-S1-P4-Ax11-Surf2	8.84	E10-S1-P5-Ax11-Surf2
	Xenon Eq.	8.87	E10-S1-P4-Ax11-Surf2	9.15	E10-S1-P4-Ax12-Surf2	9.20	E10-S1-P5-Ax12-Surf2
	EOC	8.89	E10-S1-P4-Ax12-Surf2	9.34	E7-S1-P4-Ax11-Surf2	9.36	E10-S1-P5-Ax12-Surf2
187	BOC	8.67	E10-S1-P4-Ax12-Surf2	8.82	E10-S1-P4-Ax11-Surf2	8.85	E10-S1-P5-Ax11-Surf2
	Xenon Eq.	8.69	E10-S1-P4-Ax11-Surf2	9.17	E10-S1-P4-Ax12-Surf2	8.93	E24-S1-P18-Ax9-Surf2
	EOC	8.83	E10-S1-P4-Ax12-Surf2	9.31	E10-S1-P4-Ax11-Surf2	9.21	E24-S1-P18-Ax10-Surf2
188	BOC	8.80	E10-S1-P4-Ax11-Surf2	9.00	E10-S1-P4-Ax11-Surf2	9.08	E10-S1-P5-Ax11-Surf2
	Xenon Eq.	8.76	E10-S1-P4-Ax11-Surf2	9.38	E10-S1-P4-Ax13-Surf2	9.33	E10-S1-P5-Ax11-Surf2
	EOC	9.00	E10-S1-P4-Ax13-Surf2	9.50	E10-S1-P4-Ax11-Surf2	9.60	E10-S1-P5-Ax11-Surf2
189	BOC	8.00	E10-S1-P4-Ax11-Surf2	8.31	E10-S1-P4-Ax12-Surf2	8.14	E10-S1-P5-Ax11-Surf2
	Xenon Eq.	8.19	E10-S1-P4-Ax11-Surf2	8.62	E10-S1-P4-Ax12-Surf2	8.48	E10-S1-P5-Ax11-Surf2
	EOC	8.27	E10-S1-P4-Ax11-Surf2	8.70	E10-S1-P4-Ax11-Surf2	8.67	E10-S1-P5-Ax11-Surf2
190	BOC	8.23	E10-S1-P4-Ax12-Surf2	8.56	E10-S1-P4-Ax11-Surf2	8.41	E10-S1-P5-Ax11-Surf2
	Xenon Eq.	8.46	E10-S1-P4-Ax11-Surf2	8.82	E10-S1-P4-Ax12-Surf2	8.73	E10-S1-P5-Ax11-Surf2
	EOC	8.49	E10-S1-P4-Ax12-Surf2	8.94	E10-S1-P4-Ax12-Surf2	8.84	E10-S1-P5-Ax11-Surf2
min. ONB power (MW)		8.00		8.31		8.14	
margin to ONB (%)		14.3%		18.7%		16.3%	

The results obtained for the reference design with and without fins are presented in Table 22. The reference design with fins presented enough ONB margins through the entire fuel management sequence with a minimum found at cycle 189 EOC. The limiting element is element 27 (adjacent to the reflector). This is expected since the meat thickness is constant and the power tends to peak on the edge of the element. The effect is amplified by the proximity of the reflector. As explained in section 4.2.1, the importance of the fins is significant on the ONB margins. The limiting ONB power obtained for the reference design without fins is about the half of the case with fins.

The six remaining candidate designs present sufficient ONB margin through the entire fuel management sequence. The limiting ONB power through the entire fuel sequence found for these configurations varying from 8.59MW (18B25) to 9.67MW (19B25). Limiting power at each core state and corresponding location for each configuration is shown from Table 23 to Table 28. Progression of the core minimum ONB power for the six remaining candidate configurations is shown in Figure 26. Though magnitudes differ, the shape for each configuration is relatively similar. For these six designs, the variation between configurations at each core state remain in an about 1 MW band. For the vast majority of the core states analyzed, the top of the band (best ONB margins) correspond to configuration 19B25 whereas the bottom of the band (less ONB margins) corresponds to configuration 18B25. Except for configuration

19B30, the limiting ONB power through the fuel management sequence is found in core 189 BOC, element 10, in the channel adjacent to the first not-reduced meat. Recall that element 10 in core 189 is a fresh element in the freshest core. 19B30 is also limited in core 189 but in element 27 in an end channel adjacent to the reflector. These results highlight how sensitive the efficiency of the meat thickness variation is to the relocation of the power peaking and consequently on the location of the limiting ONB power.

The impact of the channel gap closure due to irradiation-induced plate swelling has also been studied using the procedure described in Section 3.2.3. The new core limiting ONB power and corresponding location is also presented in Table 23 to Table 28. In these tables, the change of the minimum ONB power through the fuel management sequence due to the plate swelling is also indicated. As one can see, for each configuration, the ONB margins tend to increase slightly (about 2%) when channel gap closure treatment is included. This result can be explained by the fact that for a given flow rate, the channel gap reduction in the core leads to a slight increase in coolant velocity which allow a better plate cooling and consequently better ONB margins. It is also observed that the location of the minimum ONB power generally remains in the same location, which except for design 19B30 is limited in a fresh element at BOC despite the reduction in channels of depleted elements. This section addresses the thermal hydraulic effects of axially-averaged swelling impacting thermal hydraulics. More details of plate swelling on a local basis relevant to fuel performance are provided in section 5.5. Oxide formed at the cladding-coolant interface also reduces the thermal hydraulic channel; however, the impact is similarly expected to be beneficial to ONB power in cases where a fresh element is limiting, and of minimal impact otherwise due to the increase in velocity associated with net core flow area reduction.

The impact of the nominal volumetric flow rate has also been studied. The flow rate has been varied from 1800 to 2200 gpm for each core limiting position of each configuration. Results are shown in Figure 27. As one can see, in the flow range considered the ONB power decreases linearly with the flow decrease. From this plot one can deduce what minimum flow is required to remain above the LSSS power requirement. The minimum required flow for each design is provided in Table 29. Large differences exist between designs where the minimum flow varies from 1900 gpm (19B25) to 2150 gpm (18B25), but each of them require a flow rate that is above the current HEU LSSS flow rate by 5-20%.

Table 22. Reference LEU Design Thermal Hydraulic Margin with and without Fins and Fuel Swelling.

		with fins		no fins		no fins with swelling	
Cycle	**Core state**	**ONB power (MW) & location**		**ONB power (MW) & location**		**ONB power (MW) & location**	
185	BOC	10.04	E12-S4-P18-Ax18-	6.55	E27-S1-P1-Ax8-Surf1	7.52	E27-S1-P1-Ax8-su1
	Xenon Eq.	9.66	E27-S1-P1-Ax13-Surf1	6.18	E27-S1-P1-Ax10-Surf1	6.96	E27-S1-P1-Ax12-su1
	EOC	9.53	E27-S1-P1-Ax13-Surf1	6.27	E27-S1-P1-Ax13-Surf1	6.92	E27-S1-P1-Ax13-su1
186	BOC	10.48	E12-S4-P18-Ax18-	6.65	E14-S1-P18-Ax7-Surf2	7.68	E27-S1-P1-Ax8-su1
	Xenon Eq.	9.80	E27-S1-P1-Ax13-Surf1	6.41	E27-S1-P1-Ax11-Surf1	7.10	E27-S1-P1-Ax13-su1
	EOC	9.95	E27-S1-P1-Ax13-Surf1	6.52	E27-S1-P1-Ax13-Surf1	7.14	E27-S1-P1-Ax13-su1
187	BOC	10.36	E12-S4-P18-Ax18-	6.31	E25-S4-P1-Ax8-Surf1	7.33	E25-S4-P1-Ax8-su1
	Xenon Eq.	9.61	E25-S4-P1-Ax12-Surf1	5.96	E25-S4-P1-Ax10-Surf1	6.83	E25-S4-P1-Ax10-su1
	EOC	9.61	E25-S4-P1-Ax13-Surf1	6.15	E25-S4-P1-Ax10-Surf1	6.95	E25-S4-P1-Ax12-su1
188	BOC	10.71	E12-S4-P18-Ax18-	6.34	E24-S1-P18-Ax8-Surf2	7.42	E24-S1-P18-Ax8-su2
	Xenon Eq.	9.79	E24-S1-P18-Ax13-	6.30	E24-S1-P18-Ax10-Surf2	7.16	E25-S4-P18-Ax11-su2
	EOC	10.00	E24-S1-P18-Ax13-	6.51	E24-S1-P18-Ax12-Surf2	7.28	E25-S4-P18-Ax13-su2
189	BOC	10.50	E2-S1-P1-Ax18-Surf1	6.32	E27-S1-P1-Ax8-Surf1	7.34	E27-S1-P1-Ax8-su1
	Xenon Eq.	9.36	E27-S1-P1-Ax11-Surf1	5.89	E27-S1-P1-Ax10-Surf1	6.73	E27-S1-P1-Ax11-su1
	EOC	9.17	E27-S1-P1-Ax13-Surf1	5.91	E27-S1-P1-Ax10-Surf1	6.71	E27-S1-P1-Ax11-su1
190	BOC	10.70	E2-S1-P1-Ax18-Surf1	6.40	E27-S1-P1-Ax8-Surf1	7.41	E27-S1-P1-Ax8-su1
	Xenon Eq.	9.42	E27-S1-P1-Ax13-Surf1	6.05	E27-S1-P1-Ax11-Surf1	6.83	E27-S1-P1-Ax11-su1
	EOC	9.52	E27-S1-P1-Ax13-Surf1	6.15	E27-S1-P1-Ax11-Surf1	6.91	E27-S1-P1-Ax12-su1
min. ONB power (MW)		9.17		5.89		6.71	
margin to ONB (%)		30.9%		-15.8%		-4.1%	
variation due to swelling (%)						13.9%	

Table 23. Design 18A30 Thermal Hydraulic Margin with and without Fuel Swelling.

		no swelling		with swelling	
Cycle	**Core state**	**ONB power (MW) & location**		**ONB power (MW) & location**	
185	BOC	9.54	E10-S1-P4-Ax11-su2	9.70	E10-S1-P4-Ax11-su2
	Xenon Eq.	9.66	E25-S4-P4-Ax10-su2	9.76	E25-S4-P4-Ax10-su2
	EOC	9.66	E25-S4-P4-Ax10-su2	9.77	E25-S4-P4-Ax10-su2
186	BOC	9.69	E10-S1-P4-Ax11-su2	9.82	E10-S1-P4-Ax11-su2
	Xenon Eq.	9.90	E2-S4-P4-Ax18-su2	9.93	E2-S4-P4-Ax18-su2
	EOC	9.82	E2-S4-P4-Ax18-su2	9.86	E2-S4-P4-Ax18-su2
187	BOC	9.66	E10-S1-P4-Ax11-su2	9.76	E10-S1-P4-Ax11-su2
	Xenon Eq.	9.62	E25-S4-P4-Ax9-su2	9.70	E25-S4-P4-Ax11-su2
	EOC	9.54	E25-S4-P4-Ax10-su2	9.62	E25-S4-P4-Ax10-su2
188	BOC	9.70	E25-S4-P15-Ax8-su1	9.78	E25-S4-P15-Ax8-su1
	Xenon Eq.	9.72	E25-S4-P15-Ax9-su1	9.79	E25-S4-P15-Ax9-su1
	EOC	9.70	E25-S4-P15-Ax11-su1	9.78	E25-S4-P15-Ax11-su1
189	BOC	9.01	E10-S1-P4-Ax11-su2	9.20	E10-S1-P4-Ax11-su2
	Xenon Eq.	9.28	E10-S1-P4-Ax11-su2	9.46	E10-S1-P4-Ax11-su2
	EOC	9.38	E22-S4-P4-Ax10-su2	9.53	E22-S4-P4-Ax10-su2
190	BOC	9.29	E10-S1-P4-Ax12-su2	9.47	E10-S1-P4-Ax12-su2
	Xenon Eq.	9.41	E22-S4-P4-Ax10-su2	9.54	E22-S4-P4-Ax10-su2
	EOC	9.50	E22-S4-P4-Ax11-su2	9.66	E22-S4-P4-Ax11-su2
min. ONB power (MW)		9.01		9.20	
margin to ONB (%)		28.7%		31.4%	
variation due to swelling (%)				2.1%	

Table 24. Design 18B25 Thermal Hydraulic Margin with and without Fuel Swelling.

		no swelling		with swelling	
Cycle	**Core state**	**ONB power (MW) & location**		**ONB power (MW) & location**	
185	BOC	9.08	E10-S1-P4-Ax11-su2	9.24	E10-S1-P4-Ax11-su2
	Xenon Eq.	9.27	E10-S1-P4-Ax11-su2	9.42	E10-S1-P4-Ax11-su2
	EOC	9.60	E10-S1-P4-Ax12-su2	9.76	E10-S1-P4-Ax12-su2
186	BOC	9.32	E10-S1-P4-Ax11-su2	9.45	E10-S1-P4-Ax11-su2
	Xenon Eq.	9.68	E10-S1-P4-Ax11-su2	9.81	E10-S1-P4-Ax11-su2
	EOC	9.68	E10-S1-P4-Ax12-su2	9.83	E10-S1-P4-Ax12-su2
187	BOC	9.37	E10-S1-P4-Ax11-su2	9.45	E10-S1-P4-Ax11-su2
	Xenon Eq.	9.55	E10-S1-P4-Ax12-su2	9.64	E10-S1-P4-Ax12-su2
	EOC	9.69	E10-S1-P4-Ax11-su2	9.80	E10-S1-P4-Ax11-su2
188	BOC	9.46	E10-S1-P4-Ax11-su2	9.54	E10-S1-P4-Ax11-su2
	Xenon Eq.	9.68	E10-S1-P4-Ax12-su2	9.78	E10-S1-P4-Ax12-su2
	EOC	9.77	E10-S1-P4-Ax12-su2	9.88	E10-S1-P4-Ax12-su2
189	BOC	8.59	E10-S1-P4-Ax11-su2	8.75	E10-S1-P4-Ax11-su2
	Xenon Eq.	8.94	E10-S1-P4-Ax11-su2	9.12	E10-S1-P4-Ax11-su2
	EOC	9.05	E10-S1-P4-Ax11-su2	9.23	E10-S1-P4-Ax11-su2
190	BOC	8.93	E10-S1-P4-Ax11-su2	9.08	E10-S1-P4-Ax11-su2
	Xenon Eq.	9.06	E10-S1-P4-Ax12-su2	9.23	E10-S1-P4-Ax12-su2
	EOC	9.36	E10-S1-P4-Ax11-su2	9.54	E10-S1-P4-Ax11-su2
min. ONB power (MW)		8.59		8.75	
margin to ONB (%)		22.7%		25.0%	
variation due to swelling (%)				1.9%	

Table 25. Design 19A25 Thermal Hydraulic Margin with and without Fuel Swelling.

		no swelling		with swelling	
Cycle	**Core state**	**ONB power (MW) & location**		**ONB power (MW) & location**	
185	BOC	9.76	E7-S1-P4-Ax11-su2	9.93	E10-S1-P4-Ax11-su2
	Xenon Eq.	10.03	E10-S1-P4-Ax12-su2	10.20	E10-S1-P4-Ax12-su2
	EOC	9.91	E2-S4-P4-Ax18-su2	10.00	E2-S4-P4-Ax18-su2
186	BOC	9.98	E10-S1-P4-Ax11-su2	10.10	E10-S1-P4-Ax11-su2
	Xenon Eq.	10.15	E2-S4-P4-Ax18-su2	10.22	E2-S4-P4-Ax18-su2
	EOC	10.00	E2-S4-P4-Ax18-su2	10.06	E2-S4-P4-Ax18-su2
187	BOC	9.85	E10-S1-P4-Ax11-su2	9.93	E10-S1-P4-Ax11-su2
	Xenon Eq.	10.07	E25-S4-P4-Ax10-su2	10.14	E25-S4-P4-Ax10-su2
	EOC	10.10	E25-S4-P4-Ax11-su2	10.17	E25-S4-P4-Ax11-su2
188	BOC	10.08	E10-S1-P4-Ax11-su2	10.14	E10-S1-P4-Ax11-su2
	Xenon Eq.	10.26	E25-S4-P16-Ax10-su1	10.34	E25-S4-P16-Ax10-su1
	EOC	10.11	E2-S4-P4-Ax18-su2	10.11	E2-S4-P4-Ax18-su2
189	BOC	9.09	E10-S1-P4-Ax11-su2	9.26	E10-S1-P4-Ax11-su2
	Xenon Eq.	9.44	E10-S1-P4-Ax12-su2	9.63	E10-S1-P4-Ax12-su2
	EOC	9.72	E22-S4-P4-Ax10-su2	9.88	E22-S4-P4-Ax10-su2
190	BOC	9.51	E10-S1-P4-Ax11-su2	9.70	E10-S1-P4-Ax11-su2
	Xenon Eq.	9.63	E10-S1-P4-Ax11-su2	9.81	E10-S1-P4-Ax11-su2
	EOC	9.77	E2-S4-P16-Ax18-su1	9.83	E2-S4-P16-Ax18-su1
min. ONB power (MW)		9.09		9.26	
margin to ONB (%)		29.8%		32.3%	
variation due to swelling (%)				1.9%	

Table 26. Design 19B25 Thermal Hydraulic Margin with and without Fuel Swelling.

		no swelling		with swelling	
Cycle	**Core state**	**ONB power (MW) & location**		**ONB power (MW) & location**	
185	BOC	10.08	E10-S1-P4-Ax11-su2	10.25	E10-S1-P4-Ax11-su2
	Xenon Eq.	10.35	E23-S1-P19-Ax10-su2	10.50	E23-S1-P19-Ax10-su2
	EOC	10.37	E2-S4-P4-Ax18-su2	10.49	E2-S4-P4-Ax18-su2
186	BOC	10.48	E10-S1-P4-Ax12-su2	10.61	E10-S1-P4-Ax12-su2
	Xenon Eq.	10.68	E7-S1-P4-Ax11-su2	10.74	E2-S4-P4-Ax18-su2
	EOC	10.34	E2-S4-P4-Ax18-su2	10.41	E2-S4-P4-Ax18-su2
187	BOC	10.36	E10-S1-P4-Ax11-su2	10.45	E10-S1-P4-Ax11-su2
	Xenon Eq.	10.46	E25-S4-P4-Ax10-su2	10.55	E25-S4-P4-Ax10-su2
	EOC	10.56	E25-S4-P4-Ax11-su2	10.65	E25-S4-P4-Ax11-su2
188	BOC	10.55	E10-S1-P4-Ax11-su2	10.61	E10-S1-P4-Ax11-su2
	Xenon Eq.	10.48	E25-S4-P16-Ax10-su1	10.58	E25-S4-P16-Ax10-su1
	EOC	10.71	E2-S4-P4-Ax18-su2	10.67	E2-S4-P4-Ax18-su2
189	BOC	9.67	E10-S1-P4-Ax11-su2	9.88	E10-S1-P4-Ax11-su2
	Xenon Eq.	9.94	E27-S1-P1-Ax9-su1	10.08	E27-S1-P1-Ax9-su1
	EOC	9.96	E10-S1-P4-Ax12-su2	10.18	E10-S1-P4-Ax12-su2
190	BOC	9.96	E10-S1-P4-Ax11-su2	10.17	E10-S1-P4-Ax11-su2
	Xenon Eq.	10.17	E10-S1-P4-Ax11-su2	10.34	E22-S4-P4-Ax10-su2
	EOC	10.11	E22-S4-P4-Ax11-su2	10.27	E22-S4-P4-Ax11-su2
min. ONB power (MW)		9.67		9.88	
margin to ONB (%)		38.2%		41.2%	
variation due to swelling (%)				2.2%	

Table 27. Design 19B30 Thermal Hydraulic Margin with and without Fuel Swelling.

		no swelling		with swelling	
Cycle	**Core state**	**ONB power (MW) & location**		**ONB power (MW) & location**	
185	BOC	10.10	E23-S1-P19-Ax9-su2	10.22	E23-S1-P19-Ax9-su2
	Xenon Eq.	9.80	E23-S1-P19-Ax10-su2	9.93	E23-S1-P19-Ax10-su2
	EOC	9.98	E23-S1-P19-Ax11-su2	10.08	E23-S1-P19-Ax11-su1
186	BOC	10.42	E27-S1-P1-Ax8-su1	10.52	E27-S1-P1-Ax8-su1
	Xenon Eq.	10.26	E23-S1-P19-Ax11-su2	10.31	E23-S1-P19-Ax11-su2
	EOC	10.55	E23-S1-P19-Ax11-su2	10.61	E23-S1-P19-Ax11-su1
187	BOC	10.00	E13-S1-P19-Ax8-su2	10.13	E13-S1-P19-Ax8-su2
	Xenon Eq.	9.87	E13-S1-P19-Ax10-su2	9.93	E13-S1-P19-Ax11-su2
	EOC	9.96	E13-S1-P19-Ax10-su2	10.03	E13-S1-P19-Ax11-su2
188	BOC	10.54	E25-S4-P19-Ax10-su2	10.62	E25-S4-P19-Ax11-su2
	Xenon Eq.	10.15	E25-S4-P19-Ax10-su2	10.26	E25-S4-P19-Ax10-su2
	EOC	10.54	E25-S4-P19-Ax10-su2	10.62	E25-S4-P19-Ax11-su2
189	BOC	9.59	E27-S1-P1-Ax8-su1	9.71	E27-S1-P1-Ax8-su1
	Xenon Eq.	9.31	E27-S1-P1-Ax10-su1	9.45	E27-S1-P1-Ax10-su1
	EOC	9.45	E27-S1-P1-Ax10-su1	9.59	E27-S1-P1-Ax10-su1
190	BOC	9.92	E27-S1-P1-Ax8-su1	10.05	E27-S1-P1-Ax8-su1
	Xenon Eq.	9.63	E27-S1-P1-Ax10-su1	9.75	E27-S1-P1-Ax10-su1
	EOC	9.78	E27-S1-P1-Ax11-su1	9.93	E27-S1-P1-Ax11-su1
min. ONB power (MW)		9.31		9.45	
margin to ONB (%)		32.9%		34.9%	
variation due to swelling (%)				1.5%	

Table 28. Design 19D20 Thermal Hydraulic Margin with and without Fuel Swelling.

		no swelling		with swelling	
Cycle	**Core state**	**ONB power (MW) & location**		**ONB power (MW) & location**	
185	BOC	9.48	E7-S1-P5-Ax11-su2	9.64	E10-S1-P5-Ax11-su2
	Xenon Eq.	9.77	E10-S1-P5-Ax12-su2	9.92	E10-S1-P5-Ax12-su2
	EOC	9.95	E10-S1-P5-Ax12-su2	10.09	E10-S1-P5-Ax12-su2
186	BOC	9.73	E10-S1-P5-Ax11-su2	9.83	E10-S1-P5-Ax11-su2
	Xenon Eq.	10.06	E10-S1-P5-Ax12-su2	10.17	E10-S1-P5-Ax12-su2
	EOC	10.33	E10-S1-P5-Ax13-su2	10.41	E10-S1-P5-Ax13-su2
187	BOC	9.79	E10-S1-P5-Ax11-su2	9.87	E10-S1-P5-Ax11-su2
	Xenon Eq.	9.50	E24-S1-P19-Ax9-su2	9.67	E24-S1-P19-Ax10-su2
	EOC	9.74	E24-S1-P19-Ax10-su2	9.93	E24-S1-P19-Ax10-su2
188	BOC	9.94	E10-S1-P5-Ax11-su2	10.00	E10-S1-P5-Ax11-su2
	Xenon Eq.	10.08	E24-S1-P19-Ax9-su2	10.25	E24-S1-P19-Ax9-su2
	EOC	10.35	E10-S1-P5-Ax12-su2	10.36	E10-S1-P5-Ax18-su2
189	BOC	9.10	E10-S1-P5-Ax12-su2	9.28	E10-S1-P5-Ax12-su2
	Xenon Eq.	9.27	E10-S1-P5-Ax12-su2	9.45	E10-S1-P5-Ax12-su2
	EOC	9.52	E10-S1-P5-Ax11-su2	9.72	E10-S1-P5-Ax11-su2
190	BOC	9.34	E10-S1-P5-Ax11-su2	9.51	E10-S1-P5-Ax11-su2
	Xenon Eq.	9.68	E10-S1-P5-Ax12-su2	9.86	E10-S1-P5-Ax12-su2
	EOC	9.79	E10-S1-P5-Ax12-su2	9.97	E10-S1-P5-Ax12-su2
min. ONB power (MW)		9.10		9.28	
margin to ONB (%)		30.1%		32.6%	
variation due to swelling (%)				1.9%	

Table 29. Minimum Volumetric Flow Rate to Remain above 8.4 MW LSSS Requirement for the Six Final Design Candidates.

LEU Design Configuration	**18B25**	**18A30**	**19D20**	**19A25**	**19B25**	**19B30**
Volumetric flow rate required for 20% margin to ONB, 8.4 MW (gpm)	2150	2040	2020	2020	1900	1970

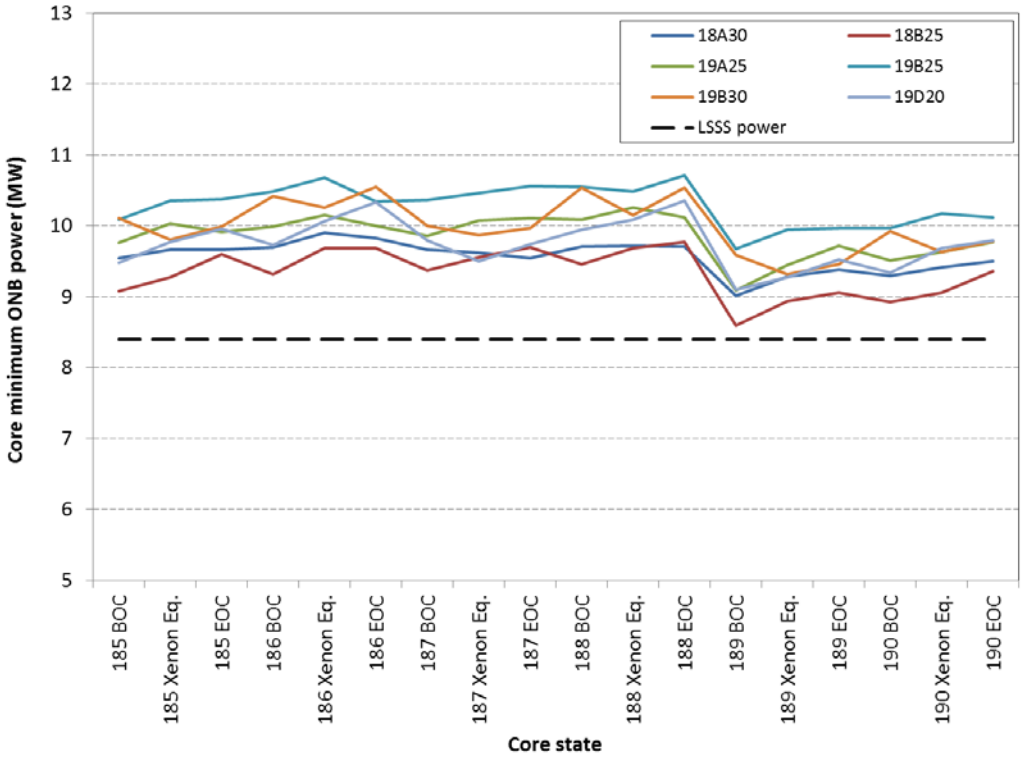

Figure 26. Minimum core ONB Power for the Six Final Design Candidates.

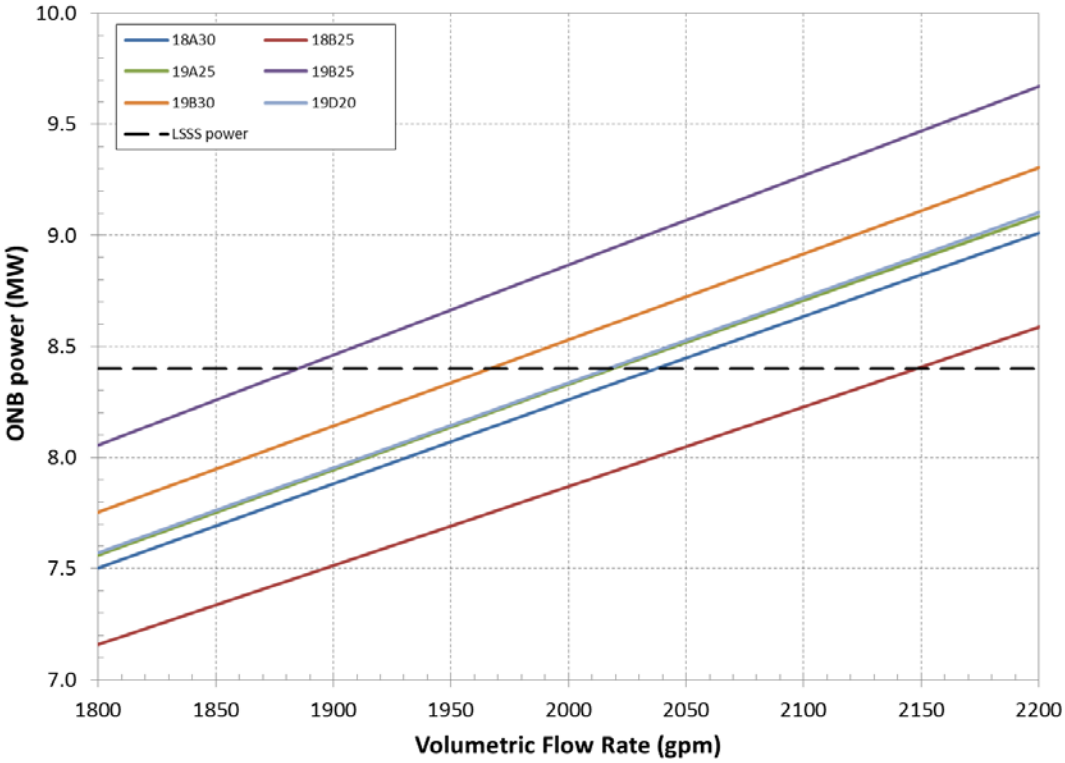

Figure 27. ONB Power versus Flow Rate for the Six Final Design Candidates.

5.3 Discussion on Peak Heat Flux of Depleted Cores

The peak heat flux results are tabulated in Table D1 to Table D14 of Appendix D. In addition, a comparison between the reference LEU design [6] and re-calculated reference LEU design results is given in Table D15. These results show that the peak heat flux results obtained in this work are in good agreement with Reference [6].

Figure 28 through Figure 33 illustrate the heat flux profile by plate for the six remaining candidate designs in key locations as explained below (see section 5.2 for an explanation of the favorable hydraulic margin of these six candidates, and the most limiting locations with regards to ONB). In this section the heat flux is assumed to be evenly transferred to each side of the plate. The Stat code does not make this assumption; however, this allows comparison of the designs based upon the power distributions generated. The fuel thickness is also plotted by plate for each design, and the reference LEU design. For comparison, the reference LEU design heat flux by plate is shown at the most limiting location as well as in element 10. Axial node 11 was selected since, for the most favorable design with regards to ONB (19B25) this axial node was limiting. Other axial nodes in the vicinity are comparable.

Also shown in these figures is the Core 189 EOC power distribution for element 27 stripe 1 by plate. For the reference LEU design, element 27 has typically been the most limiting in fresh cores among the C-ring elements. This is due to its proximity to the larger water hole for the regulating rod. The reference LEU design has also been shown to be limiting in this peak location, E27P1S1, for depleted cores. In order to estimate whether the degree of thinning has been adequate, and not overly reduced, the comparison of the maximum heat flux in Core 189 EOC E27P1S1 to the maximum in the most limiting location with regards to ONB can be made. If the fuel was thinned less, the most limiting location would be expected to return to a plate adjacent to the reflector, as is shown to be the case in Section 5.2 with the reference LEU design.

The most limiting location with regards to ONB has been found in Section 5.2 to be in element 10 of Core 189 BOC in the channel adjacent to the first plate with full meat thickness, other than for design 19B30. From these figures it can be observed that the first un-thinned plate is also the maximum with regards to heat flux other than for design 19B30. For design 19B30 core 189 is always limited in element 27 plate 1. This comparison, as tabulated numerically in Table 30, provides a gauge of how appropriate the fuel has been thinned in the outer plate in order to flatten the power profile. As discussed in the thermal hydraulic results presented in Section 5.2, the reference LEU design and 19B30 are the only two limited by element 27 plate 1. These two configurations have heat flux in core 189 EOC element 27 P1 143% and 110% of the BOC element 10 maximum which shows that the outer plate(s) have not been thinned optimally. The configurations 19D20 and 19B25, however, have the largest margin to ONB (see Section 5.2) and also have the ratio closest to 100% in Table 30.

It should be noted that these comparisons were made between the same locations for consistency, and that the most limiting accounts not only for specific local power but also enthalpy rise which is represented in the results of Section 5.2. These figures do illustrate that within the constraint to have three distinct fuel thicknesses in the MIT element, the fuel in the outer plates has been thinned sufficiently in order to flatten the power peaking typical in the MITR core. Table 31 through Table 33 summarize the peak heat fluxes, and locations, found in the designs considered.

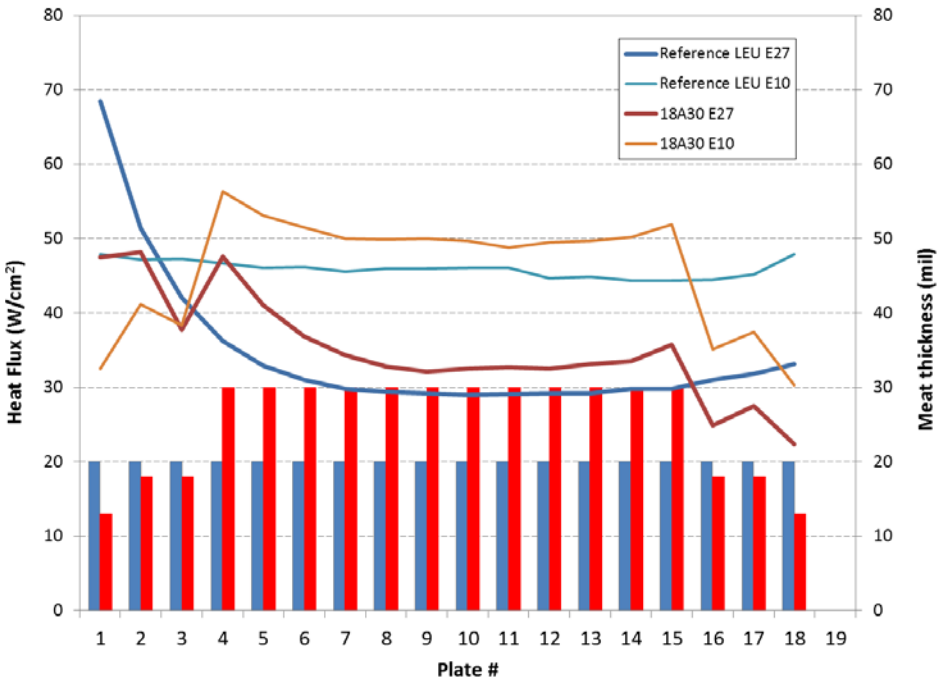

Figure 28. Heat Flux Profile by Plate for design 18A30 in both Element 10, Stripe 1, Axial Node 11 and Element 27, Stripe 1, Axial Node 11 .

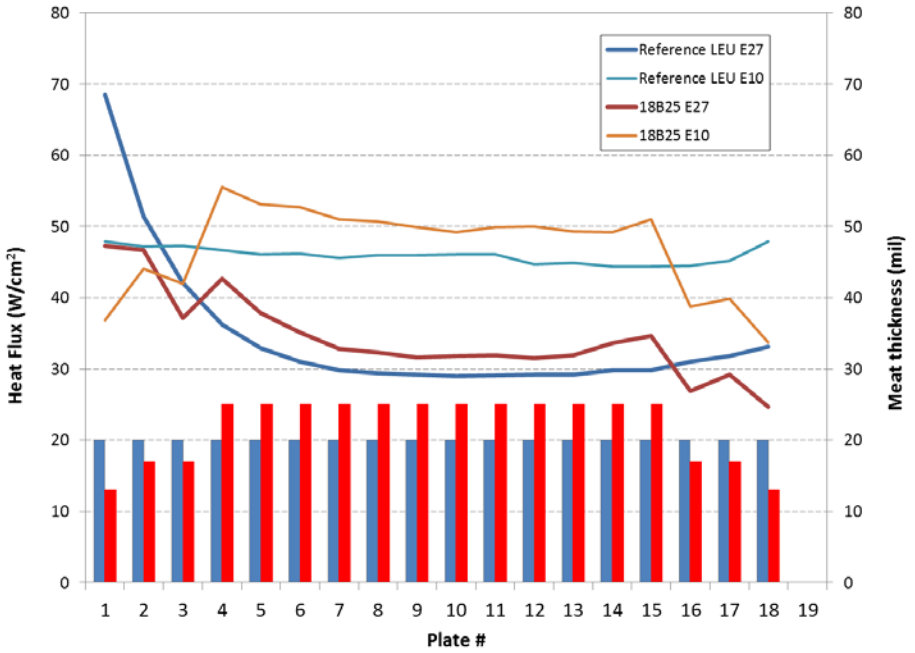

Figure 29. Heat Flux Profile by Plate for design 18B25 in both Element 10, Stripe 1, Axial Node 11 and Element 27, Stripe 1, Axial Node 11.

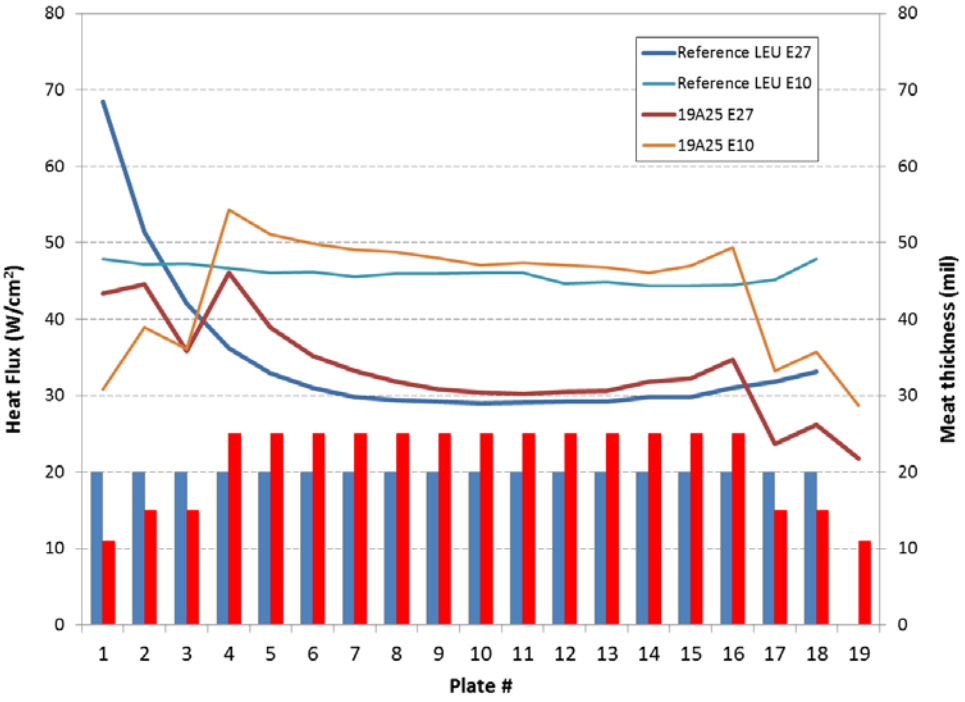

Figure 30. Heat Flux Profile by Plate for design 19A25 in bothElement 10, Stripe 1, Axial Node 11 and Element 27, Stripe 1, Axial Node 11.

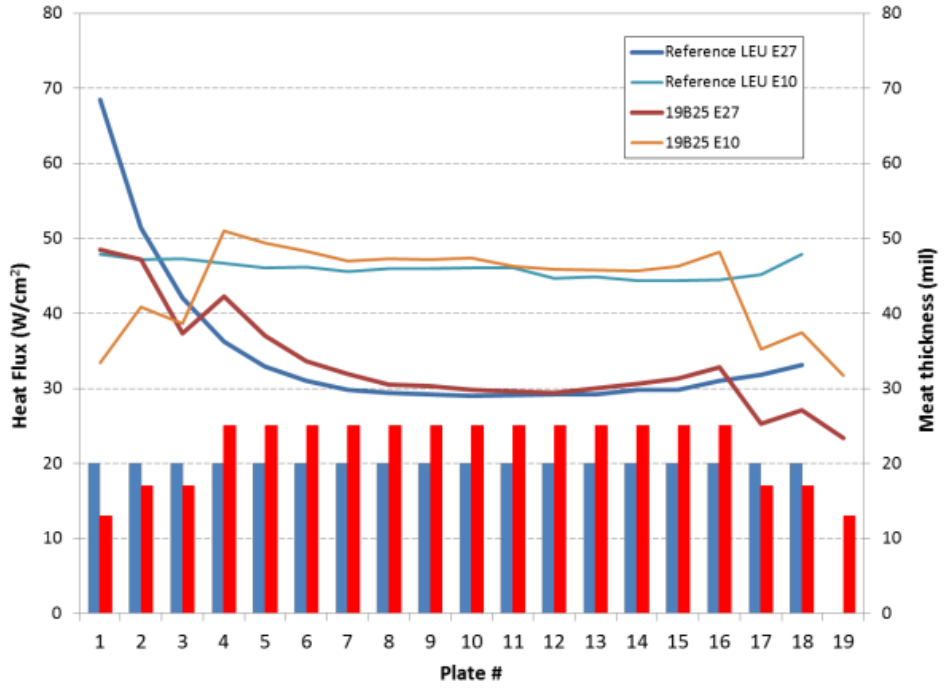

Figure 31. Heat Flux Profile by Plate for design 19B25 in both Element 10, Stripe 1, Axial Node 11 and Element 27, Stripe 1, Axial Node 11.

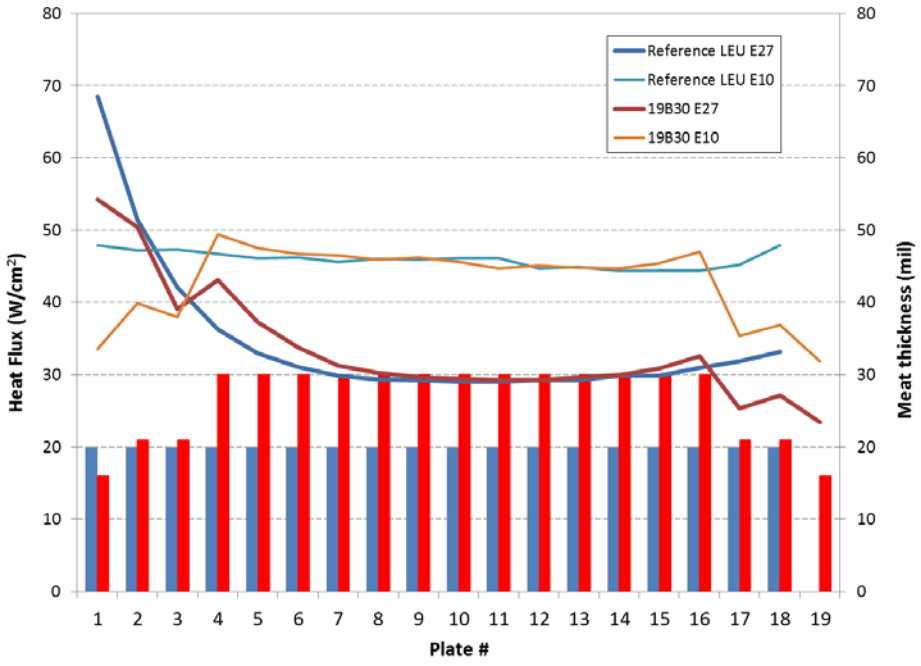

Figure 32. Heat Flux Profile by Plate for design 19B30 in both Element 10, Stripe 1, Axial Node 11 and Element 27, Stripe 1, Axial Node 11.

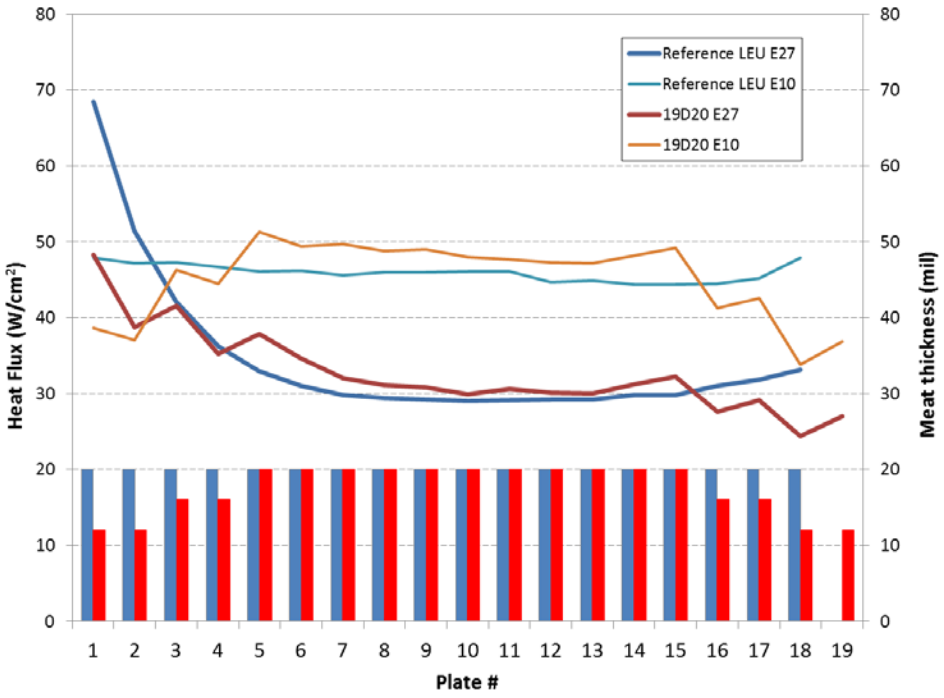

Figure 33. Heat Flux Profile by Plate for design 19D20 in both Element 10, Stripe 1, Axial Node 11 and Element 27, Stripe 1, Axial Node 11.

Table 30. Heat Flux in Plate 1 Stripe 1 of Element 27 of Core 189 EOC vs. Maximum Heat Flux in Core 189 BOC Element 10.

Axial 11	Reference LEU	18A30	18B25	19A25	19B25	19B30	19D20
Heat Flux Plate 1 Element 27 (W/cm^2)	68.5	47.4	47.3	43.4	48.5	54.2	48.3
Maximum all plates of Element 10 (W/cm^2) [a]	47.9	56.3	55.5	54.3	51.0	49.4	51.3
Heat Flux Plate 1 E27 vs. Max E10 all plates	143%	84%	85%	80%	95%	110%	94%

a. Fresh element 10 was found to be limiting for all alternate designs except 19B30 where element 27 plate 1 adjacent to the reflector was most limiting (see Section 5.4).

Table 31. Peak Heat Flux Values for Peak Spot and Stripe for Each LEU Design at BOC.

LEU Design	Peak Spot (W/cm^2)	Peak Spot Location	Peak Stripe (W/cm^2)	Peak Stripe Location
Reference	75.4	27P1S1Ax18	50.2	27P1S1
17A30	61.7	10P4S1Ax11	53.4	10P4S1
18A25	58.1	10P4S1Ax11	50.5	10P4S1
18A30	59.2	22P4S4Ax13	49.4	10P4S1
18B25	55.9	10P4S1Ax9	48.6	10P4S1
18D20	58.1	22P14S4Ax13	48.3	10P5S1
19A25	56	22P4S4Ax12	47	10P4S1
19B25	53.7	27P1S1Ax15	45.1	10P4S1
19B30	60.9	27P1S1Ax18	43.4	10P4S1
19D20	57.1	22P15S4Ax13	44.9	10P5S1

Table 32. Peak Heat Flux Values for Peak Spot and Stripe for Each LEU Design at Equilibrium Xenon.

LEU Design	Peak Spot (W/cm^2)	Peak Spot Location	Peak Stripe (W/cm^2)	Peak Stripe Location
Reference	74.2	27P1S1Ax12	55.6	27P1S1
17A30	60.1	22P4S4Ax13	51.5	10P4S1
18A25	56.5	22P4S4Ax12	48.4	10P4S1
18A30	57.8	22P4S4Ax11	47.7	10P4S1
18B25	54.6	10P4S1Ax9	46.6	10P4S1
18D20	53.7	27P1S1Ax12	46.1	10P5S1
19A25	54.3	22P4S4Ax11	45.1	10P4S1
19B25	53.7	27P1S1Ax12	43.4	10P4S1
19B30	59.2	27P1S1Ax11	44.9	27P1S1
19D20	56.7	22P15S4Ax12	43	10P5S1

Table 33. Peak Heat Flux Values for Peak Spot and Stripe for Each LEU Design at EOC.

LEU Design	Peak Spot (W/cm^2)	Peak Spot Location	Peak Stripe (W/cm^2)	Peak Stripe Location
Reference	71.6	27P1S1Ax9	57.7	27P1S1
17A30	60.4	22P4S4Ax12	50.6	10P4S1
18A25	56.1	10P4S1Ax8	47.5	10P4S1
18A30	57.6	22P4S4Ax11	46.9	10P4S1
18B25	54.2	22P4S4Ax11	45.8	10P4S1
18D20	57.4	22P14S4Ax12	44.9	10P5S1
19A25	53.9	22P4S4Ax10	44.2	10P4S1
19B25	52.3	22P4S4Ax11	42.5	10P4S1
19B30	57.3	27P1S1Ax11	45.8	27P1S1
19D20	55.2	22P15S4Ax10	42.1	10P5S1

5.4 Performance of Depleted Cores

After performing the fuel management depletions, it was necessary to perform neutron flux at two critical states to assure mission performance. Neutron flux performance results used were thermal (<0.4 eV) other than for the ICSA fast neutron flux (>0.1 MeV).Beginning of Cycle (BOC) and End of Cycle (EOC) calculations were performed for the last 6 cores (185-190) for each reactor configuration, for a total of 144 calculations. Performance results are presented for HEU in Table 34. LEU performance was assessed by comparing the LEU to HEU flux ratio by core at both BOC and EOC. Appendix E contains the performance of the six final LEU element design candidates for cores 185-190. For each of the LEU element designs, Core 190 consistently required the highest power for performance equivalent to HEU. Table 35 lists the neutron flux ratio of LEU at 7 MW to HEU at 6 MW for core 190. Also listed is the LEU power level required to obtain performance equivalent to HEU. This power is based upon providing a LEU/HEU flux ratio of at least 100% at each location. The average power required for performance equivalent to HEU over cores 185-190 is listed in Table 36. The power required for performance equivalent to 6 MW HEU operation is 7.22 for 19A25 and 7.27 MW for 19D20 at EOC. The remaining designs provide performance within 2% of the HEU reactor operations assuming a 7 MW operating power level.

Table 34. Neutron Flux Performance in All-Fresh and Historical Depleted HEU Cores at 6 MW.

	Flux (n/cm^2 s)				
Core	**In-Core Irradiation (A2)**	**Twelve-inch Beam Port**	**Two-inch Pneumatic Facility**	**Fission Converter Window**	**Below-core Thermal Beam Facility**
Energy	>0.1 MeV	<0.4 eV	<0.4 eV	<0.4 eV	<0.4 eV
HEU Fresh 22 Element	1.19E+14	1.43E+13	5.67E+13	1.04E+13	1.54E+12
HEU 185 BOC	1.31E+14	1.39E+13	5.11E+13	9.77E+12	1.47E+12
HEU 185 EOC	1.26E+14	1.34E+13	4.99E+13	9.36E+12	1.35E+12
HEU 186 BOC	1.29E+14	1.39E+13	5.21E+13	9.72E+12	1.47E+12
HEU 186 EOC	1.24E+14	1.31E+13	5.05E+13	9.26E+12	1.32E+12
HEU 187 BOC	1.29E+14	1.37E+13	5.15E+13	9.78E+12	1.46E+12
HEU 187 EOC	1.25E+14	1.32E+13	5.06E+13	9.46E+12	1.35E+12
HEU 188 BOC	1.28E+14	1.38E+13	5.18E+13	9.74E+12	1.46E+12
HEU 188 EOC	1.24E+14	1.33E+13	5.08E+13	9.40E+12	1.35E+12
HEU 189 BOC	1.31E+14	1.37E+13	5.06E+13	9.62E+12	1.47E+12
HEU 189 EOC	1.27E+14	1.35E+13	5.10E+13	9.51E+12	1.38E+12
HEU 190 BOC	1.28E+14	1.39E+13	5.20E+13	9.58E+12	1.47E+12
HEU 190 EOC	1.25E+14	1.36E+13	5.15E+13	9.38E+12	1.38E+12

Table 35. Performance of Core 190 for Various LEU Element Designs at 7 MW vs. HEU at 6 MW.

BOC or EOC	Element Design	Power (MW)	In-Core Irradiation (A2)	Twelve-inch Beam Port	Two-inch Pneumatic Facility	Fission Converter Window	Below-core Thermal Beam Facility	Power for Performance Equivalent to HEU (MW)
BOC	18A30	7	106.1%	101.2%	102.7%	103.9%	100.1%	6.99
	18B25	7	105.4%	99.2%	99.9%	101.7%	98.9%	7.08
	19A25	7	105.9%	101.0%	102.1%	103.5%	99.8%	7.02
	19B25	7	105.9%	100.7%	101.6%	103.4%	99.9%	7.00
	19B30	7	106.1%	102.0%	103.4%	104.9%	100.6%	6.96
	19D20	7	105.3%	99.0%	99.7%	101.3%	98.4%	7.11
EOC	18A30	7	105.8%	99.1%	101.3%	102.5%	99.4%	7.06
	18B25	7	105.2%	98.4%	99.7%	101.7%	98.9%	7.11
	19A25	7	104.3%	97.5%	99.3%	101.0%	97.0%	7.22
	19B25	7	104.5%	97.8%	99.9%	101.5%	97.8%	7.16
	19B30	7	105.0%	98.9%	100.7%	102.5%	98.7%	7.09
	19D20	7	103.7%	96.6%	98.3%	100.0%	96.3%	7.27

Table 36. Average LEU Core Power for Performance Equivalent to HEU at 6 MW.

	Power for Performance Equivalent to HEU (MW)		
Element Design	Core 185-190 BOC Average	Core 185-190 EOC Average	Core 185-190 Average of BOC and EOC
19B30	6.91	6.87	6.89
18A30	6.96	6.98	6.97
19B25	6.97	7.01	6.99
18B25	7.05	7.00	7.03
19A25	6.97	7.08	7.03
19D20	7.06	7.17	7.12

5.5 Fission Density and Swelling of Depleted Cores

Figure 34 presents the maximum fission density per plate calculated for the six remaining element design candidates, and for the finned reference LEU design [6]. The tabulated values are provided in Table F1 of Appendix F. The swelling values considered were the maximum local value predicted from the core sequence 185-190, and were calculated as described in Section 3.2.3 where the ^{235}U burnup is used as a conservative estimate of the fission density. Figure 35 to Figure 37 show respectively the corresponding maximum swelling by plate relative to the plate or cladding thickness for the six alternate element designs configurations as well as for the reference LEU design.

The burnup is highest in the design 19D20 compared to the reference LEU design. This can be understood from the element loading, as shown in Table 18, where the 19D20 uranium mass is 20-30% lower than the other five most promising designs.

The maximum local fuel swelling thickness is between 3-5 mil for the alternate element designs, whereas the finned reference LEU design exceeded 6 mil of swelling on an outermost plate due to the uniform fuel thickness of all plates. Fractional swelling relative to the cladding thickness is similar for each of the alternate element designs which have 12 mil cladding, or more, on all plates. The reference LEU design, which has 10 mil cladding on all plates, shows a higher swelling relative to the cladding thickness.

Fractional swelling relative to the plate thickness is highest in the finned reference LEU design in the range of 10-15% swelling vs. plate thickness. The alternate element designs exhibit swelling < 10% vs. plate thickness other than 19B25 where 9-11% swelling vs. plate thickness is predicted. Since the cladding thickness is 12 mil for all alternate designs in the central plates of the element, it should be recalled that the fueled thickness fraction will be lowest for 19D20 in the central plates of the element (45% fuel/plate thickness as-fabricated), and in the outer plates similar to design 19B25 e.g. (minimum 27% fuel/plate thickness as-fabricated). Despite this, the possible benefit to fuel performance from having a lower fueled thickness fraction may be not be realized in design 19D20 if larger swelling vs. plate thickness is relevant to fuel performance. Figure 38 shows the maximum fission density vs. fueled fraction of plate for each design configuration. The data trend shows that for a given fueled thickness fraction 19D20 has a higher fission density than all configurations other than the finned LEU reference design.

Whether the data presented in this section, or some other constraints better represent fuel performance is not addressed in this report. Prior to experimental fuel qualification results, detailed modeling may be required in order to understand the phenomena of plate deformation. Fuel swelling is treated in this work; however, the associated phenomena of fuel creep is not since mass transport is not anticipated to change the average channel dimension relevant to thermal hydraulic performance.

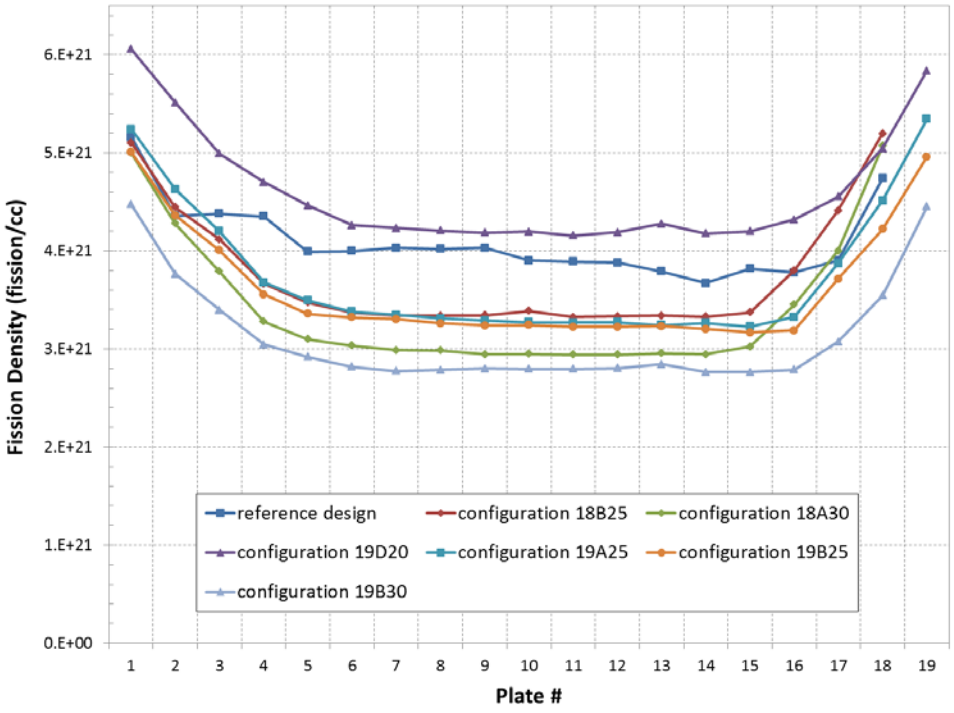

Figure 34. Maximum Fission Density by Plate.

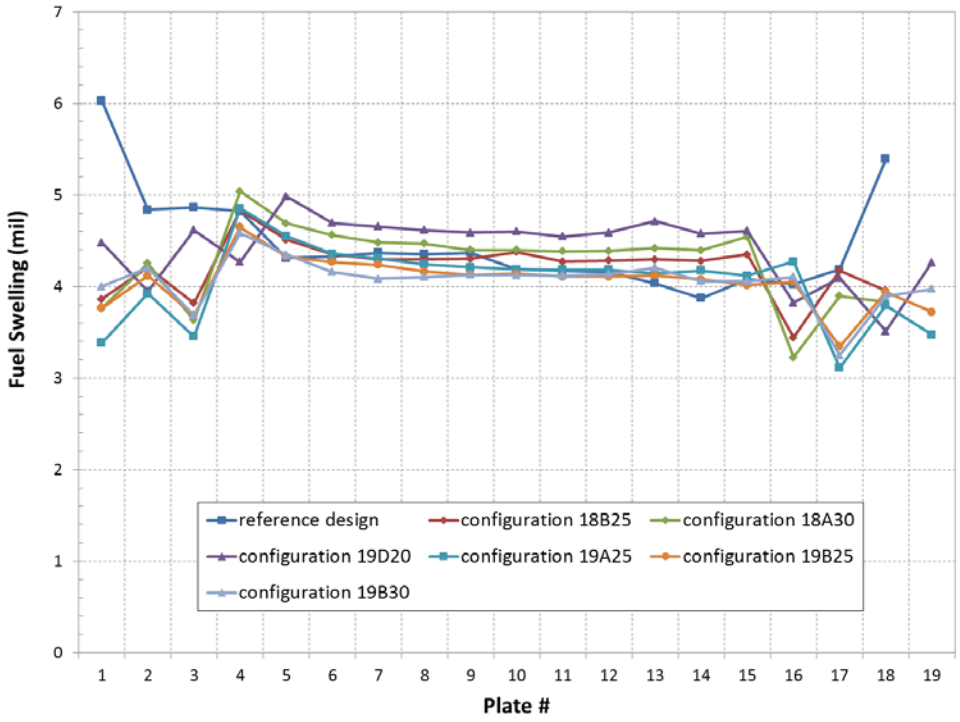

Figure 35. Maximum Swelling by Plate for each Design Configuration.

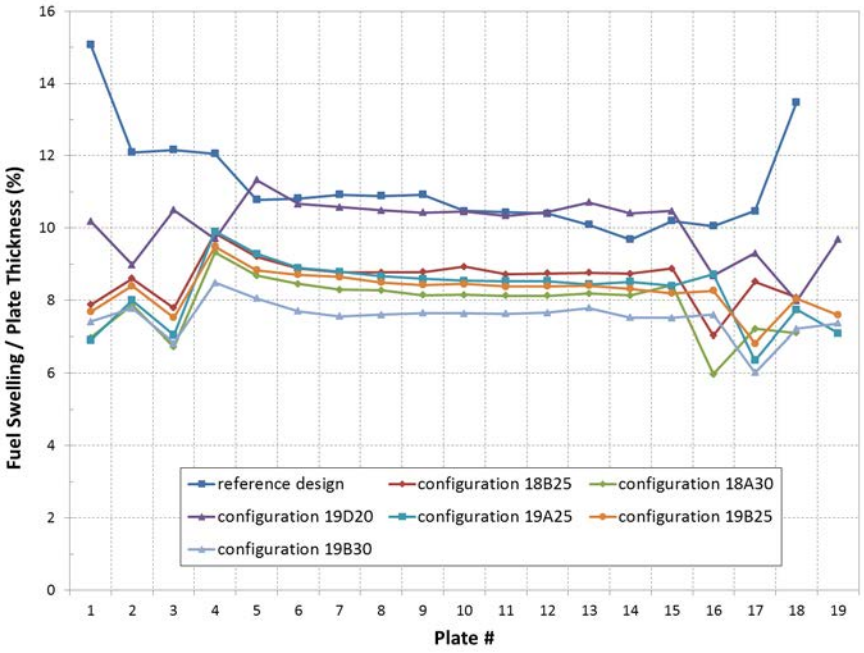

Figure 36. Maximum Fuel Meat Swelling Relative to Cladding Thickness by Plate for each Design Configuration.

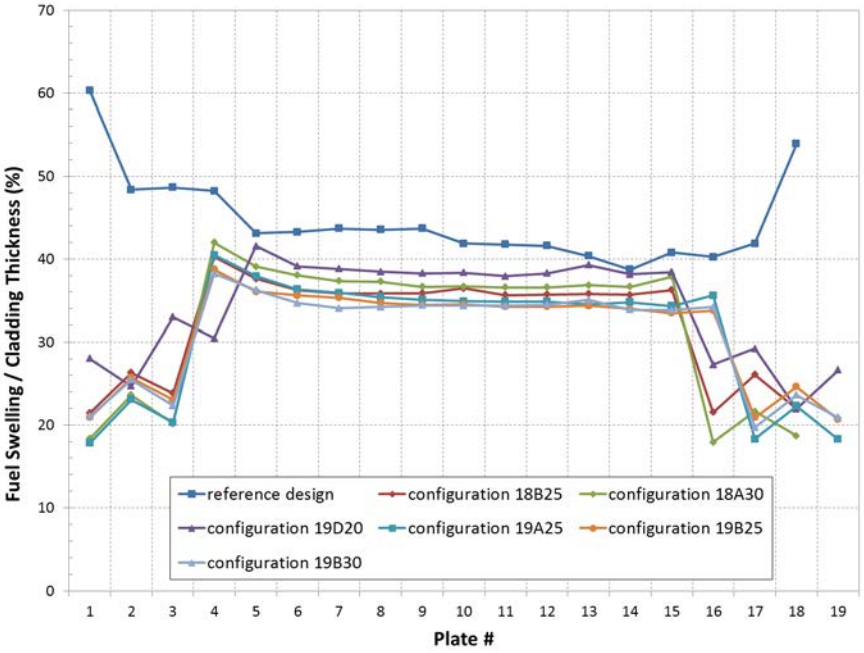

Figure 37. Maximum Fuel Meat Swelling Relative to Plate Thickness by Plate for each Design Configuration.

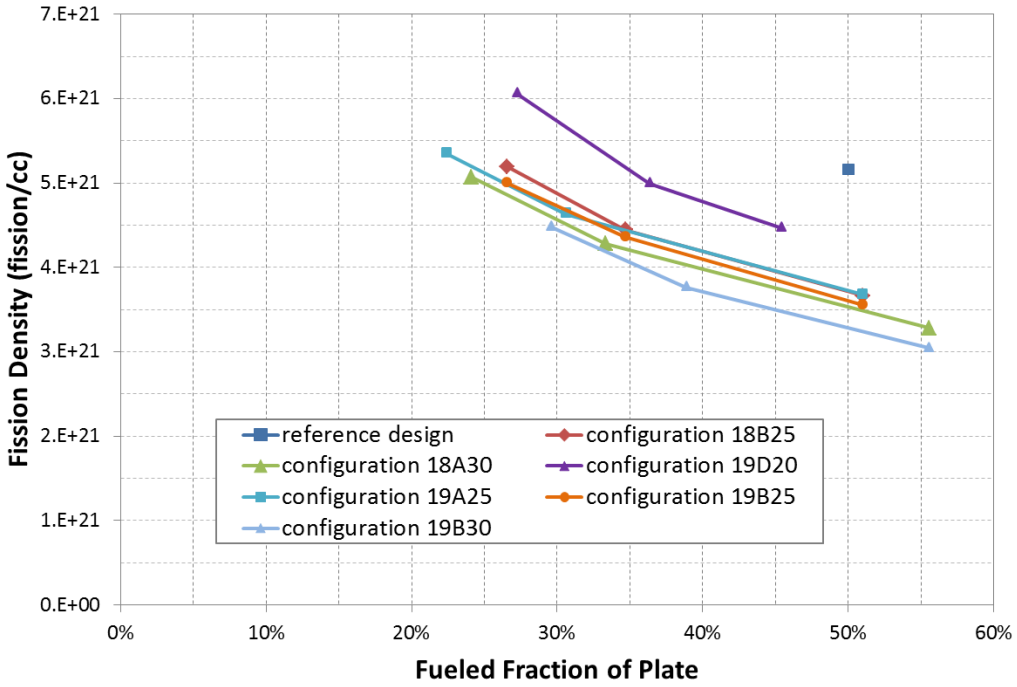

Figure 38. Maximum Fission Density vs. Fueled Fraction of Plate for each Design Configuration.

5.6 Shutdown Margins of Depleted Cores

The shutdown margins obtained for six of the nine remaining candidates is given in Table 37. The maximum uncertainty associated does not exceed 0.05% within one standard deviation. These margins are evaluated with the reactor in a cold state (10°C) with 5 blades fully inserted and one of the 6 blades and the regulating rod fully withdrawn. The limiting blade is the one that yields the smallest shutdown margin. For every case, the margins are well above the 1% Δk/k requirement.

Table 37. Shutdown Margins for Candidate LEU Configurations.

	Element Design Configuration					
	18B25	**18A30**	**19D20**	**19A25**	**19B25**	**19B30**
Δk/k (%)	2.2	3.4	2.4	3.3	3.0	3.9

6 CONCLUDING REMARKS

A summary of results obtained for the most promising LEU element design configurations with 12 mil thick cladding is shown in Table 38. Design 19B25 appears the most attractive, overall, since the analyses demonstrated the largest thermal hydraulic margin with only a small increase in core flow, and performance that matches HEU neutron flux levels within 2% by operating the LEU core at 7 MW. The 19B25 design contained 19 plates and full-thickness fuel meat of 25 mil in the interior plates of each element. The other five alternate designs demonstrated adequate, but significantly less, margin to ONB.

The 18-plate designs provided lower margin to ONB. Designs containing the thickest fuel meat (30 mil) did not demonstrate the highest margin to ONB, and required significantly more ^{235}U per element for fabrication. The designs with 30 mil thick fuel have the highest fueled thickness fraction (30 mil fuel in 54 mil plate), although this may be somewhat mitigated by having additional fuel in the core and lower fission density. Since each design has a different ^{235}U loading, and a varying degree of fuel thinning in the outer plates, more detailed results related to burnup and swelling are presented in Section 5.5.

Among the 19-plate designs, 19A25 and 19B25 are identical except for the degree of fuel thinning in the outer plates. 19B25 has the maximum ONB margin. The design 19D20 is the only design which demonstrates adequate performance with a 20 mil full-thickness fuel meat. However, the 19D20 core 188 cycle time was reduced by 4 days. Although slight, the fuel cycle of this design was the only design among the six final designs considered which required a modification to the reference LEU design fuel cycle. Also, for 19D20, as shown in Table 38, the uranium mass is approximately 20% lower than 19B25 (the design presenting the largest ONB margin among depleted cores). For this reason the ^{235}U burnup is correspondingly higher for this design. Hence, any possible benefit to fuel performance from having a lower fueled thickness fraction may be offset by additional swelling in the plate as discussed in Section 5.5.

Overall, the results of the calculations demonstrate an adequate fuel cycle including refueling on a quarterly, or less frequent, basis each year at the 7 MW LEU power required to maintain performance equivalent to 6 MW HEU operation. Several candidate LEU element designs with 12 mil cladding and no fins demonstrated sufficient margin to ONB provided core coolant flow rates can be increased, by approximately 10-20%. While this increased core coolant flow rate has been demonstrated during pre-operational tests with the current pumps, further evaluation is required. If a minimum increase in core coolant flow rate is desirable, then element design 19B25 would most easily meet safety margins. Complete safety analysis after selection of the most promising element design is also required to determine steady state core flow rates and temperatures and to finalize related uncertainty assumptions presented is this report. The performance of the LEU element design under accidents and transient scenarios also requires evaluation. The design selection will follow this report with any input available regarding fabrication from the FFC pillar, and fuel performance constraints from the FD pillar.

Fabrication input would be helpful regarding anticipated manufacturability of the designs and reasonableness of the assumed fabrication tolerances used in the safety analysis. Whereas the prior finned MITR LEU design was based upon a cladding thickness of 10 mil, recent manufacturing development experience has led to a re-evaluation of the minimum cladding thickness for reliable fabrication. In this report, all final design candidates contain 12 mil cladding on the U-10Mo fuel except the outer plates of the element where the cladding is thicker for stability. Nominal thickness of the U-

10Mo fuel foils ranges from 11-30 mil depending on the design, and plate position. For reasons of economy of fabrication it has been assumed as a constraint that there would be three distinct fuel foil thicknesses, and no more, in each element design. Thus, three distinct plates are required for proposed LEU elements. Whereas the reference LEU design had fins, all proposed plates are un-finned. The reference LEU plates were 44 mil thick (from the base of the fins). Proposed plates are 44-54 mil thick, depending on the design. Specific fabrication tolerances assumed are included in Appendix A regarding local fuel homogeneity (±10% by densitometer over 0.5 inch diameter area) and average channel tolerances as-fabricated (±4 mil interior or larger and ±12 mil end plate to outer diameter of end fitting).

Input related to fuel performance would be helpful with regards to selection among the design candidates. The fueled thickness fraction varies among the proposed designs. This, in concert with anticipated burnup (Section 5.5), and consequent fuel plate deformation, may provide a means to differentiate the designs.

With regards to future safety analysis for MITR, it should be recalled that the loading of each core remains flexible to meet experimental missions. Thus MIT analyzes the adequacy of thermal hydraulic margins prior to each core loading. The results presented for the depleted cores here are representative of current MITR fuel but do not represent conservative conditions under all conceivable fuel management operations. As a consequence, a careful analysis of the neutronic power distribution and thermal hydraulic margin for every core loading remains recommended.

Table 38. Summary of Fresh and Depleted LEU Element Design Performance.

	HEU (current design)	LEU						
		Reference design	18B25	18A30	19D20	19A25	19B25	19B30
Geometry & uranium mass								
^{235}U / U mass per element (g)	508 / 545	831 / 4210	910 / 4607	1058 / 5356	767 / 3882	940 / 4759	968 / 4900	1169 / 5917
number of plates / assembly	15	18	18	18	19	19	19	19
fins depth (mil)	10	10	no fins	no fins	no fins	no fins	no fins	no fins
plate thickness (no fins) (mil)	60	40	49	54	44	49	49	54
fuel / base clad thickness 1st plates (mil)	30 / 15	20 / 10	13 / 18	13 / 20.5	12 / 16	11 / 19	13 / 18	16 / 19
fuel / base clad thickness 2nd plates (mil)			17 / 16	18 / 18	12 / 16	15 / 17	17 / 16	21 / 16.5
fuel / base clad thickness 3rd plates (mil)			17 / 16	18 / 18	16 / 14	15 / 17	17 / 16	21 / 16.5
fuel / base clad thickness 4th plates (mil)			25 / 12	30 / 12	16 / 14	25 / 12	25 / 12	30 / 12
fuel / base clad thickness all other plates (mil)			25 / 12	30 / 12	20 /12	25 /12	25 / 12	30 / 12
end channel water gap (mil) [1]	61.5	55.5	71.5	67.2	69.9	65.7	65.7	61.4
interior channel water gap (mil) [1]	88	82	81.2	76.4	79.4	74.6	74.6	69.8
Limiting power to ONB (flow = 2200gpm) (MW) for: [2]								
22 element fresh core	n.c.	11.75	9.12	9.54	9.32	9.98	9.28	8.84
24 element fuel management sequence	n.c.	9.17	8.59	9.01	9.10	9.09	9.67	9.31
Margin to ONB (flow = 2200gpm) (MW) for: [3]								
22 element fresh core	n.c.	39%	30%	36%	33%	43%	33%	26%
24 element fuel management sequence	n.c.	9%	23%	29%	30%	30%	38%	33%
minimum flow to remain above ONB 20% margin (gpm) through 24 element fuel management sequence:	n.c.	-	2150	2040	2020	2020	1900	1970
Minimum shutdown margin Δk/k (%)								
22element fresh core	n.c.	3.1	2.4	4.0	2.4	3.7	3.4	4.6
24 element fuel management sequence	n.c.	-	2.2	3.4	2.4	3.3	3.0	3.9
Power to match HEU 6MW neutron flux performance (MW)								
22 element fresh core	-	6.9	6.9	6.8	6.9	6.8	6.8	6.8
24 element fuel management sequence at BOC [4]	-	6.80	7.08	6.99	7.11	7.02	7.00	6.96
24 element fuel management sequence at EOC [4]	-	6.99	7.11	7.06	7.27	7.22	7.16	7.09

Notes to Table 38

1) When fins are present, the dimension is the effective gap which is the average of the gap from the fin-tip to fin-tip and fin-base to fin-base.
2) Represents the minimum margin among all channels from the fuel management sequence of cores 185-190 at BOC, Xe, and EOC.
3) A 20% minimum margin to ONB is required, and is calculated with reference to a 7 MW nominal reactor power.
4) Represents the most limiting neutron flux performance from the fuel management sequence of cores 185-190 at BOC, and EOC.

ACKNOWLEDGEMENTS

The authors would like to thank U.S. Department of Energy, National Nuclear Security Administration Office of Global Threat Reduction (NA-21) for sponsoring this work. We gratefully acknowledge the expertise and knowledge of the engineering staff at both MIT and Argonne who contributed to this work. Significant recognition is due to graduate students Paul Romano and Nick Horelik of MIT who lead recent developments in the MCODE fuel management simulations, and Keng-yen Chiang who contributed to recent methods of MITR thermal hydraulic analysis. In particular Benoit Dionne, Arne Olson, John Stillman and Earl Feldman of Argonne have made many contributions towards MITR conversion that permitted this work to be accomplished, and their expertise is gratefully acknowledged. The authors are also grateful to Dr. Olson and Karen Grudzinski for valuable assistance in the preparation of this report.

REFERENCES

1. T.H. Newton, Jr., "Development of a Low Enrichment Uranium Core for the MIT Reactor," dissertation, Massachusetts Institute of Technology, Cambridge, Massachusetts, 2006.
2. T.H. Newton, Jr., E.H. Wilson, A. Bergeron, N. Horelik, and J.G. Stevens, "Neutronic Analyses for HEU to LEU Fuel Conversion of the Massachusetts Institute of Technology MITR Reactor," ANL/RERTR/TM-10-40, Argonne National Laboratory, December 2010.
3. E.H. Wilson, T.H. Newton, Jr., A. Bergeron, N. Horelik, and J.G. Stevens, "Comparison and Validation of HEU and LEU Modeling Results to HEU Experimental Benchmark Data for the Massachusetts Institute of Technology MITR Reactor," ANL/RERTR/TM-10-41, Argonne National Laboratory, December 2010.
4. L. Hu, T.H. Newton, E.H. Wilson, J.G. Stevens, "Preliminary Safety Analysis Report Methodologies and Scenarios for LEU Fuel Conversion of the MITR Reactor," MITNRL-11-01, MIT Nuclear Reactor Laboratory, Massachusetts Institute of Technology, Cambridge, Massachusetts, April 2011.
5. N.E. Horelik, "Expanding and Optimizing Fuel Management and Data Analysis Capabilities of MCODE-FM in Support of MIT Research Reactor (MITR-II) LEU Conversion," Massachusetts Institute of Technology thesis, Cambridge, Massachusetts, 2012.
6. E.H. Wilson, N. Horelik, F.E. Dunn, T.H. Newton, Jr., L. Hu, and J.G. Stevens, "Power distributions in Fresh and Depleted LEU and HEU Cores of the MITR Reactor," ANL/RERTR/TM-12-3 Revision 0, Argonne National Laboratory, February 2012.
7. L. Hu, K. Chiang, E.H. Wilson, F.E. Dunn, T.H. Newton, Jr., and J.G. Stevens, "Thermal Hydraulic Limits Analysis for LEU Fuel Conversion of the MIT Reactor," MITNRL-12-01, Massachusetts Institute of Technology, March 2012.
8. E.H. Wilson, N.E. Horelik, A. Bergeron, T.H. Newton, Jr., F. Dunn, L. Hu, J.G. Stevens, "Neutronic Modeling of the MIT Reactor LEU Conversion," Trans. Am. Nuclear Soc. 106, 1, 849-852 (2012).
9. E. Wilson, T. Newton, Jr., N. Horelik, T. Gerrity, H. Connaway, and B. Forget, "Neutronic Analysis Capabilities for Conversion of the MIT Reactor to LEU Fuel," Proceedings of the RERTR Conference, Warsaw, Poland, October 2012.
10. E.H. Wilson and F.E. Dunn, T.H. Newton, Jr. and L. Hu, "Safety Analysis of the MIT Nuclear Reactor for Conversion to LEU Fuel," Fifth International Symposium on Material Testing Reactors, Columbia, Missouri, October 2012.
11. F. E. Dunn, L. Hu, K. Chiang, E. Wilson, T. H. Newton, Jr., and J.G. Stevens, "Calculations of LSSS Limits for Use of LEU Fuel in the MITR-II Reactor," Conf. of Am. Nucl. Soc., San Diego, California, November 2012.
12. J. Roglans-Ribas, C. Landers, "Research and Test Reactor Conversion To Low Enriched Uranium Fuel: Technical And Programmatic Progress," International Conference on Research Reactors: Safe Management and Effective Utilization, Rabat, Morocco, November 2011.
13. "Reduced Enrichment for Research and Test Reactors, Meeting of U.S. High Performance Working Group, Summary" U.S. High Performance Research Reactor Working Group Meeting, Cambridge, Massachusetts, July 22-23, 2008.

14. "Safety Analysis Report for the MIT Research Reactor," MITNRL-11-02, MIT Nuclear Reactor Laboratory, Massachusetts Institute of Technology, Cambridge, Massachusetts, August 2011.
15. Z. Xu, P. Hejzlar, and M.S. Kazimi, "MCODE, Version 2.2 — An MCNP-ORIGEN Depletion Program," Center for Advanced Nuclear Systems," Massachusetts Institute of Technology, Cambridge, Massachusetts, April 2006.
16. Paul K. Romano, "Developing Fuel Management Capabilities Based on Coupled Monte Carlo Depletion in Support of the MIT Research Reactor (MITR) Conversion," Cambridge, MA, Ph.D. Thesis 2009.
17. P. Hejzlar, M. Driscoll, and M. Kazimi Z. Xu, "An Improved MCNP-ORIGEN Depletion Program (MCODE) and its Verification for High-Burnup Applications," PHYSOR, Seoul, South Korea, October 2002.
18. "MCNP - A General Monte Carlo N-Particle Transport Code, Version 5 User's Guide Manual," X-5 Monte Carlo Team, LA-UR-03-1987, Los Alamos National Laboratory, April, 2003.
19. A.G. Croff, "ORIGEN2: a Versatile Computer Code for Calculating the Nuclide Compositions and Characteristics of Nuclear Materials," Nuclear Technology, vol. 62, pp. 335-352, September 1983.
20. Y.S. Kim, and G.L. Hofman, "Fission Product Induced Swelling of U-Mo Alloy Fuel," Journal of Nuclear Materials 419 (2011) 291-301.
21. F.E. Dunn, A.P. Olson, E.H. Wilson, K. Sun, T.H. Newton, Jr., and L. Hu, "Preliminary Accident Analyses for Conversion of the Massachusetts Institute of Technology Reactor (MITR) from Highly Enriched to Low Enriched Uranium," ANL/GTRI/TM-13/5, Argonne National Laboratory, July 2013.
22. E.H. Wilson, T.H. Newton, Jr., L. Hu, and F.E. Dunn, Irradiation Experiment Conceptual Design Parameters for MITR LEU U-Mo Fuel Conversion, ANL/GTRI/TM-13/6 Argonne National Laboratory, Argonne, Illinois, June 2013.
23. The RELAP5-3D© Code Development Team, RELAP5-3D© Code Manual, Version 2.3, INEEL-EXT-98-00834, Idaho National Laboratory, April 2005.
24. E. Wilson et al., "Power Distributions in Fresh and Depleted LEU and HEU Cores of the MITR Reactor," ANL/RERTR/TM-12-3 REVISION 0, Argonne National Laboratory (2012).
25. Y. Sudo et al., "Experimental Study of Incipient Nucleate Boiling in Narrow Vertical Rectangular Channel Simulating Subchannel of Upgraded JRR-3", J. of Nuclear Science and Technology, 23[1], Jan. 1986.
26. T.C. Carnavos, "Heat Transfer Performance of Internally Finned Tubes in Turbulent Flow," Heat Transfer Engineering, 1: 4, 32-37, 1980.
27. Marvin Zelen and Norman C. Severo, Handbook of Mathematical Functions, pp. 931-933, Milton Abramowitz and Irene A. Stegun, editors, Dover Publications, New York (1965)
28. K-Y. Chiang, L.-W Hu, B. Forget, "Evaluation of Thermal Hydraulic Limits Based on Statistical Propagation of Parametric Uncertainties", RERTR 2011, Santiago, Chile, October 2011.
29. "Guidelines for Preparing and Reviewing Applications for the Licensing of Non-Power Reactors, Standard Format and Content," NUREG-1537, Part 2, U.S. Nuclear Regulatory Commission, February 1996.

APPENDICES

A. Parameters and Associated Uncertainties Used in Stat7 Analyses

Table A1. General Parameters and Associated Uncertainties Used in Stat7 Analyses.

Parameter	Nominal value	3-sigma uncertainty (%)
Reactor power (MW)	-	5
Fraction of power deposited in the core, f_c	0.965 [a]	-
Fraction of power deposited in the fuel	0.94 [a]	-
Local power	-	14.1 [b]
Pump mass flow rate (kg/s), W_p	137.0 [c]	5
Coolant height above top of the fuel plates (m)	3.05	-
Film heat transfer coefficient, h	-	20
Coolant core flow fraction, f_f	0.921	-
Plenum flow disparity factor, d_f	0.93	-
Fraction of the coolant channel flow in the stripe region, f_{sf} (accounts for neglecting the flow between the side plate and the edge of the fuel foil)	0.91	-

a) Fraction of the power deposited by region assumed to be a fixed value independent of design; however, values to be reevaluated for safety analysis of the selected design configuration.

b) The uncertainty considered in this work is 14% based upon the RMS combination of an assumed 10% uncertainty in the calculated power distribution, and a ±10% uncertainty in the local fuel homogeneity in a 0.5 inch diameter area [4].

c) Mass flow rate of 137 kg/s corresponds to 2200 gpm. Where stated other values have also been used in this study.

Table A2. Configuration Specific Parameters and Associated Uncertainties Used in Stat7 Analyses.

Configuration	Interior channel dimension [a]			End channel dimension [b]		
	Thickness (mil)	As-fabricated channel average tolerance (±mil)	3-sigma uncertainty (%)	Thickness (mil)	As-fabricated channel average tolerance (±mil)	3-sigma uncertainty with core surface uncertainty (±mil)
Ref. design finned	72.0	4.0	5.6%	50.5	12	17
Ref. design no fins	82.0	4.6	5.6%	55.5	12	17
17A30	83.7	4.6	5.6%	73.7	12	17
18A25	81.2	4.5	5.6%	71.4	12	17
18A30	76.4	4.2	5.6%	67.2	12	17
18B25	81.2	4.5	5.6%	71.4	12	17
18D20	86.0	4.8	5.6%	75.7	12	17
19A25	74.6	4.1	5.6%	65.6	12	17
19B25	74.6	4.1	5.6%	65.6	12	17
19B30	69.8	4.0	5.6%	61.4	12	17
19D20	79.4	4.4	5.6%	69.9	12	17

a) Assumed LEU interior channel tolerances are based upon the same fractional variation as specified for the HEU element which is 5.7% at 3-sigma (1.9% at 1-sigma) for all alternate element designs considered.

b) End channel thickness is defined from the end plate to outer diameter of end fitting, and tolerance as-fabricated assumed to be ±12 mil from end plate to outer diameter of end fitting as described below. End channel thickness is based on the distance from the outer plate surface to the outer dimension of the end fitting/nozzle (2.405 inch OD) as described in Section 2.1 of Reference [6]. Assumed LEU end channel tolerances are based upon assumed fabrication tolerance from the outer plate surface to the outer dimension of the end fitting/nozzle, as described in Section 2.2 of Reference [6]. Whereas Reference [6] considers that the exterior plate to nozzle outer dimension is ±0.008 inch, it has been considered more reasonable to estimate that the tolerance would be ±0.012 inch since the end fitting is welded to the element at a fabrication step after element plate and side plate assembly is completed. There is some variation in the adjacent (e.g. core structural) surfaces, which is considered to be ±0.005 inch consistent with reactor drawings [6]. Thus the total uncertainty of the end channel from the outer plate surface to the adjacent structural surface is thus assumed to be ±0.017 inch (the sum of the 0.012 inch and 0.005 inch components). Although this assumed uncertainty is large, possible variation in manufacturing should be anticipated in order to simplify fabrication constraints. Whereas, with regards to ONB, the reference LEU design was limited in the end channel, the design options presented in this report have been found to be limited on interior channels even with the large end channel uncertainties assumed uncertainty in the end channel.

B. Target Element Masses for Different Reactor Configurations

Table B1. Target Element Masses for Core Configurations: Reference LEU design to 18B25.

Element	Ring before Cores 179-190 Location	1st Insertion Location into Cores 178-190	Reference LEU	17A30	18A25	18A30	18B25
Fresh (g ^{235}U)			**831.4**	**988.5**	**882.2**	**1057.7**	**909.9**
MIT337	A/B	B7	813	970	864	1039	891
MIT300	C	C3	645	802	696	871	723
MIT347	F	F	831	989	882	1058	910
MIT345	F	F	831	989	882	1058	910
MIT356	F	F	831	989	882	1058	910
MIT341	F	F	831	989	882	1058	910
MIT331	A/B	B6	791	948	841	1017	869
MIT329	C	C15	759	916	810	986	838
MIT330	A/B	C6	808	965	858	1034	886
MIT346	F	F	831	989	882	1058	910
MIT354	F	F	831	989	882	1058	910
MIT338	A/B	B2	831	989	882	1058	910
MIT317	A/B	C13	715	872	766	942	794
MIT323	A/B	A2	777	934	827	1003	855
MIT279	C	C6	610	767	660	836	688
MIT343	F	F	831	989	882	1058	910
MIT304	C	C5	635	792	686	861	714
MIT302	C	C1	732	889	783	958	811
MIT355	F	F	831	989	882	1058	910
MIT290	C	C3	661	818	712	887	740
MIT299	C	C1	661	818	712	887	740
MIT342	F	F	831	989	882	1058	910
MIT292	C	C10	670	827	721	897	749
MIT333	A/B	C11	759	916	809	985	837
MIT327	C	C13	813	970	863	1039	891
MIT344	F	F	831	989	882	1058	910
MIT353	F	F	831	989	882	1058	910
MIT325	C	C1	791	948	842	1017	869
MIT334	A/B	B9	740	898	791	967	819
MIT282	C	C5	631	788	682	857	709
MIT303	C	C2	648	805	699	874	726
MIT301	C	C11	695	852	746	921	773
MIT294	C	C10	661	818	712	887	739
MIT335	A/B	B1	812	969	863	1038	891
MIT348	F	F	831	989	882	1058	910
MIT324	C	C7	792	949	843	1018	870
MIT322	C	C10	700	857	751	926	779
MIT295	C	C6	649	806	700	875	728

Table B1. Cont'd

Element	Ring before Cores 179-190 Location	1st Insertion Location into Cores 178-190	Reference LEU	17A30	18A25	18A30	18B25
MIT352	F	F	831	989	882	1058	910
MIT332	A/B	C4	810	967	860	1036	888
MIT297	C	C6	652	809	703	878	730
MIT293	C	C12	678	836	729	905	757
MIT326	A/B	C9	798	955	849	1024	877
MIT339	A/B	B5	831	989	882	1058	910
MIT306	C	C8	722	879	773	948	801
MIT281	C	C5	643	801	694	870	722
MIT288	C	C2	634	791	685	860	713
MIT305	C	C4	669	826	719	895	747
MIT307	C	C5	683	840	734	909	761
MIT336	A/B	B4	810	967	861	1036	888
MIT351	F	F	831	989	882	1058	910
MIT318	C	C9	715	872	765	941	793
MIT340	A/B	B8	831	989	882	1058	910
MIT328	C	C14	783	940	834	1009	862
MIT349	F	F	831	989	882	1058	910
MIT285	C	C12	590	747	641	816	669
MIT319	A/B	C3	751	908	802	977	829

Table B2. Target Element Masses for Core Configurations 18D20 to 19D20.

Element	Ring before Cores 179-190 Location	1st Insertion Location into Cores 178-190	Reference LEU	17A30	18A25	18A30	18B25
Fresh (g ^{235}U)			**720.6**	**940**	**967.7**	**1168.6**	**766.7**
MIT337	A/B	B7	702	922	949	1150	748
MIT300	C	C3	534	754	781	982	580
MIT347	F	F	721	940	968	1169	767
MIT345	F	F	721	940	968	1169	767
MIT356	F	F	721	940	968	1169	767
MIT341	F	F	721	940	968	1169	767
MIT331	A/B	B6	680	899	927	1128	726
MIT329	C	C15	648	868	896	1096	695
MIT330	A/B	C6	697	916	944	1145	743
MIT346	F	F	721	940	968	1169	767
MIT354	F	F	721	940	968	1169	767
MIT338	A/B	B2	721	940	968	1169	767
MIT317	A/B	C13	604	824	852	1052	651
MIT323	A/B	A2	666	885	913	1114	712
MIT279	C	C6	499	718	746	947	545
MIT343	F	F	721	940	968	1169	767
MIT304	C	C5	524	744	771	972	570
MIT302	C	C1	621	841	868	1069	667
MIT355	F	F	721	940	968	1169	767
MIT290	C	C3	550	770	797	998	596
MIT299	C	C1	550	770	797	998	596
MIT342	F	F	721	940	968	1169	767
MIT292	C	C10	560	779	807	1008	606
MIT333	A/B	C11	648	867	895	1096	694
MIT327	C	C13	702	921	949	1150	748
MIT344	F	F	721	940	968	1169	767
MIT353	F	F	721	940	968	1169	767
MIT325	C	C1	680	899	927	1128	726
MIT334	A/B	B9	630	849	877	1078	676
MIT282	C	C5	520	740	767	968	566
MIT303	C	C2	537	757	784	985	583
MIT301	C	C11	584	804	831	1032	630
MIT294	C	C10	550	769	797	998	596
MIT335	A/B	B1	701	921	948	1149	747
MIT348	F	F	721	940	968	1169	767
MIT324	C	C7	681	900	928	1129	727
MIT322	C	C10	589	809	836	1037	636
MIT295	C	C6	538	758	785	986	585

Table B2. Cont'd

Element	Ring before Cores 179-190 Location	1st Insertion Location into Cores 178-190	Reference LEU	17A30	18A25	18A30	18B25
MIT352	F	F	721	940	968	1169	767
MIT332	A/B	C4	699	918	946	1147	745
MIT297	C	C6	541	760	788	989	587
MIT293	C	C12	568	787	815	1016	614
MIT326	A/B	C9	687	907	934	1135	734
MIT339	A/B	B5	721	940	968	1169	767
MIT306	C	C8	611	831	858	1059	657
MIT281	C	C5	533	752	780	981	579
MIT288	C	C2	523	743	770	971	570
MIT305	C	C4	558	777	805	1006	604
MIT307	C	C5	572	791	819	1020	618
MIT336	A/B	B4	699	918	946	1147	745
MIT351	F	F	721	940	968	1169	767
MIT318	C	C9	604	823	851	1052	650
MIT340	A/B	B8	721	940	968	1169	767
MIT328	C	C14	672	892	919	1120	718
MIT349	F	F	721	940	968	1169	767
MIT285	C	C12	479	699	726	927	525
MIT319	A/B	C3	640	859	887	1088	686

C. Control Blades Heights of Depleted Cores

Table C1. Core 179 to 184 Blade Heights (cm) for Reference LEU to 18B25.

Core	EFPD	Reference LEU	17A30	18A25	18A30	18B25
Core 179	0	19.371	18.56	18.332	22.029	16.845
	1	28.015	26.887	26.907	29.284	24.671
	3	30.945	27.957	29.156	30.68	26.615
	10	30.945	28.727	30.815	31.806	27.755
	40	35.221	32.825	33.817	35.977	32.07
	47	35.221	32.825	33.817	35.977	31.074
Core 180	47	22.778	22.258	22.852	25.577	21.025
	48	31.978	29.095	30.37	32.606	28.731
	50	34.103	30.702	32.098	34.534	30.77
	57	34.423	31.78	32.951	34.534	30.77
	87	37.807	35.04	35.94	38.738	33.268
	94	37.807	35.04	37.55	38.738	34.051
Core 181	94	24.126	23.386	23.252	25.777	21.891
	95	34.262	30.729	30.762	33.78	29.92
	97	35.494	31.744	34.648	35.244	31.677
	104	35.494	33.474	34.648	36.129	32.813
	134	38.529	35.324	38.993	38.384	35.808
	141	39.55	37.046	38.993	40.287	36.965
Core 182	141	27.624	25.604	26.345	28.998	24.842
	142	38.139	33.251	35.797	37.428	32.943
	144	41.034	36.827	38.437	40.629	36.91
	151	42.305	36.827	39.206	40.629	36.91
	176	47.615	41.004	42.728	44.7	40.271
Core 183	176	27.918	25.51	26.48	28.749	24.664
	177	38.252	32.851	34.753	37.611	33.786
	179	39.858	36.16	38.394	39.339	35.424
	186	40.809	36.16	39.15	39.339	37.303
	223	47.123	41.439	44.047	44.741	41.077
Core 184	223	27.826	26.536	26.816	29.527	25.089
	224	39.483	34.657	37.144	38.459	33.401
	226	39.483	37.019	39.388	39.771	37.402
	233	41.525	38.653	40.301	41.582	38
	263	46.465	41.817	45.304	44.788	40.637
	270	49.012	42.35	45.304	47.889	42.399

Table C2. Core 185 to 190 Blade Heights (cm) for Reference LEU to 18B25.

Core	EFPD	Reference LEU	17A30	18A25	18A30	18B25
Core 185	270	27.764	25.606	25.358	28.429	24.482
	271	36.834	33.068	35.43	36.543	32.33
	273	40.122	36.208	38.906	40.172	36.78
	280	40.893	36.964	39.925	41.023	36.304
	310	48.447	41.586	44.083	45.85	41.975
	317	48.447	42.729	44.083	46.525	41.975
Core 186	317	27.586	26.566	26.658	30.014	25.056
	318	36.693	34.258	36.156	36.836	33.271
	320	42.286	37.202	41.162	41.041	36.839
	327	42.286	38.96	41.162	41.041	37.526
	357	47.766	40.453	43.319	46.111	40.91
	364	49.765	41.982	44.333	46.111	41.499
Core 187	364	25.28	24.349	25.75	27.734	23.225
	365	34.619	31.678	34.548	35.057	31.744
	367	37.654	35.84	36.059	38.634	34.419
	374	38.639	35.84	37.783	38.634	35.441
	404	43.838	39.311	42.427	42.519	37.796
	411	43.838	39.311	42.427	42.519	38.716
Core 188	411	29.016	27.549	28.332	31.345	26.809
	412	39.707	35.955	38.356	40.564	34.913
	414	42.8	38.246	42.224	41.598	38.306
	421	42.8	39.914	42.224	41.598	38.306
	451	49.022	43.454	47.937	48.895	43.859
	458	50.868	44.08	48.804	49.665	43.263
Core 189	458	24.07	23.605	23.235	26.222	22.623
	459	32.714	29.714	32.755	33.645	28.574
	461	35.553	32.462	34.459	35.31	31.395
	468	36.797	32.462	35.332	36.526	33.246
	498	40.708	36.96	39.902	39.938	36.817
	505	43.001	36.96	39.902	41.056	36.817
Core 190	505	26.668	25.291	26.01	28.797	25.078
	506	37.454	33.869	34.815	36.696	33.271
	508	40.768	36.494	37.816	39.934	35.446
	515	40.768	36.494	39.622	39.934	36.73
	545	44.294	40.749	43.813	43.778	40.543
	552	44.294	40.749	43.813	43.778	40.543

Table C3. Core 179 to 184 Blade Heights (cm) for 18D20 to 19D20.

Core	EFPD	18D20	19A25	19B25	19B30	19D20
Core 179	0	16.299	22.086	20.173	24.132	18.703
	1	25.051	29.435	26.978	31.096	25.845
	3	27.596	31.223	29.535	32.653	29.374
	10	27.596	32.894	29.535	33.39	30.271
	40	32.675	36.009	34.355	36.797	35.377
	47	32.675	36.716	35.045	36.797	35.377
Core 180	47	20.154	25.602	23.953	27.288	22.146
	48	29.986	32.966	30.572	34.147	32.322
	50	31.57	35.353	32.95	35.259	33.282
	57	32.602	36.606	33.945	36.58	34.054
	87	35.523	40.005	37.797	39.679	38.715
	94	37.631	40.005	37.797	39.679	38.715
Core 181	94	21.074	25.717	23.88	27.806	23.119
	95	30.754	34.511	32.132	34.12	31.857
	97	32.03	35.804	34.279	37.29	35.3
	104	34.231	37.73	35.385	38.198	35.3
	134	36.402	43.091	37.877	41.194	40.278
	141	37.841	43.091	40.304	41.194	40.278
Core 182	141	24.137	28.36	27.607	30.952	26.135
	142	35.782	38.802	35.944	37.976	36.787
	144	38.97	41.473	40.061	41.341	41.495
	151	38.97	42.248	40.061	42.04	41.495
	176	44.276	47.052	43.471	45.641	47.92
Core 183	176	23.893	29.028	27.474	30.574	26.407
	177	35.675	38.894	36.136	38.776	36.998
	179	38.353	40.464	39.069	42.265	40.681
	186	38.353	42.998	39.069	42.265	40.681
	216	45.704	48.078	45.366	46.862	47.497
Core 184	223	46.428	49.055	45.366	46.862	47.497
	223	25.512	29.435	28.363	31.438	27.022
	224	36.281	40.046	36.238	39.016	37.905
	226	40.269	42.408	41.54	41.647	41.881
	233	40.269	43.494	41.54	42.372	41.881
	263	44.744	49.54	46.158	46.294	48.655

Table C4. Core 185 to 190 Blade Heights (cm) for 18D20 to 19D20.

Core	EFPD	18D20	19A25	19B25	19B30	19D20[a]
Core 185	270	24.425	28.359	27.349	30.428	25.746
	271	34.974	39.195	36.689	38.355	37.412
	273	37.923	40.682	38.272	41.458	40.067
	280	39.251	43.617	39.065	41.458	40.067
	310	45.169	50.324	46.186	46.966	48.889
	317	48.688	51.198	46.186	46.966	50.385
Core 186	317	18D20	19A25	19B25	19B30	19D20
	318	24.499	29.11	28.7	31.288	26.271
	320	36.844	38.989	36.222	39.969	39.176
	327	39.081	43.423	40.978	41.949	41.14
	357	40.289	44.188	40.978	42.881	41.14
	364	45.305	49.523	44.591	46.238	45.751
Core 187	364	45.305	51.571	45.537	46.238	51.211
	365	22.218	27.013	26.104	29.257	23.696
	367	32.813	37.515	34.485	35.396	34.366
	374	36.355	38.637	36.756	38.886	38.457
	404	36.355	40.37	38.596	39.874	38.457
	411	42.354	45.921	42.487	42.831	42.985
Core 188	411	42.354	45.921	42.487	42.831	44.255
	412	26.283	30.302	29.531	32.322	27.647
	414	38.495	40.123	37.79	39.88	38.469
	421	39.855	45.72	41.604	44.557	44.097
	451	42.167	45.72	41.604	44.557	44.919
	458[a]	49.709	52.717	46.958	48.023	52.004
Core 189	458	49.709	52.717	46.958	50.121	52.004
	459	21.603	26.3	24.845	28.217	22.652
	461	30.927	34.874	32.658	35.061	32.888
	468	32.723	36.881	34.201	36.954	34.637
	498	33.814	38.45	35.183	38.683	35.76
	505	38.37	41.819	40.298	42.231	40.57
Core 190	505	40.337	42.761	41.16	42.231	41.676
	506	23.889	28.688	27.579	30.883	26.684
	508	35.772	39.373	36.188	39.118	37.699
	515	37.54	40.593	38.337	40.372	39.787
	545	38.368	42.084	40.439	41.425	39.787
	552	44.194	46.564	43.728	45.143	46.859

a) 19D20 core 188 was ended at 454 EFPD due to limited reactivity.

Table C5. Core 185-190 Average Change in Blade Height for BOC and EOC.

	Average BOC Delta Blade Height vs. Prior Core	Average EOC Delta Blade Height vs. Prior Core
Reference LEU Design	-0.2	-0.4
17A30	-0.2	-0.3
18A25	-0.1	-0.2
18A30	-0.1	-0.7
18B25	0.0	-0.3
18D20	-0.3	-0.6
19A25	-0.1	-0.4
19B25	-0.1	-0.1
19B30	-0.1	-0.2
19D20	-0.1	-0.3

Note: Designs 18C25 and 19B20 were dropped since unable to maintain criticality through the series of fuel management representative cores.

D. Peak Heat Flux of Depleted Cores

Table D1. Peak Heat Flux for Cores 185-190 for Reference LEU Design.

Core	Core State	Heat Flux (W/cm2)			
		Peak Spot	Peak Stripe	Peak Plate	Peak Element
185	BOC	71.8	50.2	47.8	35.3
	Xe. Eq.	69.7	55.1	48.1	33.9
	EOC	67.3	56.3	50.1	33.2
186	BOC	70.6	48.8	46.5	34.8
	Xe. Eq.	68.5	54.2	47.7	33.2
	EOC	65.5	54.9	49.9	32.6
187	BOC	73.6	49.7	46.3	34.4
	Xe. Eq.	73.2	55.2	50.1	32.9
	EOC	70.3	56.2	51.7	32.2
188	BOC	73.6	49.4	45	33.6
	Xe. Eq.	70.2	53.9	49.6	32.2
	EOC	67.8	54.4	51.8	31.7
189	BOC	75.4	49.5	44.4	35.7
	Xe. Eq.	74.2	55.6	48.4	34.1
	EOC	71.6	57.7	51	33.4
190	BOC	73	49.6	43.4	35.2
	Xe. Eq.	71.1	56.2	49.4	33.5
	EOC	69.5	56.1	49.7	33.2

Table D2. Peak Heat Flux for Cores 185-190 for Design 18A30.

Core	Core State	Heat Flux (W/cm2)			
		Peak Spot	Peak Stripe	Peak Plate	Peak Element
185	BOC	57.7	47.4	42.9	34.9
	Xe. Eq.	56.7	45.6	41	33.5
	EOC	55.8	45.1	40.3	33
186	BOC	56.6	46.5	41.7	34.3
	Xe. Eq.	55.2	44.9	40.1	33.2
	EOC	54.5	44.3	39.7	32.7
187	BOC	58.9	47	41.4	33.9
	Xe. Eq.	57.4	45.4	39.7	32.7
	EOC	56.8	44.9	39.4	32.3
188	BOC	57.5	45.9	40.6	33.3
	Xe. Eq.	56.2	44.7	39.4	32.3
	EOC	55	45.2	38.7	31.8
189	BOC	59.2	49.4	42.4	35.1
	Xe. Eq.	57.8	47.7	40.9	33.9
	EOC	57.6	46.9	40.3	33.3
190	BOC	58.5	48.2	41.9	34.6
	Xe. Eq.	55.9	46.5	40.3	33.4
	EOC	56.8	46	39.9	33

Table D3. Peak Heat Flux for Cores 185-190 for Design 18B25.

Core	Core State	Heat Flux (W/cm2)			
		Peak Spot	Peak Stripe	Peak Plate	Peak Element
185	BOC	54.7	46.6	42.3	35.6
	Xe. Eq.	52.9	44.9	40.3	34
	EOC	51.9	44	39.5	33.5
186	BOC	54	45.7	41.1	35.1
	Xe. Eq.	51.6	43.8	39.3	33.7
	EOC	51.5	43.2	38.7	33.2
187	BOC	53.7	46	40.7	34.7
	Xe. Eq.	53.6	44.1	38.9	33.2
	EOC	53.1	43.7	38.4	32.7
188	BOC	53.8	45	39.9	34
	Xe. Eq.	52.3	43.4	38.4	32.6
	EOC	51.7	42.8	37.8	32.1
189	BOC	55.9	48.6	41.5	35.8
	Xe. Eq.	54.6	46.6	40	34.6
	EOC	54.2	45.8	39.3	33.9
190	BOC	54.4	47.4	40.9	35.3
	Xe. Eq.	53.6	45.6	39.2	33.9
	EOC	52.9	44.7	38.7	33.4

Table D4. Peak Heat Flux for Cores 185-190 for Design 19A25.

Core	Core State	Heat Flux (W/cm2)			
		Peak Spot	Peak Stripe	Peak Plate	Peak Element
185	BOC	54.5	45	41.3	33.1
	Xe. Eq.	52.9	43.3	39.6	31.8
	EOC	50.7	42.4	38.6	31.1
186	BOC	52.5	44.1	40.2	32.7
	Xe. Eq.	50.4	42.2	38.3	31.3
	EOC	50.1	41.6	37.8	30.8
187	BOC	53.9	44.6	39.7	32.3
	Xe. Eq.	53.6	42.7	38.2	31
	EOC	52.6	42.2	37.4	30.4
188	BOC	54.1	43.8	39.1	31.7
	Xe. Eq.	52.5	41.9	37.3	30.3
	EOC	50.9	42.2	36.9	29.9
189	BOC	56	47	40.5	33.3
	Xe. Eq.	54.3	45.1	38.9	32.1
	EOC	53.9	44.2	38.2	31.5
190	BOC	54.8	45.8	39.8	32.8
	Xe. Eq.	53.6	44.1	38.3	31.6
	EOC	52.8	43.1	37.6	31

Table D5. Peak Heat Flux for Cores 185-190 for Design 19B25.

Core	Core State	Heat Flux (W/cm2)			
		Peak Spot	Peak Stripe	Peak Plate	Peak Element
185	BOC	52.5	43.5	39.6	33.3
	Xe. Eq.	50.7	42	37.9	32
	EOC	50.2	41	37.1	31.4
186	BOC	51.3	42.2	38.3	32.7
	Xe. Eq.	49.5	40.8	36.8	31.4
	EOC	49.5	40.6	36.4	31
187	BOC	52.4	42.7	38	32.4
	Xe. Eq.	51.8	41.2	36.6	31.2
	EOC	51.5	40.5	36.1	30.7
188	BOC	52.1	41.9	37.4	31.8
	Xe. Eq.	50.2	40.5	36	30.6
	EOC	50	40.4	35.5	30.2
189	BOC	53.7	45.1	38.9	33.6
	Xe. Eq.	53.7	43.4	37.5	32.4
	EOC	52.3	42.5	36.9	31.7
190	BOC	52.9	44	38.4	33
	Xe. Eq.	51.4	42.3	36.9	31.8
	EOC	51	41.7	36.2	31.2

Table D6. Peak Heat Flux for Cores 185-190 for Design 19B30.

Core	Core State	Heat Flux (W/cm2)			
		Peak Spot	Peak Stripe	Peak Plate	Peak Element
185	BOC	58	42.1	37.8	32.7
	Xe. Eq.	55.7	44.4	38.5	31.6
	EOC	54.3	45	39.3	31.1
186	BOC	55.4	41.3	37.1	32.2
	Xe. Eq.	53.5	42.6	37.1	31.2
	EOC	51.7	42.5	37.9	30.9
187	BOC	58.2	41.6	36.8	32
	Xe. Eq.	56.6	43.9	38.3	30.9
	EOC	55	44.2	38.8	30.6
188	BOC	52.2	43.1	39.9	30
	Xe. Eq.	54.5	43.2	39.4	30.3
	EOC	52.2	43.1	39.9	30
189	BOC	60.9	43.4	37.7	32.9
	Xe. Eq.	59.2	44.9	38.6	31.9
	EOC	57.3	45.8	39.8	31.4
190	BOC	58.7	42.5	37.3	32.4
	Xe. Eq.	57	44.7	38.8	31.5
	EOC	54.7	45.5	39.8	31

Table D7. Peak Heat Flux for Cores 185-190 for Design 19D20.

Core	Core State	Heat Flux (W/cm2)			
		Peak Spot	Peak Stripe	Peak Plate	Peak Element
185	BOC	50.7	43.1	38.5	33.7
	Xe. Eq.	49.2	41.2	36.5	32.1
	EOC	48.1	40.6	35.8	31.4
186	BOC	50.3	42.2	37.3	33.1
	Xe. Eq.	49.8	40.3	35.4	31.5
	EOC	47.1	39.3	36.3	30.9
187	BOC	52.9	42.5	36.8	32.7
	Xe. Eq.	52.4	40.4	35.4	31
	EOC	50.4	39.6	36.7	30.5
188	BOC	53.1	41.6	36.2	32
	Xe. Eq.	50.6	39.4	36.4	30.4
	EOC	47.7	39.2	37.7	29.9
189	BOC	52.7	45	37.8	34
	Xe. Eq.	52.6	43.1	36	32.4
	EOC	50.8	41.9	35.5	31.8
190	BOC	50.8	43.7	37	33.2
	Xe. Eq.	49.6	41.6	35.3	31.8
	EOC	48.6	41.2	35.3	31.2

Table D8. Peak to Core Average Heat Flux or Cores 185-190 for Reference LEU Design.

Core	Core State	Peak/Core Average			
		Peak Spot	Peak Stripe	Peak Plate	Peak Element
185	BOC	2.663	1.863	1.772	1.31
	Xe. Eq.	2.587	2.044	1.783	1.257
	EOC	2.495	2.09	1.858	1.232
186	BOC	2.62	1.811	1.727	1.291
	Xe. Eq.	2.543	2.01	1.771	1.231
	EOC	2.429	2.035	1.851	1.209
187	BOC	2.732	1.845	1.719	1.274
	Xe. Eq.	2.716	2.047	1.859	1.219
	EOC	2.607	2.085	1.919	1.196
188	BOC	2.731	1.831	1.668	1.248
	Xe. Eq.	2.604	2	1.84	1.194
	EOC	2.515	2.019	1.921	1.176
189	BOC	2.797	1.837	1.648	1.325
	Xe. Eq.	2.751	2.063	1.797	1.266
	EOC	2.657	2.14	1.891	1.239
190	BOC	2.707	1.84	1.608	1.305
	Xe. Eq.	2.637	2.083	1.834	1.243
	EOC	2.577	2.08	1.844	1.23

Table D9. Peak to Core Average Heat Flux or Cores 185-190 for Design 18A30.

Core	Core State	Peak/Core Average			
		Peak Spot	Peak Stripe	Peak Plate	Peak Element
185	BOC	2.14	1.758	1.59	1.293
	Xe. Eq.	2.103	1.693	1.522	1.243
	EOC	2.069	1.674	1.496	1.224
186	BOC	2.101	1.723	1.545	1.273
	Xe. Eq.	2.049	1.665	1.489	1.23
	EOC	2.023	1.642	1.472	1.214
187	BOC	2.186	1.742	1.534	1.259
	Xe. Eq.	2.13	1.684	1.473	1.214
	EOC	2.106	1.666	1.461	1.2
188	BOC	2.133	1.704	1.505	1.237
	Xe. Eq.	2.084	1.656	1.461	1.197
	EOC	2.042	1.675	1.434	1.178
189	BOC	2.196	1.831	1.572	1.302
	Xe. Eq.	2.146	1.769	1.518	1.259
	EOC	2.136	1.74	1.493	1.237
190	BOC	2.171	1.788	1.553	1.284
	Xe. Eq.	2.075	1.726	1.494	1.237
	EOC	2.108	1.708	1.479	1.224

Table D10. Peak to Core Average Heat Flux or Cores 185-190 for Design 18B25.

Core	Core State	Peak/Core Average			
		Peak Spot	Peak Stripe	Peak Plate	Peak Element
185	BOC	2.03	1.73	1.57	1.321
	Xe. Eq.	1.961	1.664	1.496	1.262
	EOC	1.924	1.633	1.466	1.243
186	BOC	2.004	1.697	1.523	1.303
	Xe. Eq.	1.914	1.624	1.459	1.249
	EOC	1.909	1.603	1.436	1.231
187	BOC	1.992	1.707	1.508	1.286
	Xe. Eq.	1.989	1.637	1.443	1.231
	EOC	1.968	1.62	1.426	1.212
188	BOC	1.995	1.67	1.479	1.26
	Xe. Eq.	1.941	1.61	1.424	1.21
	EOC	1.917	1.587	1.401	1.192
189	BOC	2.073	1.804	1.54	1.329
	Xe. Eq.	2.025	1.73	1.484	1.284
	EOC	2.011	1.698	1.459	1.259
190	BOC	2.019	1.757	1.518	1.309
	Xe. Eq.	1.989	1.691	1.454	1.259
	EOC	1.962	1.657	1.434	1.238

Table D11. Peak to Core Average Heat Flux or Cores 185-190 for Design 19A25.

Core	Core State	Peak/Core Average			
		Peak Spot	Peak Stripe	Peak Plate	Peak Element
185	BOC	2.136	1.764	1.619	1.297
	Xe. Eq.	2.07	1.694	1.549	1.247
	EOC	1.987	1.662	1.511	1.22
186	BOC	2.057	1.728	1.572	1.28
	Xe. Eq.	1.972	1.652	1.499	1.225
	EOC	1.96	1.627	1.478	1.205
187	BOC	2.109	1.746	1.555	1.263
	Xe. Eq.	2.097	1.672	1.494	1.213
	EOC	2.061	1.653	1.466	1.191
188	BOC	2.119	1.715	1.53	1.242
	Xe. Eq.	2.054	1.641	1.462	1.187
	EOC	1.992	1.653	1.445	1.171
189	BOC	2.192	1.842	1.585	1.305
	Xe. Eq.	2.128	1.766	1.523	1.256
	EOC	2.111	1.731	1.496	1.235
190	BOC	2.146	1.793	1.558	1.285
	Xe. Eq.	2.099	1.726	1.501	1.237
	EOC	2.066	1.689	1.472	1.215

Table D12. Peak to Core Average Heat Flux or Cores 185-190 for Design 19B25.

Core	Core State	Peak/Core Average			
		Peak Spot	Peak Stripe	Peak Plate	Peak Element
185	BOC	2.055	1.705	1.552	1.302
	Xe. Eq.	1.986	1.644	1.483	1.253
	EOC	1.967	1.606	1.451	1.228
186	BOC	2.007	1.651	1.5	1.282
	Xe. Eq.	1.939	1.599	1.442	1.231
	EOC	1.937	1.589	1.426	1.216
187	BOC	2.052	1.673	1.489	1.269
	Xe. Eq.	2.026	1.614	1.435	1.221
	EOC	2.015	1.586	1.415	1.202
188	BOC	2.039	1.642	1.463	1.246
	Xe. Eq.	1.965	1.584	1.409	1.198
	EOC	1.956	1.582	1.391	1.184
189	BOC	2.102	1.766	1.525	1.315
	Xe. Eq.	2.104	1.697	1.47	1.267
	EOC	2.047	1.665	1.443	1.241
190	BOC	2.072	1.722	1.504	1.294
	Xe. Eq.	2.013	1.656	1.444	1.246
	EOC	1.998	1.631	1.419	1.222

Table D13. Peak to Core Average Heat Flux or Cores 185-190 for Design 19B30.

Core	Core State	Peak/Core Average			
		Peak Spot	Peak Stripe	Peak Plate	Peak Element
185	BOC	2.269	1.647	1.48	1.28
	Xe. Eq.	2.182	1.74	1.506	1.236
	EOC	2.125	1.761	1.539	1.219
186	BOC	2.168	1.618	1.453	1.262
	Xe. Eq.	2.095	1.667	1.453	1.222
	EOC	2.024	1.666	1.484	1.209
187	BOC	2.279	1.629	1.443	1.252
	Xe. Eq.	2.217	1.719	1.5	1.211
	EOC	2.155	1.729	1.519	1.198
188	BOC	2.045	1.689	1.562	1.176
	Xe. Eq.	2.132	1.692	1.543	1.188
	EOC	2.045	1.689	1.562	1.176
189	BOC	2.383	1.7	1.478	1.287
	Xe. Eq.	2.319	1.757	1.512	1.25
	EOC	2.245	1.792	1.557	1.231
190	BOC	2.299	1.665	1.459	1.269
	Xe. Eq.	2.232	1.752	1.519	1.232
	EOC	2.141	1.78	1.56	1.213

Table D14. Peak to Core Average Heat Flux or Cores 185-190 for Design 19D20.

Core	Core State	Peak/Core Average			
		Peak Spot	Peak Stripe	Peak Plate	Peak Element
185	BOC	1.985	1.686	1.507	1.318
	Xe. Eq.	1.926	1.613	1.43	1.256
	EOC	1.882	1.588	1.402	1.228
186	BOC	1.971	1.652	1.46	1.298
	Xe. Eq.	1.949	1.577	1.386	1.233
	EOC	1.846	1.54	1.423	1.208
187	BOC	2.07	1.662	1.441	1.28
	Xe. Eq.	2.05	1.582	1.388	1.213
	EOC	1.974	1.551	1.437	1.195
188	BOC	2.079	1.627	1.418	1.251
	Xe. Eq.	1.981	1.543	1.425	1.19
	EOC	1.868	1.536	1.476	1.172
189	BOC	2.064	1.762	1.48	1.331
	Xe. Eq.	2.059	1.686	1.411	1.27
	EOC	1.991	1.642	1.391	1.245
190	BOC	1.989	1.711	1.448	1.3
	Xe. Eq.	1.944	1.629	1.383	1.244
	EOC	1.904	1.615	1.382	1.222

Table D15. Relative Difference in Maximum Heat Flux between Reference LEU design [6] and Re-calculated Results.

Core	Relative Difference in Heat Flux (%)[1]			
	Peak Spot	Peak Stripe	Peak Plate	Peak Element
185-BOC	0.3%	-0.4%	-0.2%	-0.3%
185-EOC	1.1%	0.0%	0.0%	0.0%
186-BOC	0.0%	0.4%	0.2%	0.3%
186-EOC	-0.8%	1.1%	2.7%	-0.6%
187-BOC	-0.9%	-0.8%	0.2%	0.3%
187-EOC	-1.1%	0.0%	0.0%	-0.3%
188-BOC	0.1%	-0.2%	0.2%	0.0%
188-EOC	1.6%	0.0%	-0.2%	0.0%
189-BOC	-1.6%	-0.4%	0.0%	0.0%
189-EOC	-0.8%	0.9%	1.4%	-0.6%
190-BOC	-0.7%	-1.2%	0.5%	0.3%
190-EOC	1.0%	-0.7%	-0.8%	0.3%

1) This table compares for the finned reference LEU design the peak heat flux values in various regions as reported in Reference [6] to values re-calculated in this work.

E. Performance of Depleted Cores

Table E1. Performance of Six Final Element Design Candidates for Cores 185-190 at BOC.

		LEU 7 MW Performance vs. HEU 6 MW Performance					Power for Performance Equivalent to HEU (MW)
Core	Element Design	In-Core Irradiation (A2)	Twelve-inch Beam Port	Two-inch Pneumatic Facility	Fission Converter Window	Below-core Thermal Beam Facility	
185	18A30	105.5%	101.9%	102.6%	102.3%	100.9%	6.94
186	18A30	105.3%	100.9%	103.5%	103.2%	100.1%	6.99
187	18A30	105.5%	101.6%	103.7%	103.4%	101.5%	6.89
188	18A30	105.2%	100.9%	103.2%	102.7%	100.0%	7.00
189	18A30	104.8%	102.3%	104.0%	103.6%	100.7%	6.95
190	18A30	106.1%	101.2%	102.7%	103.9%	100.1%	6.99
185	18B25	105.0%	100.1%	100.1%	100.1%	99.8%	7.01
186	18B25	105.2%	99.6%	101.6%	101.4%	99.7%	7.03
187	18B25	105.3%	99.4%	100.8%	100.8%	100.2%	7.04
188	18B25	104.9%	99.7%	101.2%	101.1%	99.5%	7.04
189	18B25	104.0%	99.5%	100.8%	100.8%	98.6%	7.10
190	18B25	105.4%	99.2%	99.9%	101.7%	98.9%	7.08
185	19A25	105.4%	101.7%	102.4%	102.2%	100.6%	6.96
186	19A25	105.7%	100.9%	103.7%	103.4%	100.4%	6.97
187	19A25	105.6%	101.5%	103.4%	103.2%	101.4%	6.90
188	19A25	105.6%	101.2%	103.3%	102.9%	100.4%	6.97
189	19A25	104.5%	101.4%	103.6%	103.1%	100.1%	6.99
190	19A25	105.9%	101.0%	102.1%	103.5%	99.8%	7.02
185	19B25	105.3%	101.2%	102.0%	101.9%	100.8%	6.94
186	19B25	105.2%	100.7%	103.0%	102.9%	100.1%	6.99
187	19B25	105.5%	101.3%	103.1%	102.8%	101.4%	6.91
188	19B25	105.2%	101.0%	102.7%	102.4%	100.1%	6.99
189	19B25	104.5%	101.5%	103.1%	102.7%	100.2%	6.99
190	19B25	105.9%	100.7%	101.6%	103.4%	99.9%	7.00
185	19B30	105.5%	102.5%	103.9%	103.6%	101.4%	6.91
186	19B30	105.8%	102.1%	104.6%	104.4%	101.0%	6.93
187	19B30	105.9%	102.9%	104.8%	104.6%	102.2%	6.85
188	19B30	105.8%	102.4%	104.3%	103.6%	101.1%	6.93
189	19B30	105.0%	103.1%	105.5%	104.8%	101.4%	6.90
190	19B30	106.1%	102.0%	103.4%	104.9%	100.6%	6.96
185	19D20	105.2%	99.9%	99.9%	100.4%	99.4%	7.04
186	19D20	105.2%	99.4%	101.8%	101.7%	99.5%	7.04
187	19D20	105.3%	99.7%	101.2%	101.3%	100.0%	7.02
188	19D20	105.0%	99.9%	101.3%	101.1%	99.5%	7.04
189	19D20	104.6%	99.4%	100.7%	100.6%	98.5%	7.11
190	19D20	105.3%	99.0%	99.7%	101.3%	98.4%	7.11

Table E2. Performance of Six Final Element Design Candidates for Cores 185-190 at EOC.

		LEU 7 MW Performance vs. HEU 6 MW Performance					Power for Performance Equivalent to HEU (MW)
Core	Element Design	In-Core Irradiation (A2)	Twelve-inch Beam Port	Two-inch Pneumatic Facility	Fission Converter Window	Below-core Thermal Beam Facility	
185	18A30	105.5%	100.0%	101.9%	102.8%	100.8%	7.00
186	18A30	106.2%	102.2%	103.7%	104.4%	103.1%	6.85
187	18A30	106.1%	101.6%	103.3%	103.9%	102.1%	6.89
188	18A30	104.7%	99.1%	101.0%	101.7%	99.2%	7.06
189	18A30	105.2%	100.0%	101.6%	102.3%	100.0%	7.00
190	18A30	105.8%	99.1%	101.3%	102.5%	99.4%	7.06
185	18B25	105.7%	99.9%	101.4%	102.4%	100.9%	7.01
186	18B25	106.2%	101.8%	103.4%	104.0%	103.4%	6.88
187	18B25	105.7%	100.8%	102.6%	103.3%	102.2%	6.95
188	18B25	105.0%	99.4%	100.9%	101.9%	99.9%	7.04
189	18B25	105.2%	99.7%	100.8%	101.7%	100.3%	7.02
190	18B25	105.2%	98.4%	99.7%	101.7%	98.9%	7.11
185	19A25	104.7%	98.5%	100.6%	101.4%	98.9%	7.11
186	19A25	104.9%	100.4%	102.2%	102.8%	101.0%	6.97
187	19A25	105.0%	100.0%	102.4%	102.5%	100.4%	7.00
188	19A25	104.1%	98.4%	100.3%	101.1%	98.1%	7.13
189	19A25	104.9%	99.3%	100.9%	101.7%	99.1%	7.07
190	19A25	104.3%	97.5%	99.3%	101.0%	97.0%	7.22
185	19B25	105.4%	99.8%	101.7%	102.6%	100.4%	7.01
186	19B25	106.0%	101.9%	103.6%	104.1%	102.9%	6.87
187	19B25	105.7%	100.8%	103.3%	103.4%	101.6%	6.95
188	19B25	104.9%	99.8%	101.3%	101.9%	99.8%	7.01
189	19B25	104.5%	99.5%	101.0%	101.6%	99.2%	7.06
190	19B25	104.5%	97.8%	99.9%	101.5%	97.8%	7.16
185	19B30	105.9%	101.1%	103.3%	103.6%	101.6%	6.92
186	19B30	106.9%	103.0%	104.5%	105.4%	104.1%	6.80
187	19B30	106.5%	102.5%	104.6%	104.7%	103.2%	6.83
188	19B30	109.3%	106.2%	106.3%	107.4%	109.3%	6.59
189	19B30	105.3%	100.6%	102.5%	103.0%	100.5%	6.97
190	19B30	105.0%	98.9%	100.7%	102.5%	98.7%	7.09
185	19D20	104.2%	97.3%	98.8%	100.2%	97.5%	7.19
186	19D20	103.9%	98.7%	101.1%	101.6%	99.4%	7.09
187	19D20	104.5%	98.9%	101.3%	101.8%	99.5%	7.08
188	19D20	103.4%	97.2%	99.0%	99.6%	96.8%	7.23
189	19D20	103.9%	97.9%	99.7%	100.3%	97.7%	7.16
190	19D20	103.7%	96.6%	98.3%	100.0%	96.3%	7.27

F. Fission Density of Depleted Cores

Table F1. Maximum Local Fission Density by Plate of Six Final Element Design Candidates (fission/cc).

Plate	Reference LEU Design	18A30	18B25	19A25	19B25	19B30	19D20
1	5.2E+21	5.0E+21	5.1E+21	5.2E+21	5.0E+21	4.5E+21	6.1E+21
2	4.4E+21	4.3E+21	4.4E+21	4.6E+21	4.4E+21	3.8E+21	5.5E+21
3	4.4E+21	3.8E+21	4.1E+21	4.2E+21	4.0E+21	3.4E+21	5.0E+21
4	4.4E+21	3.3E+21	3.7E+21	3.7E+21	3.6E+21	3.0E+21	4.7E+21
5	4.0E+21	3.1E+21	3.5E+21	3.5E+21	3.4E+21	2.9E+21	4.5E+21
6	4.0E+21	3.0E+21	3.4E+21	3.4E+21	3.3E+21	2.8E+21	4.3E+21
7	4.0E+21	3.0E+21	3.3E+21	3.3E+21	3.3E+21	2.8E+21	4.2E+21
8	4.0E+21	3.0E+21	3.3E+21	3.3E+21	3.3E+21	2.8E+21	4.2E+21
9	4.0E+21	2.9E+21	3.3E+21	3.3E+21	3.2E+21	2.8E+21	4.2E+21
10	3.9E+21	2.9E+21	3.4E+21	3.3E+21	3.2E+21	2.8E+21	4.2E+21
11	3.9E+21	2.9E+21	3.3E+21	3.3E+21	3.2E+21	2.8E+21	4.2E+21
12	3.9E+21	2.9E+21	3.3E+21	3.3E+21	3.2E+21	2.8E+21	4.2E+21
13	3.8E+21	3.0E+21	3.3E+21	3.2E+21	3.2E+21	2.8E+21	4.3E+21
14	3.7E+21	2.9E+21	3.3E+21	3.3E+21	3.2E+21	2.8E+21	4.2E+21
15	3.8E+21	3.0E+21	3.4E+21	3.2E+21	3.2E+21	2.8E+21	4.2E+21
16	3.8E+21	3.5E+21	3.8E+21	3.3E+21	3.2E+21	2.8E+21	4.3E+21
17	3.9E+21	4.0E+21	4.4E+21	3.9E+21	3.7E+21	3.1E+21	4.6E+21
18	4.7E+21	5.1E+21	5.2E+21	4.5E+21	4.2E+21	3.5E+21	5.0E+21
19	-	-	-	5.3E+21	5.0E+21	4.5E+21	5.8E+21

Nuclear Engineering Division
Argonne National Laboratory
9700 South Cass Avenue, Bldg. 208
Argonne, IL 60439

www.anl.gov